BONDING PERFORMANCES OF EPOXY-BASED COMPOSITES REINFORCED BY CARBON NANOTUBES

A Dissertation
Submitted to the Graduate Faculty
of the
North Dakota State University
of Agriculture and Applied Science

By

Dawei Zhang

In Partial Fulfillment of the Requirements
for the Degree of
DOCTOR OF PHILOSOPHY

Major Department:
Civil, Construction and Environmental Engineering

April 2022

Fargo, North Dakota

North Dakota State University

Graduate School

Title

BONDING PERFORMANCES OF EPOXY-BASED COMPOSITES REINFORCED BY CARBON NANOTUBES

By

Dawei Zhang

The Supervisory Committee certifies that this ***disquisition*** complies with North Dakota State University's regulations and meets the accepted standards for the degree of

DOCTOR OF PHILOSOPHY

SUPERVISORY COMMITTEE:

Dr. Ying Huang
Chair

Dr. Fardad Azarmi (Co-Advisor)

Dr. Zhibin Lin

Dr. Annie Tangpong

Approved:

April 13th 2022 — Date

Dr. Xuefeng (Michael) Chu — Department Chair

ABSTRACT

Epoxy resin has been exclusively used in many civil engineering applications such as adhesive joints and anti-corrosive coatings, but most of the usages of epoxy resin highly rely on a solid adhesive bonding between the epoxy matrix and the substrate material. In order to improve the bonding performance of epoxy resin, carbon nanotubes (CNTs) are incorporated into the epoxy resin due to their extraordinary mechanical properties. Although CNTs are expected to be promising additives for epoxy resin, the reinforcing efficiency of CNTs is still far from satisfactory, the bonding performance of CNT reinforced epoxy composites remains an essential research issue. In this dissertation, a systematic study was carried out to investigate the bonding performances of epoxy-based composites reinforced using CNTs. The influences of two main influential parameters (surface roughness and bondline thickness) on the bonding performance of epoxy-based composites were examined. It was found that rougher steel substrates or thinner epoxy bondlines yielded better bonding performances for both unreinforced and CNT reinforced epoxy composites. However, according to the SEM image analyses, the reinforcing efficiency of CNTs was restricted by the non-uniform dispersion of CNTs in the epoxy matrix resulted from CNT agglomeration and entanglement. Given that the great variances of CNT geometries may inevitably result in extensive differences on CNT dispersion status and reinforcing efficiencies in CNT reinforced epoxy composites, the dispersion characterizations and bonding performance of CNT reinforced epoxy composites with different CNT geometries were studied. The experimental results indicated that CNTs with larger diameter (50-100 nm) had a greater ability to achieve more uniform dispersion which further led to better bonding performance. Although CNT length did not have an evident effect on the CNT dispersion, epoxy-based composites reinforced by normal-length CNTs (5-20 μm) had higher bonding strength and toughness than those by shorter CNTs

(0.5-2 μm). To further improve the dispersion effectiveness of CNTs, a novel CNT mixing method using carboxymethyl cellulose (CMC) was proposed. It was proved that better CNT dispersion resulted from the CMC surface treatment significantly improved the bonding performance of CNT reinforced epoxy composites.

ACKNOWLEDGEMENTS

As the time flying so fast, I couldn't believe it has been 4 years since I reached the land of the US and started my doctoral journey at North Dakota State University. This dissertation may not be possible without the help and support from a number of people. Before sending my gratitude to them, I would like to acknowledge that this work was supported by the National Science Foundation under Grand No. CMMI-1750316.

First of all, I must express my deepest gratitude to my advisor, Dr. Ying Huang for her insightful supervision and invaluable assistance throughout my doctoral study. Her guidance and suggestions not only helped me organize my experiments and learn journal paper writing in my academic research, but also solve many issues in my personal life and indicate the directions of my future career development. I am so lucky to have her as my advisor and as a life mentor.

Further, many thanks to all of my committee members, Dr. Fardad Azarmi as my co-advisor as well as Dr. Zhibin Lin and Dr. Annie Tangpong. Thank you so much for their review and feedbacks on this dissertation and dissertation presentation.

Big thanks also go to my colleagues and friends in the office and lab including but not limited to Dr. Fodan Deng, Dr. Xingyu Wang, Mr. Leonard Chia, Mrs. Zi Zhang, Mr. Xin Bai, Miss Li Yao, Mr. Shuomang Shi and Mrs. Ratna Yasoda, for their ideas and help in my experiments.

At last, I am so grateful to my parents and my family for their unconditional and unfailing support and encouragement. They made my life much easier both emotionally and economically especially alone in a foreign country.

TABLE OF CONTENTS

ABSTRACT iii

ACKNOWLEDGEMENTS v

LIST OF TABLES x

LIST OF FIGURES xi

CHAPTER 1. INTRODUCTION 1

1.1. Research Background 1

1.2. Two Main Influential Parameters 2

1.2.1. Surface roughness 3

1.2.2. Bondline thickness 3

1.3. Carbon Nanotubes (CNTs) as Reinforcing Additives 4

1.4. Dispersion of CNTs 6

1.4.1. CNT geometry 7

1.4.2. Mixing methods 8

1.5. Problem Statement and Significance of This Study 9

1.6. Objectives and Organization of This Dissertation 11

CHAPTER 2. INFLUENCES OF SURFACE ROUGHNESS AND BONDLINE THICKNESS ON THE BONDING PERFORMANCE OF NEAT EPOXY RESIN 13

2.1. Experimental Setup 13

2.1.1. Experimental design 13

2.1.2. Sample preparation 15

2.1.3. Testing procedure 16

2.2. Experimental Results 17

2.2.1. Surface roughness and morphology 17

2.2.2. Thickness control 18

2.2.3. SLS test results 19
2.3. Influences of Surface Roughness and Bondline Thickness 24
2.3.1. Influence of surface roughness 24
2.3.2. Influence of bondline thickness 28
2.4. Summary 34
CHAPTER 3. INFLUENCES OF SURFACE ROUGHNESS ON THE BONDING PERFORMANCE OF CNT REINFORCED EPOXY COMPOSITES 36
3.1. Experimental Setup 36
3.1.1. Materials 36
3.1.2. Surface preparation and roughness measurements 37
3.1.3. Contact angle tests 37
3.1.4. SLS tests 38
3.2. Experimental Results 39
3.2.1. Surface characterizations 39
3.2.2. SLS test results 41
3.3. Data Analysis and Discussion 43
3.3.1. Influence of the addition of CNTs in epoxy-based composites 43
3.3.2. Influence of surface roughness for the CNT reinforced epoxy composites 49
3.4. Summary 52
CHAPTER 4. INFLUENCES OF BONDLINE THICKNESS AND CNT WEIGHT FRACTION ON THE BONDING PERFORMANCE OF CNT REINFORCED EPOXY COMPOSITES 54
4.1. Experimental Setup 54
4.2. Results and Discussions 55
4.2.1. Stress-strain curve 55
4.2.2. Bonding strength and fracture strain 60

4.2.3. Failure mode analysis 63

4.2.4. SEM image analysis 64

4.3. Summary 68

CHAPTER 5. INFLUENCES OF CNT GEOMETRIES ON THE DISPERSION CHARACTERIZATIONS AND BONDING PERFORMANCE OF CNT REINFORCED EPOXY COMPOSITES 69

5.1. Experimental Setup 69

5.1.1. Materials 69

5.1.2. Preparation of CNT suspensions 70

5.1.3. Preparation of CNT reinforced epoxy composites 70

5.1.4. Testing 71

5.2. Results and Discussions 73

5.2.1. Validation of CNT geometries with a new mixing protocol 73

5.2.2. Dispersion characterizations 74

5.2.3. Bonding performances 80

5.2.4. SEM analysis on fracture surfaces 85

5.3. Summary 88

CHAPTER 6. CNT REINFORCED EPOXY COMPOSITES USING CMC SURFACE TREATMENT AS A NOVEL MIXING METHOD 90

6.1. Experimental Setup 90

6.1.1. Materials 90

6.1.2. CMC surface treatment to CNTs 90

6.1.3. Dispersion characterizations 91

6.1.4. Bonding performance 92

6.2. Experimental Results and Discussions 92

6.2.1. Raman spectroscopy 92

6.2.2. Particle size analysis 94
6.2.3. TEM analysis 96
6.2.4. Contact angle test 98
6.2.5. SLS test 99
6.2.6. SEM analysis 102
6.3. Summary 103
CHAPTER 7. CONCLUSIONS 105
7.1. Main Conclusions 105
7.2. Main Contributions 106
7.3. Future Work 107
REFERENCES 108

LIST OF TABLES

Table Page

1. SLS test matrix in Chapter 2 15

2. Surface roughness for different surface treatments 18

3. Results of the bondline thickness (unit: mm) 19

4. Results of SLS tests in Chapter 2 23

5. Fitting parameter values in Chapter 2 27

6. SLS test matrix in Chapter 3 39

7. Results of SLS tests in Chapter 3 42

8. Fitting parameter values in Chapter 3 51

9. Results of SLS tests in Chapter 4 55

10. CNT geometries and other properties 70

11. Experimental matrix in Chapter 5 71

12. Particle size distribution and its statistical analysis 77

13. Results of SLS tests in Chapter 6 92

LIST OF FIGURES

Figure Page

1. Epoxy resin and its applications as protective coatings: (a) epoxy resin coated steel bars; (b) pipelines with anti-corrosive epoxy coating 1

2. CNTs: (a) schematic of atomic structure of a multi-walled CNT (MWCNT); (b) MWCNTs in a TEM image 5

3. Detailed sample configurations: (a) cross-section view and (b) top view 14

4. SLS test setup 17

5. SEM images of steel substrates under 100 μm magnification from different surface treatments: (a) ground; (b) fine-blasted; (c) medium-blasted; and (d) coarse-blasted surfaces 20

6. Stress-strain curves for (a) G1, (b) F1, (c) M1, and (d) C1 groups 21

7. Stress-strain curves for (a) G0.5, (b) F0.5, (c) M0.5, and (d) C0.5 groups 22

8. Stress-strain curves for (a) G0.25, (b) F0.25, (c) M0.25, and (d) C0.25 groups 23

9. Average stress-strain curves with different surface roughnesses for each bondline thickness: (a) 1 mm; (b) 0.5 mm; (c) 0.25 mm 25

10. Influence of surface roughness on the bonding strength and the fracture strain with different bondline thicknesses: (a) 1 mm; (b) 0.5 mm; (c) 0.25 mm 26

11. (a) Fracture surfaces and (b) SEM image of bottom surface under 50 μm magnification in G0.5 group; (c) fracture surfaces and (d) SEM image of bottom surface under 50 μm magnification in C0.5 group 29

12. Comparisons of the toughness with different bondline thicknesses 30

13. Typical failure surfaces: (a) 0.25 mm ground samples and (b) 0.25 mm coarse-blasted samples 31

14. SEM images of the fracture surfaces on the coarse-blasted substrate under 50 μm magnification: (a) top surface of the sample with 1 mm bondline thickness; (b) non-whitened area; and (c) whitened area of the sample of with 0.25 mm bondline thickness.....33

15. SEM images of the major crack of 0.25 mm coarse-blasted sample: (a) under 100 μm magnification; (b) under 50 μm magnification 34

16. The detailed SLS specimen configuration (unit: mm).....38

17. SEM images of steel substrates of four roughness levels at a magnification of 100X: (a) smooth; (b) fine; (c) medium; and (d) coarse substrates 40

18. Contact angles of water droplets on four different roughness substrates: (a) smooth; (b) fine; (c) medium; and (d) coarse substrates 41

19. Average stress-strain curves with different surface roughness: (a) the neat; and (b) the CNT reinforced epoxy composites 42

20. Increments between the neat and the CNT reinforced epoxy coatings: (a) bonding strength; (b) fracture strain; and (c) toughness 44

21. Typical fracture surfaces on smooth substrates: (a) the neat; and (b) the CNT reinforced epoxy composites 45

22. Contact angles of the neat and CNT reinforced epoxy droplets: (a) neat epoxy on the smooth substrates; (b) neat epoxy on the fine substrates; (c) neat epoxy on the medium substrates; (d) neat epoxy on the coarse substrates; (e) CNT reinforced epoxy on the smooth substrates; (f) CNT reinforced epoxy on the fine substrates; (g) CNT reinforced epoxy on the medium substrates; and (h) CNT reinforced epoxy on the coarse substrates.....46

23. Typical fracture surfaces on coarse substrates: (a) neat epoxy coating; (b) SEM image of the fractured neat epoxy resin at a magnification of 500X; (c) CNT reinforced epoxy composites; (d) SEM image of the fractured CNT reinforced epoxy composites at a magnification of 500X 47

24. Detection of CNTs: (a) on fracture surfaces at a magnification of 5000X; (b) on fracture surfaces at a magnification of 10,000X; (c) on the main crack at a magnification of 500X; (d) on the main crack at a magnification of 10,000X.....49

25. Changes of bonding strengths and fracture strains of the CNT reinforced epoxy composites with different surface roughness 51

26. Typical fracture surfaces of the CNT reinforced epoxy composites on top surfaces at a magnification of 500X: (a) on the smooth substrate; (b) on the coarse-blasted substrate 52

27. Comparisons between original experimental stress-strain curves and the average fitting curves in each testing conditions: (a) E1; (b) E0.5; (c) E0.25; (d) HC1; (e) HC0.5; (f) HC0.25; (g) C1; (h) C0.5; (i) C0.25 56

28. Average stress-strain curves of epoxy-based composites: (a) neat epoxy; (b): 0.375% CNTs; (c) 0.75% CNTs 58

29. Comparisons of toughness between different bondline thickness (including increments from 1 mm to 0.5 mm and 0.5 mm to 0.25 mm) with each CNT addition 59

30. Comparisons between different bondline thickness (including increments from 1 mm to 0.5 mm and 0.5 mm to 0.25 mm) with each CNT addition: (a) bonding strength; (b) fracture strain 62

31. Typical fracture surfaces of epoxy-based composites: (a) 1 mm neat epoxy; (b): 1 mm 0.75% CNT reinforced epoxy; (c) 0.25 mm neat epoxy; (d) 0.25 mm 0.75% CNT reinforced epoxy 64

32. SEM images of the typical fracture surfaces: (a) 1 mm neat epoxy; (b): 1 mm 0.75% CNT reinforced epoxy; (c) 0.25 mm neat epoxy; (d) 0.25 mm 0.75% CNT reinforced epoxy 65

33. SEM images of the presence of CNTs in the epoxy bondlines at higher magnifications: (a) the presence of CNTs; (b): CNT pulling-out from epoxy bondlines 66

34. SEM images of a CNT cluster on the fracture surface of 0.75% CNT reinforced epoxy composites: (a) a CNT cluster at a magnification of ×2300; (b): enlarged view of (a) at a magnification of ×15000.....67

35. The complete mixing procedures: (a) CNT suspensions; (b) CNT reinforced epoxy composites 72

36. TEM images showing the diameters of CNTs: (a) N10; (b) N20; (c) N50 74

37. TEM images showing the lengths CNTs: (a) N20; (b) S20.....74

38. Volume weighted particle size distributions of CNT suspensions of different CNT geometries: (a) 0.5%; (b) 1%; (c) 2% CNT fractions 76

39. TEM images showing the real dispersion states of CNTs with different geometries and fractions: (a) N10-2; (b) N20-0.5; (c) N20-2; (d) N20-1; (e) N50-2; (f) S20-2.....80

40. Average stress-strain curves of CNT reinforced epoxy composites with different CNT geometries: (a) 0.5%; (b) 1%; (c) 2% CNT fractions 81

41. Bonding strenths of CNT reinforced epoxy composites with different CNT geometries: (a) 0.5%; (b) 1%; (c) 2% CNT fractions 82

42. Toughness of CNT reinforced epoxy composites with different CNT geometries: (a) 0.5%; (b) 1%; (c) 2% CNT fractions 84

43. SEM images on the fracutre surfaces of CNT reinforced epoxy composites: (a) N10-0.5; (b) N20-1; (c) N20-0.5; (d) N20-2; (e) N50-0.5; (f) S50-0.5 87

44. SEM images at high magnification: (a) N10-0.5; (b) N50-0.5.....88

45. CMC and CNT mixing procedures 91

46. Raman spectra of pristine CNTs and CMCs coated CNTs with different CNT fractions: (a) 0.5%; (b) 1%; (c) 2%. 93

47. Particle size distributions of pristine CNTs and CMCs coated CNTs with different CNT fractions: (a) C0.5; (b) CC0.5; (c) C1; (d) CC1; (e) C2; (f) CC2 95

48. TEM observations of pristine CNTs and CMCs coated CNTs with different CNT fractions: (a) C0.5; (b) CC0.5; (c) C1; (d) CC1; (e) C2; (f) CC2 97

49. Typical TEM images of individual pristine CNTs and CMCs coated CNTs at a higher magnification: (a) pristine CNTs; (b) CMCs coated CNTs 98

50. CNTs reinforced epoxy droplets and their contact angles: (a) C0.5; (b) C1; (c) C2; (d) CC0.5; (e) CC1; (f) CC2 99

51. SLS test results: (a) stress-strain curves of SLS specimens; (b) toughness of SLS specimens 100

52. Increments of the bonding strength and fracture strain between pristine CNTs and CMCs/CNTs reinforced epoxy composites with different CNT fractions: (a) bonding strength; (b): fracture strain 101

53. Typical CNT clusters on the fracture surfaces of 2% pristine CNTs and CMCs/CNTs reinforced epoxy composites: (a) C2; (b) close-view of the CNT cluster of C2; (c); CC2; (d) close-view of the CNT cluster of CC2 102

CHAPTER 1. INTRODUCTION

1.1. Research Background

Polymeric materials are generally believed to have a great potential of possessing many advanced properties by designing or modifying the component, structure, and morphology [1,2]. Such properties have drawn intensive research attentions and motivated their vital usage in a wide spectrum of applications [3,4]. For example, in civil engineering, polymeric adhesive bonding has been broadly recognized as a favorable method of joining various structural materials in the form of adhesive joints [5]. Compared to traditional joints, polymeric adhesive joints provide many advantages such as light weight, high strength, uniform stress distribution and low manufacturing cost [6]. Polymeric composites are also extensively used to protect steel substrates from corrosion as a protective coating on underground, underwater, and offshore infrastructures [7,8]. Epoxy resins, with high strength-to-weight ratio, good chemical and environmental resistance, no toxic substance, and easy to apply in practice, have become a favorable polymeric material in those applications. Figure 1(a) shows the main applications of epoxy resin.

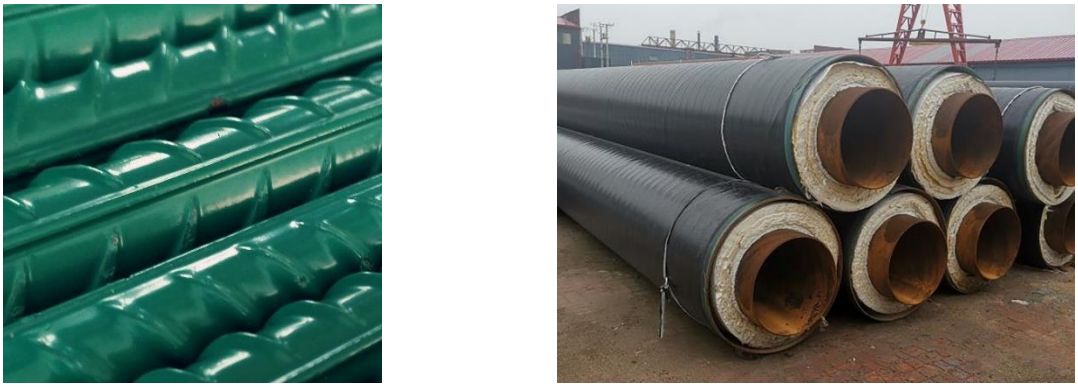

(a) (b)

Figure 1. Epoxy resin and its applications as protective coatings: (a) epoxy resin coated steel bars; (b) pipelines with anti-corrosive epoxy coating

However, epoxy-based composites also suffer from some drawbacks especially their relatively poor bonding performances which may easily lead to the early failure of adhesive joints

or the debonding of protective coatings under external disturbances [9–11]. Epoxy-based composites have relatively weak bonding performances not only because they are brittle materials which yield relatively low ductility and resistance to crack propagations [12], but also given the fact that steel and epoxy resin are dissimilar materials, the interfacial adhesion forces between steel and epoxy resin are mainly hydrogen and Van der Waals force in the form of secondary bonding which are weaker compared to adhesion between similar materials [13,14]. The brittleness of the neat epoxy resin results in the low shear capacity of adhesive composites due to poor mechanical properties [15], while the secondary bonding forces between the neat epoxy and substrate lead to premature adhesive failure in which the composites delaminate from the substrate before it fully deforms [16]. In fact, neat epoxy resin also has many initial defects. The growth and propagation of these initial defects inside the composite matrix normally have a detrimental impact on the bonding performance of epoxy-based composites [17]. Therefore, the bonding performance of epoxy-based composites are not only determined by the mechanical properties of the epoxy adhesive, the interfacial adhesion between the epoxy adhesive and the substrate are also crucial and definitive.

1.2. Two Main Influential Parameters

Both strong adhesive joints and effective corrosion preventions highly rely on a solid adhesive bonding between the epoxy-based composite and the substrate material, leading to an increasing demand of improving the bonding performance of epoxy-based composites. Many researches have attempted to improve the bonding performance of epoxy-based composites. Modifying epoxy adhesives and substrates using different fabrication methods is regarded as one of the most straightforward and cost-effective approaches since it does not involve any extra treatments or additions. Among all manufacturing parameters, two factors have been identified as

main parameters affecting the bonding performance of epoxy-based composites, including the surface roughness of the adherend substrate and the bondline thickness of the epoxy adhesive [18,19].

1.2.1. Surface roughness

Surface roughness of the substrate is of vital importance to the interfacial adhesion between the epoxy adhesive and the substrate as well as the overall bonding performance of the epoxy-based composites. There is a variety of surface treatment methods used to adjust surface roughness, such as hydroxide immersion [20], acid treatment [21], mechanical blasting [22], and thermal spraying treatments [23]. The literature indicates that sufficient surface roughness plays a critical role in obtaining a reliable bond by enlarging the contact area between the adhesive and the adherend [24]. However, most of the previous studies on surface roughness only compared the bonding strength with or without a certain surface roughness condition. Few studies have been conducted to compare the bonding strength resulting from several different surface roughness levels. Unfortunately, these studies yielded inconsistent findings. For instance, Uehara and Sakurai showed that there was no clear relationship between the shear strength and the surface roughness of adherends [25], but some recent studies found the existence of an optimum surface roughness [26] which varies with respect to different combinations of adhesives and adherends [27]. Several other studies showed that the increase of surface roughness improved joint strength [16,28].

1.2.2. Bondline thickness

Similar to surface roughness, results of existing discussions on the influence of bondline thickness are also controversial. It was found by classical theoretical methods that stress and strain were more uniformly distributed within thicker bondlines, which consequently resulted in higher bonding strength. However, other researches showed there was no clear evidence implying that

the variation of bondline thickness result in considerable modifications on the strength [29] and stiffness [30] of epoxy-based composites. By contrast, some other experimental and analytical studies indicated that bondline thickness decisively influenced the bonding performance. The bonding strength was expected to be weakened with the increase of bondline thickness [31], although the impact varied with different failure modes [32]. This trend of weakened bonding strength with thicker bondlines could also be predicted by statistical [33] and finite element analyses [34]. Thicker bondlines yielded weaker bonding strengths because of a variety of factors, with the porosity of the epoxy adhesive being one of the most critical. Thicker bondlines increased the likelihood of more internal voids and micro cracks, which might lead to a greater possibility of early failure [35]. Bending moment [36], constrain effect [37], and global yielding [38] have also been used to explain the adverse effects of bondline thickness on the bonding strength of epoxy-based composites.

1.3. Carbon Nanotubes (CNTs) as Reinforcing Additives

Nanocomposites consist of a polymer matrix embedded with at least one kind of inorganic particles in nano-dimension [39], and the usage of nanocomposites has gained ever increasing popularity in a wide range of applications in the last few decades. A variety of nanofillers have been incorporated into polymeric materials to enhance their mechanical, electrical, and thermal properties as polymer reinforcement [39–42]. Since first discovered by Iijima in 1991 [43], carbon nanotubes with extraordinarily high shear strength and young's modulus [44], have intrigued exclusive research attentions among all the nanofillers. It is well established that adding a small percentage of CNTs into the epoxy matrix as additives is a promising way to improve the bonding performance of epoxy-based composites, which makes CNTs an ideal reinforcement for epoxy-based composites [45–47]. Research findings showed that the added CNTs are able to constrain

and resist crack propagation within the adhesive matrix by increasing the fracture toughness [48,49], and eventually improve the bonding performance of epoxy-based composites [50]. Figure 2(a) shows schematic of atomic structure of a multi-walled CNT, and Figure 2(b) displays MWCNTs in a TEM image.

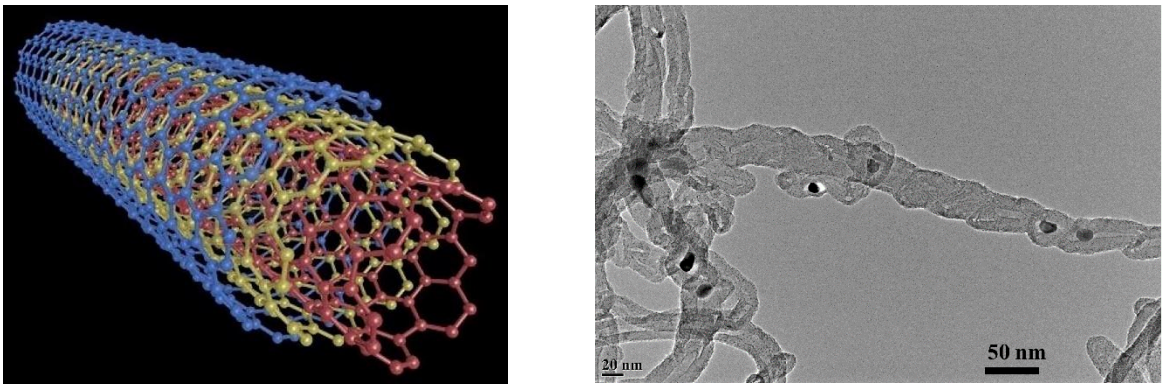

(a) (b)

Figure 2. CNTs: (a) schematic of atomic structure of a multi-walled CNT (MWCNT); (b) MWCNTs in a TEM image

A lot of research efforts has been focusing on the bonding performance of CNT reinforced epoxy composite, but unfortunately, these researches are inconsistent with their conclusions regarding the improvement in bonding strength. Some studies showed that the bonding strength of CNT reinforced epoxy composites was as much as 39% higher than that of neat epoxy resin [40,51]. However, it was also reported by some other studies that the addition of CNTs did not seem to significantly affect the bonding strength, only a slight increase in bonding strength (typically less than 10%) was obtained by CNT reinforced epoxy adhesive with the same CNT weight fraction (around 5%) [49,52].

Since surface roughness and bondline thickness are recognized as the two main influential parameters, the inconsistency in the research findings may be induced by the variations of those parameters. Previous studies conclude that the bonding strength improvement by CNT addition was mainly due to the improvement of mechanical properties of the reinforced epoxy-based

composite [53,54]. However, when the interfacial adhesion is not strong enough, only a small part of the composites contributes to the bond, which may easily lead to the premature failure. The interfacial adhesion is directly related to the surface roughness of the substrate. Thus, only improving the mechanical properties by CNT addition might be insufficient to achieve a firm bond if the surface roughness does not create a reliable interfacial adhesion between the epoxy adhesive and the substrate [55]. Previous researches only compare the bonding performances of CNT reinforced epoxy composites with or without a certain surface treatment method. It still lacks investigations on the bonding performance with a wide roughness range using the same surface treatment method, since different roughness made from different treatment methods might also contribute to the inconsistent results mentioned previously.

As discussed above in the last section, epoxy-based composites with thicker bondline layers tend to have more voids and micro-cracks, implying higher porosity, higher possibility of a brittle failure and lower bonding strength. However, for CNT reinforced epoxy composites, the addition of CNTs was found to reduce the porosity of epoxy bondlines which could deviate and bridge the crack within the epoxy matrix [52,56]. Thus, the negative effect of thicker bondline thickness could probably be mitigated or even reversed with the CNT reinforcement. Because when the epoxy bondlines are free of any imperfections, the classic theoretical analysis showed that thicker bondlines positively influence the bonding performances of neat epoxy as a result of a more uniform stress and strain distribution within the bondline layer.

1.4. Dispersion of CNTs

Most of the existing studies contain discussions with regard to the influence of CNT weight fraction on the bonding performance of CNT reinforced epoxy composites. Literature shows that shows that the bonding strength of epoxy-based composites increase as the increase of CNT

addition until a threshold (around 1%), and then decrease [51,56]. The existence of an optimal CNT fraction is mainly due to the non-uniform dispersion of CNTs in the epoxy matrix when the CNT fraction is too high [57,58]. CNTs are difficult to be uniformly and evenly dispersed in the epoxy matrix not only because of the relatively high viscosity of epoxy resin, but also owing to the extremely high aspect ratios and extremely large surface areas of CNTs, resulting in strong Van der Waals forces on the surface [59]. Without any external stimulus to break the intermodular interactions, CNTs are more likely to agglomerate and entangle into CNT clusters which normally weaken the strength, cause stress concentration and other detrimental effects as defects or imperfections [60]. The dispersion characterizations of CNTs plays an important role on the bonding performance of CNT reinforced epoxy composites [61,62]. Thus, the bonding strength improvements of CNTs reinforced epoxy-based composites may vary a lot among different dispersion qualities, which may also cause the inconsistency mentioned above.

1.4.1. CNT geometry

As the most obvious properties of CNTs, CNT geometry including diameter and length of the tubes definitely have a non-ignorable influence on the dispersion of CNTs. CNTs fall into the category of nanomaterials because the diameter of the tubes is in nanometer scale, but diameters also vary a lot from several nanometers to more than one hundred nanometers [44]. Since the aspect ratio of CNTs is always extraordinary high, the length of CNTs is typically far larger than the diameter. Due to different production methods, the length of CNTs could be as short as micro level, or as long as centimeter level. The huge variances of CNTs in diameter and length inevitably result in extensive differences in aspect ratio and other material properties, which further affect dispersion characterizations and reinforcing efficiency of CNT reinforced epoxy composites [63,64]. In the literature, different researchers use CNTs with different geometries, while very few

researches only focus on the effect of CNT geometries on the thermal and electrical properties of CNT reinforced epoxy composites [65,66]. To the best of the authors' knowledge, there is no relevant research involving investigations on the mechanical properties of CNT reinforced epoxy composites with different CNT geometries, especially bonding performance.

1.4.2. Mixing methods

The dispersion of CNTs is also governed by mixing methods. To promote the dispersion of CNTs into epoxy resin, varieties of methods have been developed. Most of the prevalent methods fall into three categories: mechanical mixing, chemical, and physical surface treatments [67]. Mechanical mixing including ultrasonic mixing [68] and three-roll milling [69] is the most prevalent method to improve the dispersion by breaking up CNTs clusters, but it is not able to maintain the dispersion state constantly [70]. Moreover, the disassembling process by ultrasonic methods may also cut off the length and shorten the aspect ratio of CNTs [68,71].

On the other side, the principal mechanism of both chemical and physical surface treatments is to add soluble moieties and let them attach on the tube surface, which prevents CNTs from agglomeration [72]. Chemical treatments are usually covalent functionalization such as amino [73] and silane [74] functionalization, and it is proven that they are effective to modify the dispersion in practical applications [75]. However, chemical treatments could also cause structural damages on the tube walls, which in turn consequently affects the mechanical and electrical properties of CNTs and the polymer matrix as a whole [76,77]. Among all those methods, physical surface treatments are regarded as non-covalent functionalization with less aggressive surfactants forming physical absorption on the surface of CNTs [78,79]. Compared to covalent functionalization, physical treatments are expected to improve the dispersion while preserving the chemical structure and original properties of the CNTs [80].

Carboxymethyl cellulose (CMC) is a water dispersible cellulose derivative, and its sodium salt has been exclusively used in food, cosmetic and pharmaceutical industries as a thicker, stabilizer or binder [81]. Recently, CMC found its new applications as a surfactant to functionalize CNTs for a better dispersion, and physical treatment using CMC is a prospective method to improve the mechanical and electrical properties of carbon nanomaterials [82,83]. Another advantage of CMC is that CMC is an environmental-friendly, biocompatible, and disposable material without any harsh chemicals, which makes it even more favorable over some other solvents. However, the current application of CMC is only limited in obtaining a uniform and stabilized CNT dispersion in cementitious materials [36], no studies have incorporated CMCs into CNTs reinforced polymer materials like CNTs reinforced epoxy resin.

1.5. Problem Statement and Significance of This Study

All the previous studies provide valuable information and data to investigate the bonding performance of epoxy-based composites. The following findings and research gaps are identified based on the literature review:

1) A solid adhesive bonding is the prerequisite for effective and sustainable application of epoxy-based composites. How to optimize the bonding performance of epoxy-based composites has become a critical issue owing to weak interfacial adhesion between the epoxy and the substrate and the brittleness of epoxy resin.
2) Surface roughness of the substrate and bondline thickness of the epoxy-based composites are the two universal influential parameters which are able to enhance the interfacial adhesion and overcome the brittleness of epoxy resin respectively, but there is a lack of consistency in the understanding of those two parameters.

3) Adding a small percentage of CNTs into epoxy-based composites as reinforcements is believed to be a promising way to improve the bonding performance of epoxy-based composites. The conclusions of bonding strength improvements by CNT addition are not yet consistent.
4) Surface roughness still have their impact on CNT reinforced epoxy composites. Most current researches only focus on the influence of CNT weight fractions, it still lacks investigations on the bonding performance of epoxy-based composites with several different roughness levels covering a wide range.
5) The influence of bondline thickness on CNT reinforced epoxy composites may be very different from that on neat epoxy resin. However, there is a severe lack of relevant studies on CNT reinforced epoxy composites with different bondline thicknesses.
6) CNTs naturally tend to agglomerate and entangle into CNT clusters leading to the non-uniform dispersion in the epoxy-based composites, which further influences the reinforcing efficiency. The dispersion characterizations of CNTs are governed by CNT geometries and mixing methods.
7) CNT geometries include the diameter and length of the tubes. No relevant research involving investigations on the bonding performance of CNT reinforced epoxy composites with different CNT geometries.
8) CMC surface treatment is believed to be a novel CNT mixing method for better CNT dispersion, but no studies have incorporated CMCs into CNTs reinforced polymer materials like CNTs reinforced epoxy resin.

1.6. Objectives and Organization of This Dissertation

In this dissertation, the main objective is to investigate the bonding performance of epoxy-based composites reinforced by CNTs. To achieve this objective, this study is carried out on the basis of four specific tasks which can be summarized as follow:

1) Have a clear understanding of the influence of surface roughness and bondline thickness on the bonding performance of neat epoxy resin.
2) Have a clear understanding of the influence of CNT addition on the bonding performance of CNT reinforced epoxy composites with different surface roughness.
3) Investigate the influence of bondline thickness and CNT weight fraction on the bonding performance of CNT reinforced epoxy composites.
4) Investigate the influence of CNT geometries (diameter and length) on the dispersion characterizations and bonding performance of CNT reinforced epoxy composites.
5) Develop a new physical surface treatment method using CMCs and verify whether the dispersion or bonding performances of CNT reinforced epoxy composites were improved by using newly-developed physical treatment methods.

This dissertation is thus organized as follows: in Chapter 1, an introduction of epoxy-based composites and a detailed literature review of the influences of different parameters; in Chapter 2, Experimental studies about the influences of surface roughness and bondline thickness on the bonding performance of neat epoxy resin; in Chapter 3, Experimental studies about the influence of surface roughness on the bonding performance of CNT reinforced epoxy composites; in Chapter 4, Experimental studies about the influence of bondline thickness and CNT weight fractions on the bonding performance of CNT reinforced epoxy composites; in Chapter 5, Experimental studies about the influence of CNT geometries (diameter and length) on the dispersion characterizations

and bonding performance of CNT reinforced epoxy composites; in Chapter 6, CNT reinforced epoxy composites using CMC surface treatment as a novel mixing method; and in Chapter 7, main conclusion, contributions and future work.

CHAPTER 2. INFLUENCES OF SURFACE ROUGHNESS AND BONDLINE THICKNESS ON THE BONDING PERFORMANCE OF NEAT EPOXY RESIN

Surface roughness of the substrate and bondline thickness of the epoxy-based composites are the two main influential parameters for all kinds of epoxy-based composites, regardless of any treatments, additions, or applications. To actually investigate the influences of those two parameters, it is necessary to use neat epoxy resin as the composite material before adding CNTs. The bonding performance of polymers or composites could be examined by several testing methods, single bonding (SLS) tests were extensively deployed to investigate the influence of different parameters on the bonding performance of epoxy-based composites. In this chapter, experimental studies using SLS tests were performed to investigate the influences of surface roughness and bondline thickness on the bonding performances of neat epoxy resin. The evaluated bonding performances included the bonding strength, fracture strain, and failure mode of epoxy-based composites which were fabricated with four different surface roughnesses and three bondline thicknesses. SEM analyses were performed to understand the bonding mechanism of epoxy-based composites by examining the mechanical properties and surface morphology before and after fracture.

2.1. Experimental Setup

2.1.1. Experimental design

In this chapter, SLS tests were conducted to evaluate the bonding performance of neat roughness's epoxy-based composites. Specifically, tension loading was applied on a series of SLS samples to produce shear on the neat epoxy resin to determine their bonding performances on mild steel substrates. An SLS sample consisted of two mild steel sheets bonded with epoxy adhesive,

as shown in Figure 3. The material of the steel sheets was low carbon A36 steel (supplied by Mid-American Steel Inc) which has been commonly used in the civil engineering industry for structural applications. The epoxy adhesive was made of a general-purpose epoxy resin (supplied by East Coast Resin) including a bisphenol A based resin and a polyamide adduct curing agent. The adhesive matrix was prepared by mixing the resin and the curing agent thoroughly at a volume ratio of 1:1. As detailed in Figure 3, the dimension of the steel sheets was 101.6 mm × 25.4 mm × 3.175 mm (length, width, and thickness) and the overlap length between the two steel sheets was 12.7 mm, following ASTM D3165-07. In addition to the two steel sheets, two steel tabs were bonded at the ends of each steel sheet using the same epoxy to balance the misalignment in the loading direction of the joint. The steel tabs had the same thickness and width as the steel sheets and a length of 25.4 mm. The thickness of the steel sheets and the tabs was chosen to be 3.175 mm to promote stability of the joint and prevent early buckling before bonding failure.

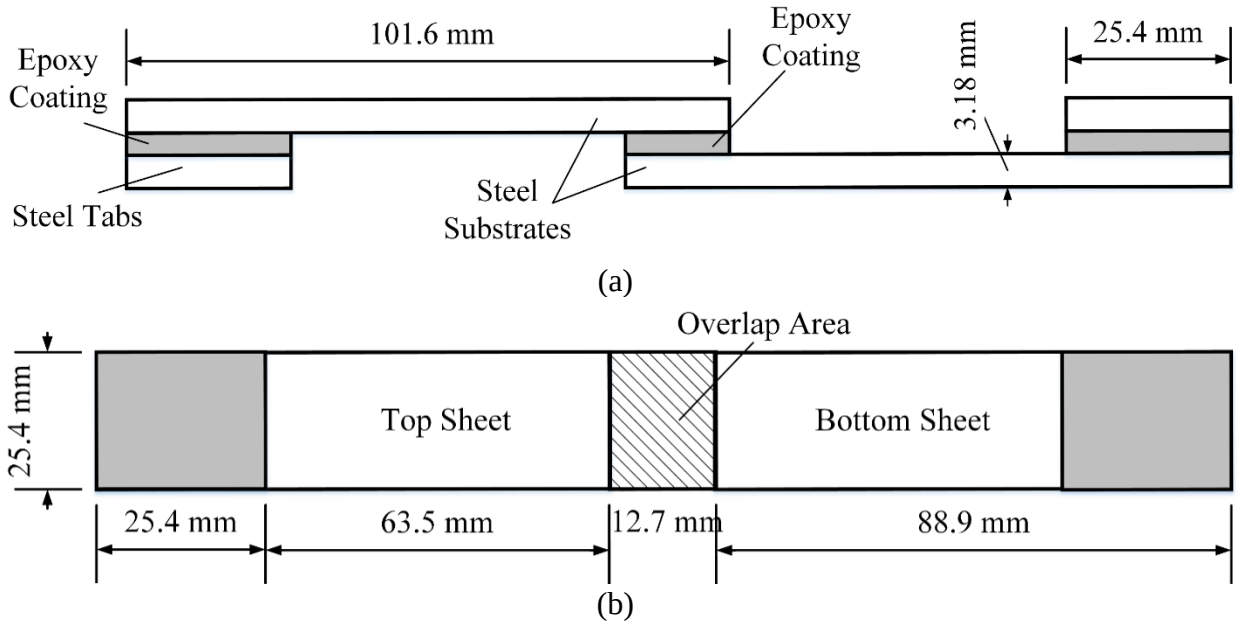

Figure 3. Detailed sample configurations: (a) cross-section view and (b) top view

Table 1 shows sample details performed in this chapter. Three different bondline thicknesses of 0.25mm, 0.5 mm, and 1 mm were prepared using steel shims. For each bondline

thickness, there were four different surface conditions of the steel adherend, including ground (G0.25, G0.5, and G1), fine- (F0.25, F0.5, and F1), medium- (M0.25, M0.5, and M1), and coarse-blasted (C0.25, C0.5, and C1) surface conditions for 0.25 mm, 0.5 mm, and 1 mm thicknesses respectively. To be statistically valid, five samples were prepared for each testing group shown in Table 1. Therefore, there were 12 testing groups, resulting in 60 total samples with four different surface roughness levels and three different bondline thicknesses.

Table 1. SLS test matrix in Chapter 2

Testing group	Surface roughness	Bondline thickness (mm)	Sample notation
P0.25	Ground	0.25	G0.25-1, G0.25-2, G0.25-3, G0.25-4, G0.25-5
F0.25	Fine	0.25	F0.25-1, F0.25-2, F0.25-3, F0.25-4, F0.25-5
M0.25	Medium	0.25	M0.25-1, M0.25-2, M0.25-3, M0.25-4, M0.25-5
C0.25	Coarse	0.25	C0.25-1, C0.25-2, C0.25-3, C0.25-4, C0.25-5
P0.5	Ground	0.5	G0.5-1, G0.5-2, G0.5-3, G0.5-4, G0.5-5
F0.5	Fine	0.5	F0.5-1, F0.5-2, F0.5-3, F0.5-4, F0.5-5
M0.5	Medium	0.5	M0.5-1, M0.5-2, M0.5-3, M0.5-4, M0.5-5
C0.5	Coarse	0.5	C0.5-1, C0.5-2, C0.5-3, C0.5-4, C0.5-5
P1	Ground	1	G1-1, G1-2, G1-3, G1-4, G1-5
F1	Fine	1	F1-1, F1-2, F1-3, F1-4, F1-5
M1	Medium	1	M1-1, M1-2, M1-3, M1-4, M1-5
C1	Coarse	1	C1-1, C1-2, C1-3, C1-4, C1-5

2.1.2. Sample preparation

To prepare the four different surface roughness conditions, mechanical surface treatments were applied, since surface roughness prepared by mechanical surface treatments can be modified quantitively using sandpapers with different mesh numbers [84] or blast abrasives with different grit sizes [85]. This study adopted sandpaper grinding and grit blasting as the surface treatment methods. Before any surface treatment, all steel sheets were immersed in pure acetone solution and cleaned ultrasonically at room temperature for 15 minutes. To achieve the ground surface, the overlap areas of steel sheets were sanded in the sequence of 60, 120, 220 and 400 grit sandpapers. To achieve the fine-blasted, medium-blasted and coarse-blasted surfaces, grit blasting was

performed with 20 grit, 36 grit and 60 grit aluminum oxides, respectively. The grit blasting pressure was 500 kPa and the standoff distance was 150 mm with a blasting angle of 90°. After grinding or grit blasting, the substrates were cleaned by compressed air to remove any grit or dust remaining on the surface, followed by ultrasonic cleaning with the same procedure described above. Furthermore, SLS samples were prepared within 24 hours after surface treatments to minimize surface oxidation. Steel shims with thicknesses of 0.25 mm, 0.5 mm and 1 mm were used to control the thickness while applying epoxy. After the samples were prepared, they were cured at 32℃ for 24 hours, followed by curing at room temperature for at least 7 days before testing.

2.1.3. Testing procedure

To provide accurate measurements of surface roughness, each surface was measured by a roughness tester (PCE-RT 1200 supplied by PCE Americas, Inc.) right after all of the surface treatments. Three roughness parameters were measured, including the average roughness (R_z), the arithmetic mean roughness (R_a), and the maximum roughness (R_t). Among those three roughness parameters, R_z is the arithmetic mean of the maximum height difference among several adjoining individual measuring sections. R_a is the arithmetic mean of the absolute values of the profile deviations within the reference line, while R_t is the distance between the highest and the lowest points of the measuring section [86]. For each measured substrate, the mean value of five measurements at different locations was used to reduce random errors. In one roughness measurement, five measuring sections were included with the cut-off length of 0.8 mm. In addition, the prepared surfaces were also evaluated using SEM image analyses at the Electron Microscopy Center of North Dakota State University. The SLS tests were conducted using MTS Flex Test® SE loading frame with displacement control at a loading rate of 1.3 mm/min under monotonic

loading, as shown in Figure 4. Each sample was loaded till shear failure occurred. The real-time uniaxial shear load and displacement in shear loading direction were recorded and studied. The fractured surfaces of epoxy-based composites in each group were also evaluated using SEM image analyses.

Figure 4. SLS test setup

2.2. Experimental Results

2.2.1. Surface roughness and morphology

Table 2 displays the average measured values and standard deviations of R_z, R_a, and R_t based on the roughness measurements of the four different surface treatments. It is obvious that surface roughnesses varied significantly among each surface treatment, but all three parameters shared a similar trend in terms of the four surface treatments. Among these roughness parameters, R_a considers every height of the whole profile instead of only the heights of peaks like R_z, and R_a has been widely recognized as an internationally applied roughness parameter. Although all the three roughness parameters were recorded and reported in this study, only R_a was used to represent

surface roughness in the further analysis. The roughness values of ground, fine-, medium- and coarse-blasted surfaces were 0.20 µm, 3.54 µm, 5.62 µm, and 8.52 µm, respectively.

Table 2. Surface roughness for different surface treatments

Surface treatment	Grit size	R_z (µm)	R_a (µm)	R_t (µm)
Ground	Sandpaper 60, 120, 220, 400	1.81 ± 0.11	0.20 ± 0.02	2.03 ± 0.19
Fine-blasted	Aluminum oxides 60	24.13 ± 0.98	3.54 ± 0.17	27.43 ± 2.19
Medium-blasted	Aluminum oxides 36	36.11 ± 0.13	5.62 ± 0.34	35.60 ± 1.51
Coarse-blasted	Aluminum oxides 20	45.66 ± 1.58	8.52 ± 0.43	47.57 ± 2.91

Figure 5(a ~ d) shows SEM images of representative substrates from the four different surface conditions under 100 µm magnification. In agreement with Table 2, when comparing Figure 5(a ~ d), it can be seen that the ground surface was very smooth and flat with very few humps. The fine-blasted surface has small humps and cavities, while the medium-blasted surface has deeper cavities and higher humps than fine-blasted surface. For the coarse-blasted surface, the height differences between cavities and humps were the greatest. As surface roughness is determined by the heights of humps and depths of cavities on the substrate, higher humps and deeper cavities increased the surface roughness creating more contact areas between the epoxy adhesive and the substrate [22,51].

2.2.2. Thickness control

The bondline thickness was measured as the thickness of the overlap area minus the thickness of each sheet in the sample using a Vernier caliper. The average thickness was obtained from five readings at different locations. The results of the bondline thicknesses for each sample as well as the average thicknesses and standard deviations for each testing group are shown in Table 3. In this dissertation, all the standard deviations in percentage were calculated by dividing the actual standard deviations of each parameter with the average values of that parameter. It can be seen from the table that all the variances of bondline thickness among five samples in one group

were within 16% of the corresponding target thicknesses, indicating consistent thicknesses of the prepared samples in each group.

Table 3. Results of the bondline thickness (unit: mm)

Sample Number	1	2	3	4	5	Average	Standard Deviation (%)
G1	1.22	0.85	0.86	0.94	1.03	0.98 ± 0.14	14
F1	1.12	1.09	1.23	0.82	0.84	1.02 ± 0.16	16
M1	0.80	1.11	0.98	1.06	0.93	0.98 ± 0.11	11
C1	1.25	0.97	1.06	0.92	0.93	1.03 ± 0.12	12
G0.5	0.40	0.37	0.58	0.50	0.46	0.46 ± 0.07	15
F0.5	0.40	0.38	0.39	0.46	0.39	0.41 ± 0.03	7
M0.5	0.37	0.38	0.43	0.53	0.54	0.45 ± 0.07	16
C0.5	0.41	0.53	0.52	0.46	0.57	0.50 ± 0.06	12
G0.25	0.23	0.25	0.25	0.25	0.21	0.24 ± 0.02	8
F0.25	0.28	0.22	0.26	0.27	0.20	0.25 ± 0.03	12
M0.25	0.24	0.22	0.25	0.26	0.28	0.25 ± 0.02	8
C0.25	0.21	0.22	0.22	0.23	0.25	0.23 ± 0.02	9

2.2.3. SLS test results

The recorded shear load and displacement were converted into the corresponding shear stress (τ) and shear strain (γ) using the following equations:

$$\tau = P/A = P/LW \quad (1)$$

$$\gamma \approx tan\gamma = D/t \quad (2)$$

where, P is the shear load, A is the overlap area calculated by multiplying its length (L) and width (W), D is the applied displacement and t is the bondline thickness. Thus, load-displacement curves can be presented as stress-strain curves. To better compare the impact of surface roughness on the bonding performance among different testing groups, five individual curves in each group were fitted into one average stress-strain curve using the X-function mathematical algorithm.

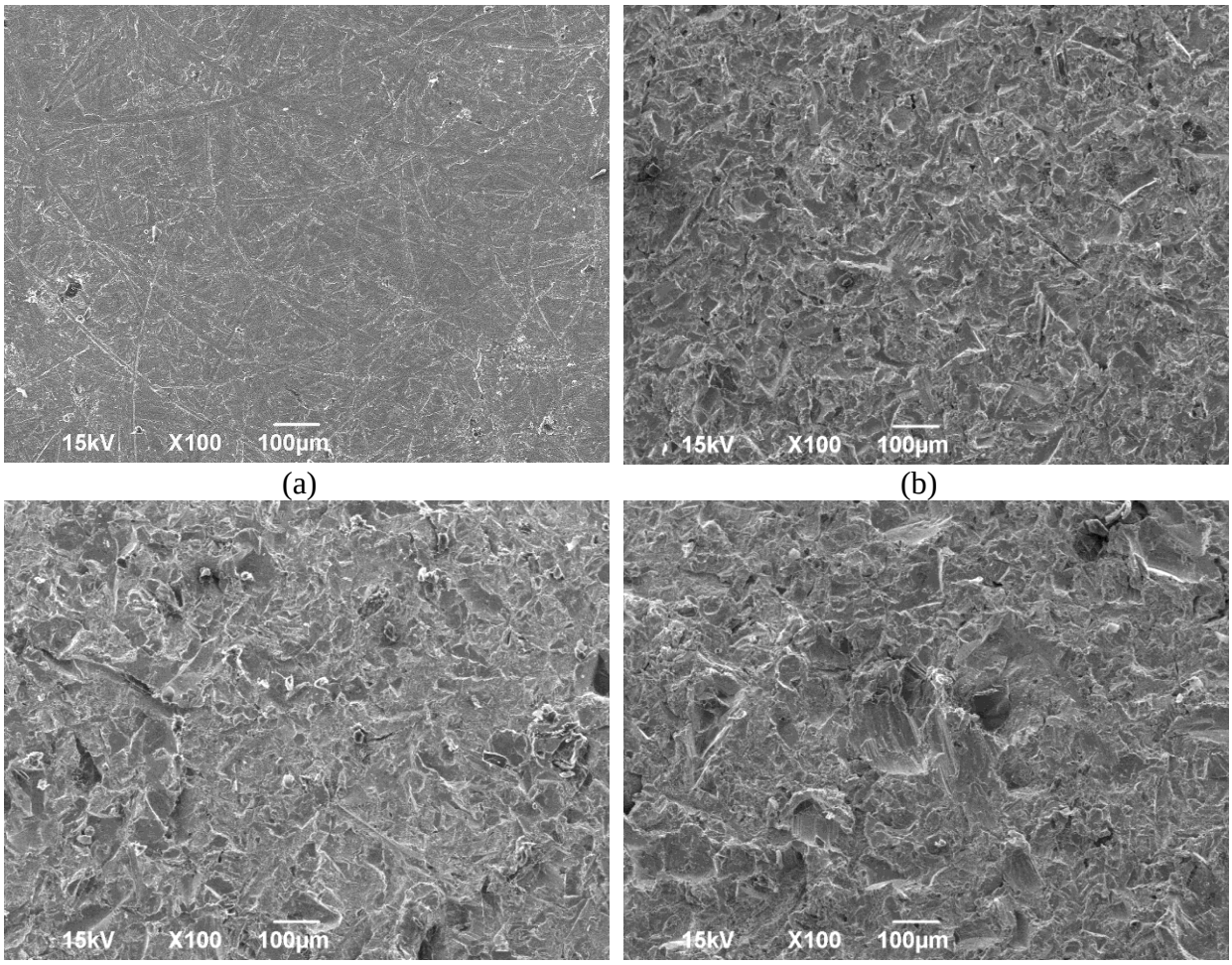

Figure 5. SEM images of steel substrates under 100 µm magnification from different surface treatments: (a) ground; (b) fine-blasted; (c) medium-blasted; and (d) coarse-blasted surfaces

Figure 6 ~ 8 illustrate comparisons between measured stress-strain curves of the five samples and the corresponding average curves in each group with bondline thicknesses of 1 mm, 0.5 mm, and 0.25 mm, respectively. For all the groups, although there were some fluctuations at the beginning, the measured stress-strain curves as well as the average curves basically shared a similar growing trace and ended up with similar ultimate stresses and strains. The stress-strain curves of each group could be represented by the corresponding average curves in the same group. Thus, in the further analysis, the average stress-strain curves were used to represent the associated testing groups and to study the influence of surface roughness and bondline thickness.

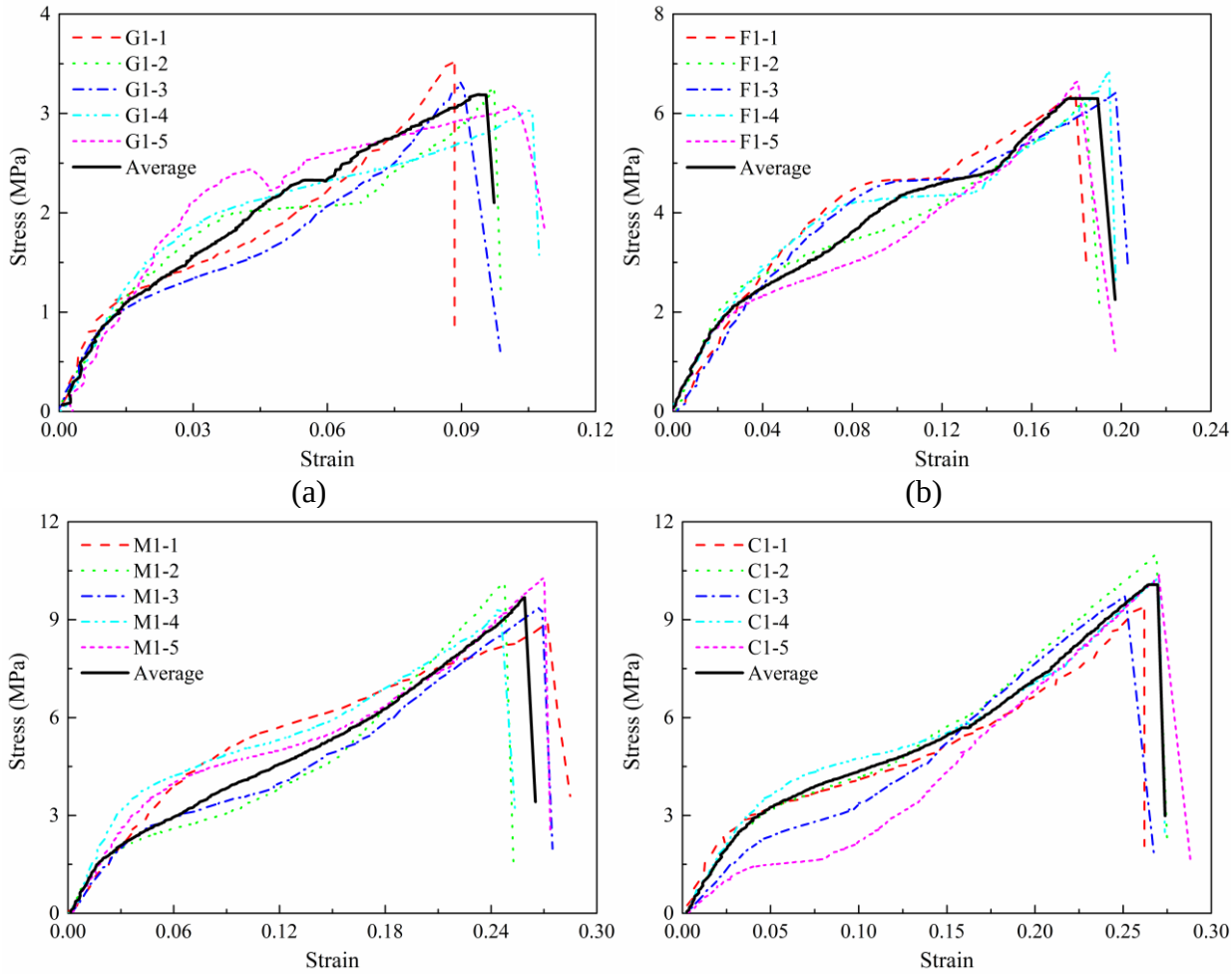

Figure 6. Stress-strain curves for (a) G1, (b) F1, (c) M1, and (d) C1 groups

From Figure 6 ~ 8, the bonding performance of neat epoxy resin can be evaluated by bonding strength and fracture strain. The bonding strength was identified as the peak stress in the stress-strain curves, and the fracture strain was determined as the fracture strain when the joints fractured or failed, with the former describing the ultimate stress and the latter reflecting the fracture strain. Table 4 presents the average bonding strengths and fracture strains as well as corresponding standard deviations for each testing group. Table 4 shows that both surface roughness and bondline thickness had a significant influence on the bonding strength and fracture strain of neat epoxy resin. For the same bondline thickness, the increase of surface roughness

improved the bonding strength and the fracture strain. For a given surface condition, thinner bondlines yielded larger bonding strengths and fracture strains.

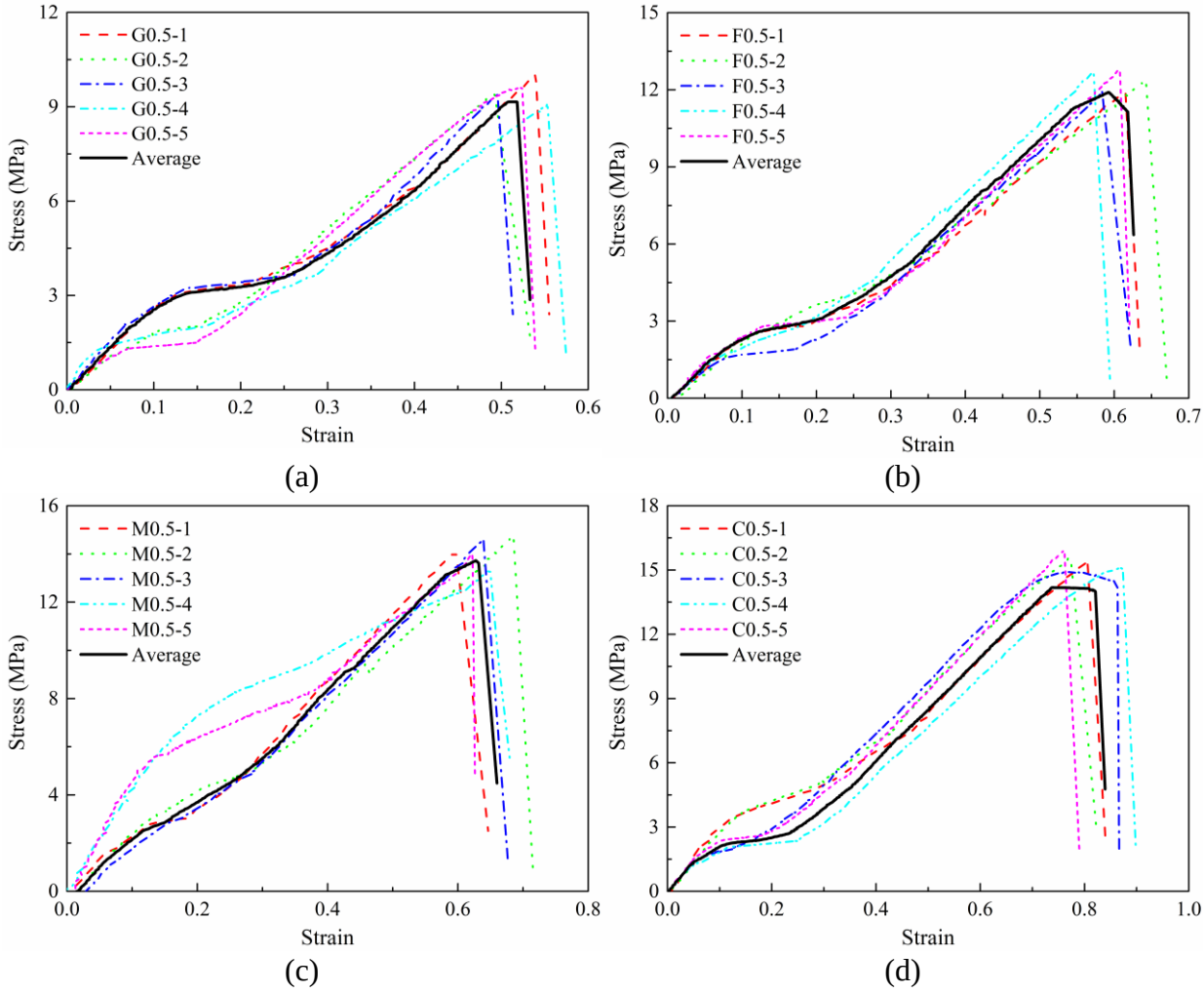

Figure 7. Stress-strain curves for (a) G0.5, (b) F0.5, (c) M0.5, and (d) C0.5 groups

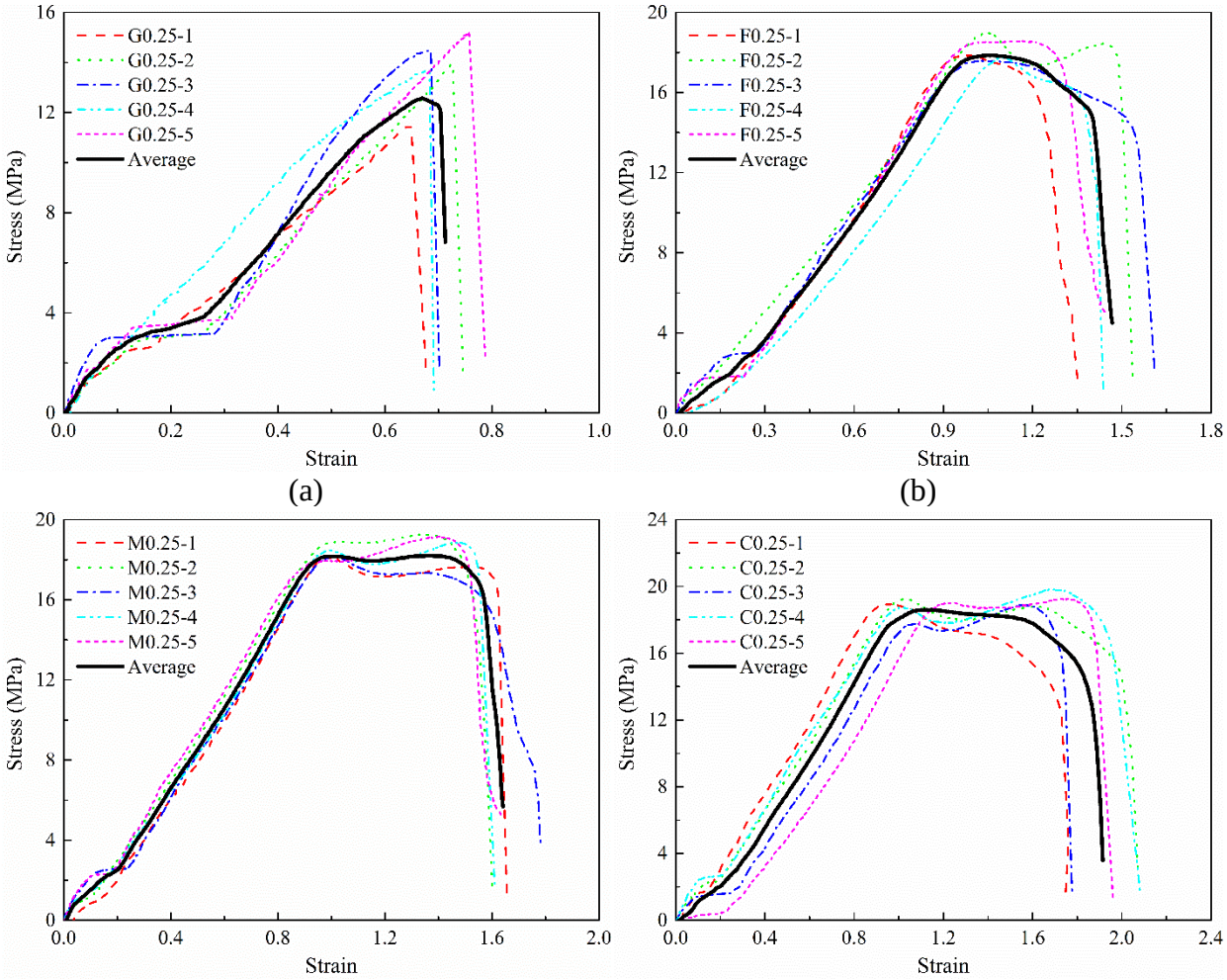

Figure 8. Stress-strain curves for (a) G0.25, (b) F0.25, (c) M0.25, and (d) C0.25 groups

Table 4. Results of SLS tests in Chapter 2

Group No.	R_a (μm)	Bonding strength (MPa)	Standard deviation (%)	Fracture strain	Standard deviation (%)
G1	0.20	3.3 ± 0.4	12	0.100 ± 0.016	16
F1	3.54	6.5 ± 0.4	6	0.188 ± 0.014	7
M1	5.62	9.6 ± 1.1	11	0.268 ± 0.028	10
C1	8.52	10.2 ± 1.1	11	0.273 ± 0.020	7
G0.5	0.20	9.5 ± 0.7	7	0.543 ± 0.046	8
F0.5	3.54	12.4 ± 0.8	6	0.628 ± 0.055	9
M0.5	5.62	14.5 ± 1.1	8	0.669 ± 0.068	10
C0.5	8.52	15.4 ± 0.8	5	0.881 ± 0.103	12
G0.25	0.20	13.8 ± 1.4	10	0.721 ± 0.046	6
F0.25	3.54	18.2 ± 1.1	6	1.476 ± 0.100	7
M0.25	5.62	18.7 ± 0.7	4	1.669 ± 0.074	4
C0.25	8.52	19.2 ± 1.0	5	1.971 ± 0.156	8

2.3. Influences of Surface Roughness and Bondline Thickness

2.3.1. Influence of surface roughness

To further investigate the influence of surface roughness on the bonding performance of neat epoxy resin, Figure 9(a ~ c) illustrates the obtained average stress-strain curves with different surface roughnesses for the bondline thicknesses of 1 mm, 0.5 mm and 0.25 mm, respectively. It is noted that the bonding strength and the fracture strain on rougher substrates were inevitably larger than those on smoother substrates with the same bondline thickness. In the 1 mm and the 0.5 mm thickness groups, although the bonding strength and the fracture strain varied among each stress-strain curve, the shapes of all eight curves were similar regardless of surface roughness. For each individual curve in Figure 9(a) and 8(b), the shear stress increased linearly with the increase of strain, and then dropped sharply after reaching the ultimate stress, resulting in sudden failure. Except for a moderate nonlinearity in C0.5 group, the stress-strain curves for the bondline thicknesses of 1 mm and 0.5 mm were basically linear. The linear pattern was also seen in the G0.25 group shown in Figure 9(c). However, as seen in Figure 9(c), for the rest of three surface conditions, the stress-strain curves showed a different trend after the peak shear stress was attained. For F0.25, M0.25 and C0.25 groups, the stress kept unchanged after reaching the peak while the strain continued to increase, indicating significant nonlinear behaviors. It can also be seen that a higher surface roughness led to greater nonlinearity, which was normally an indication of more plastic deformations. With a combination of thinner bondlines and rougher surfaces, epoxy adhesive joints were expected to induce remarkable large plastic deformations before failure.

Based on Table 4 and Figure 9, Figure 10(a~ c) plots changes of bonding strength and fracture strain with respect to the surface roughness parameter, R_a, for each bondline thickness. In general, both the bonding strength and the fracture strain increased with the increase of surface

roughness. As the surface roughness increased from 0.20 μm on the ground substrate to 3.54 μm on the fine-blasted substrate, significant increases in the bonding performance were observed with increments up to 100% in bonding strength and 105% in fracture strain.

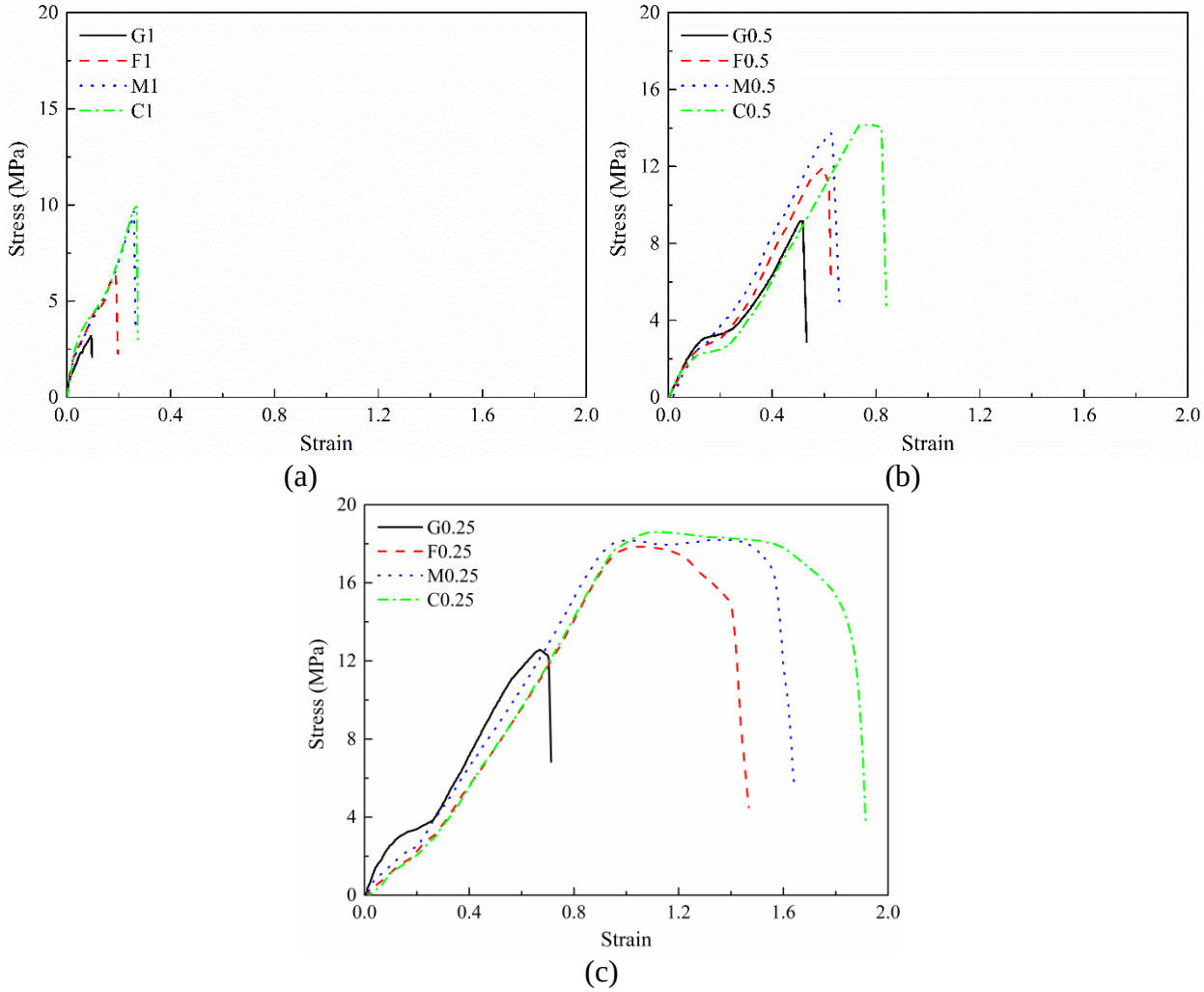

Figure 9. Average stress-strain curves with different surface roughnesses for each bondline thickness: (a) 1 mm; (b) 0.5 mm; (c) 0.25 mm

For epoxy-based composites with bondline thickness of 1 mm, as shown in Figure 10(a), the improvements in both bonding strength and fracture strain were still remarkable when the surface roughness reached 5.62 μm on the medium-blasted substrate, and then become less significant as the roughness increased to 8.52 μm on the coarse-blasted substrate. As shown in Figure 9(b), for epoxy-based composites with bondline thickness of 0.5 mm, the behavior of

fracture strain with surface roughness was slightly different. When R_a increased from 5.62 μm to 8.52 μm, the fracture strain increased substantially with an improvement of about 32%, in comparison to only 2% when bondline thickness was 1 mm. As shown in Figure 10(c), for epoxy-based composites with bondline thickness of 0.25 mm, as the surface roughness changed from 3.54 μm to 5.62 μm and from 5.62 μm to 8.52 μm, the bonding strength remained nearly constant, while the fracture strain increased considerably by about 13% and 15%, respectively. Overall, fine- or medium-blasted steel substrates with the surface roughness around 3.54 ~ 5.62 μm could yielded acceptable bonding behaviors with sufficient bonding strengths and fracture strains.

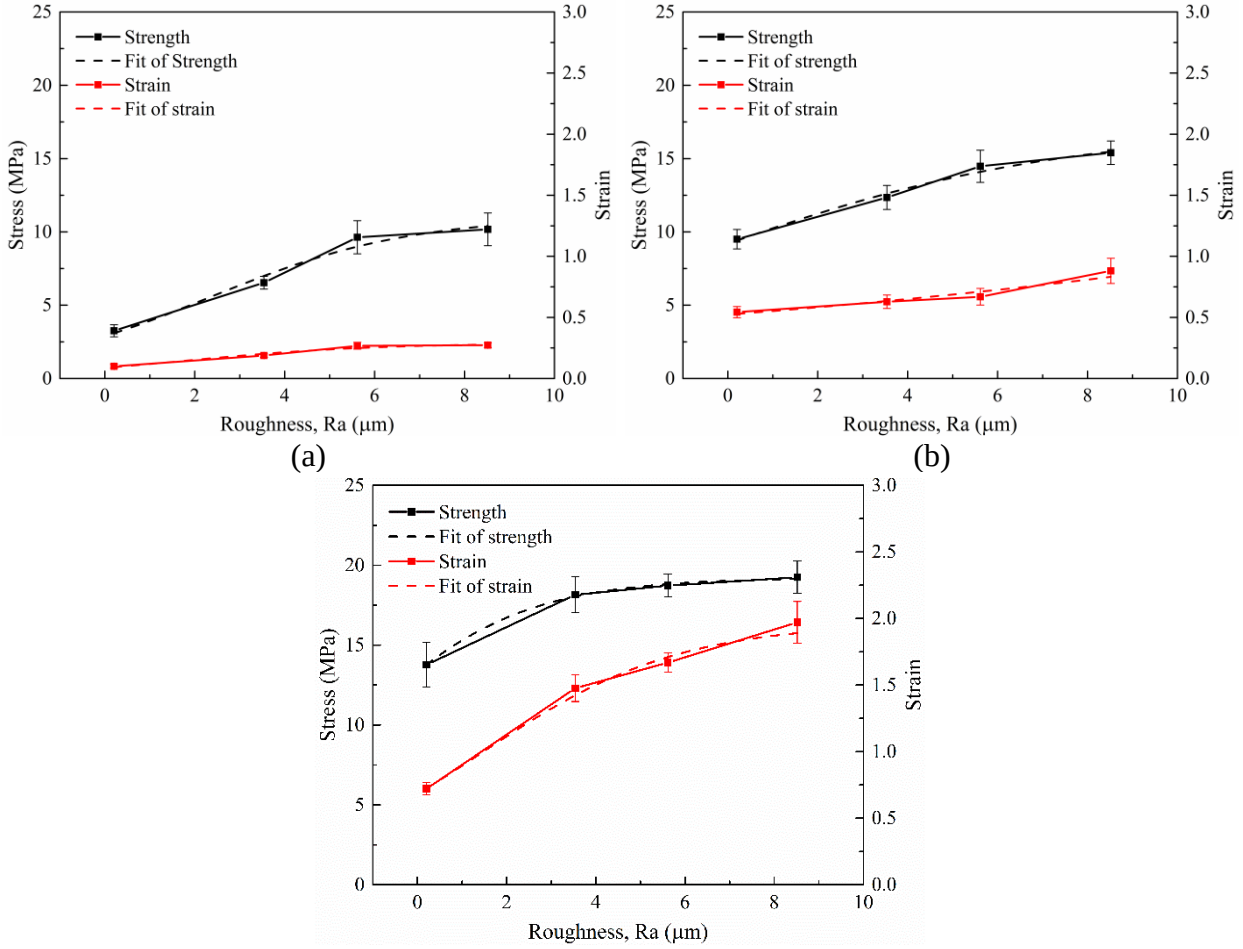

Figure 10. Influence of surface roughness on the bonding strength and the fracture strain with different bondline thicknesses: (a) 1 mm; (b) 0.5 mm; (c) 0.25 mm

Efforts were made to fit the experimentally obtained changes of bonding strength and fracture strain with different surface roughnesses using continuous mathematic functions. Although the fit might not be universally valid, it may provide some useful information on the changes of the bonding performance with any other surface roughness that was not tested in this study. After trying various functions to fit the experimental data, it was found that the S-Shape logistic function achieved the best fitting results. Specifically, the applied S-Shape logistic function followed the Equation (3):

$$y = a/\{1 + \exp[-k(x - x_c)]\} \quad (3)$$

in which a is the curve's maximum value, k is the logistic growth rate or steepness of the curve, and x_c is the value of the sigmoid's midpoint. Table 5 shows the fitted parameters from Equation (3) for all three thicknesses in this chapter. As also shown in Figure 10, all the fitting curves followed similar trends as the original data within the measured standard deviations.

Table 5. Fitting parameter values in Chapter 2

	a	x_c	k	R^2
1 mm Strength	11.07	2.33	0.45	0.989
1 mm Strain	0.29	1.75	0.48	0.990
0.5 mm Strength	17.02	-0.65	0.25	0.998
0.5 mm Strain	0.13	143.16	0.06	0.985
0.25 mm Strength	19.22	-1.52	0.54	0.990
0.25 mm Strain	1.97	1.40	0.45	0.985

To investigate the failure mode of neat epoxy resin with different surface roughnesses, Figure 11(a) shows typical fracture surfaces after SLS tests for epoxy-based composites with thickness of 0.5 mm on ground surfaces (G0.5 group), and Figure 11(b) shows the SEM image of the typical bottom surface of such epoxy adhesive joints under 50 μm magnification. As seen in Figure 11(a), on the ground substrate, the epoxy bondline delaminated from the steel substrate. All the epoxy adhesive was attached only on the top surface of the joint, and no noticeable cracks or ruptures developed inside the bondline. It was further proved in the SEM image in Figure 11(b),

no sign of epoxy was found on the bottom surface after fracture, indicating a typical interfacial adhesion failure. Since the ground surfaces were so smooth and flat, there were no deep cavities or pits existed for epoxy resin to flow into. Therefore, the epoxy was less likely to penetrate into the substrate, which led to the weak bonding performance of the epoxy adhesive joints.

For coarse-blasted substrates, Figure 11(c) illustrates the typical fracture surfaces after SLS tests for epoxy-based composites with thickness of 0.5 mm on coarse surfaces (C0.5 group), and Figure 11(d) shows the SEM image of the typical bottom surface of such epoxy-based composites under 50 μm magnification. Figure 11(c) illustrates that adhesion failure was also the dominant failure mode on the coarse-blasted substrate. No recognizable epoxy remained on the bottom surface of the joint either. However, it was evident in Figure 11(d) that some epoxy was locked into the pits and cavities on the coarse-blasted substrate created by grit blasting. While comparing Figure 11(b) and 11(d), no obvious epoxy remained on the ground substrate, but significant amounts of epoxy remained on the coarse-blasted substrate. Higher humps and deeper cavities on rougher surfaces could also create more contact areas between the adhesive and the substrate than on smoother surfaces, which also contributed to the better bonding performance of the epoxy adhesive joints.

2.3.2. Influence of bondline thickness

By comparing the bonding strength and the fracture strain of different bondline thicknesses with the same surface roughness as displayed in Table 4 and Figure 9, it was noted that bondline thickness had a strong influence on the bonding performance of neat epoxy resin. The bonding strength and the fracture strain increased significantly as the bondline thickness decreased from 1 mm to 0.25 mm. Especially on ground substrates, when compared to 1 mm thick epoxy bondlines, 188% improvement in bonding strength and 445% enhancement in fracture strain were achieved

with the bondline thickness of 0.5 mm. Moreover, when the bondline thickness further decreased to 0.25 mm, the improvements were enlarged to 322% and 659%, respectively.

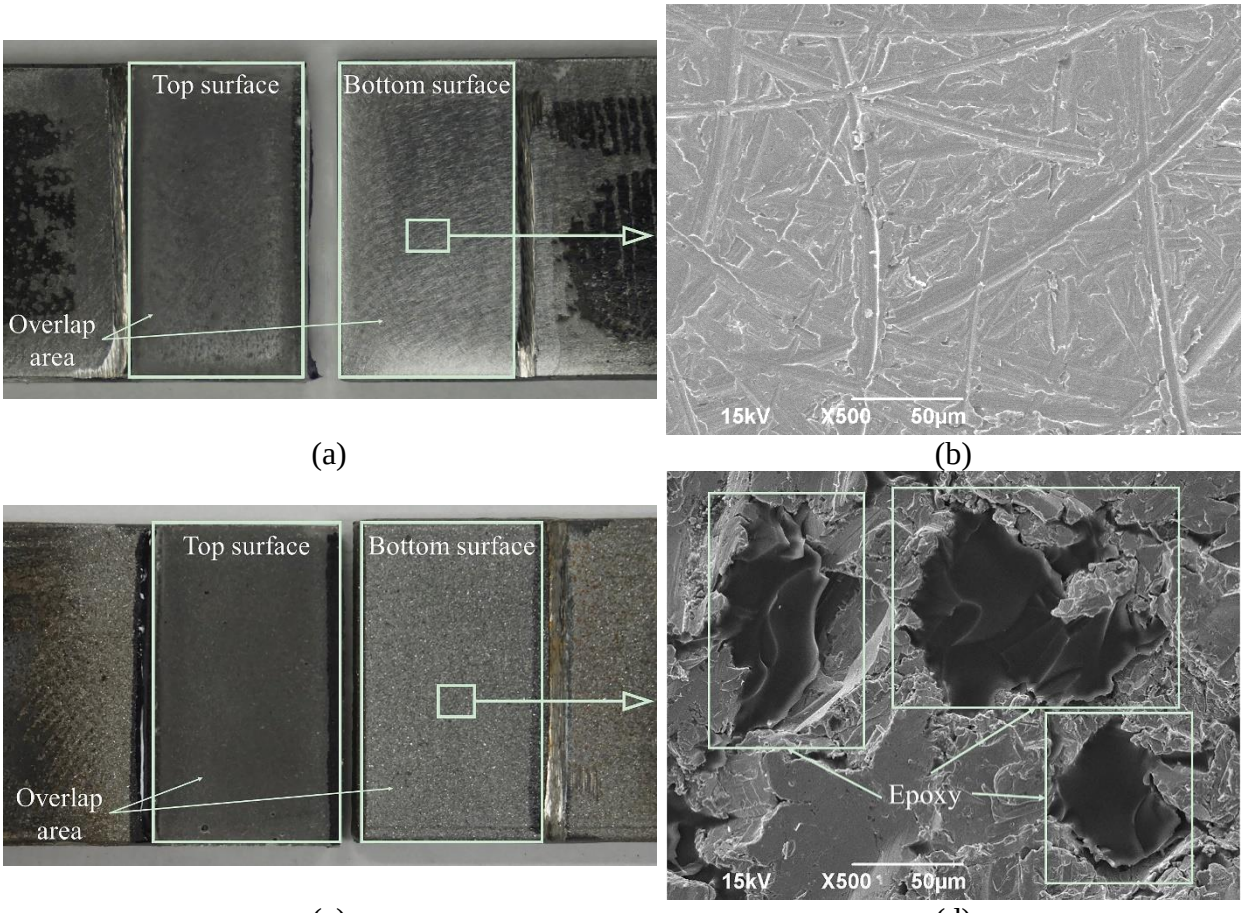

Figure 11. (a) Fracture surfaces and (b) SEM image of bottom surface under 50 μm magnification in G0.5 group; (c) fracture surfaces and (d) SEM image of bottom surface under 50 μm magnification in C0.5 group

In addition to bonding strength and fracture strain, the area under the stress-strain curves in Figure 9 reflects the toughness, which is the ability of the material to consume energy and deform plastically before fracture. Figure 9 shows that for all testing groups, the stress-strain curves became appreciably extended as the bondline thickness decreased. Figure 12 compares the toughness of neat epoxy resin with different bondline thicknesses. It could be seen clearly that the reduction of bondline thickness from 1 mm to 0.25 mm tremendously increased the toughness of epoxy-based composites when the same surface treatments were applied. Although the increases

of bonding strength become relatively limited on high-roughened surfaces, the increments of toughness were still as high as 303% and 302% from the bondline thickness of 1 mm to 0.5 mm and from 0.5 mm to 0.25 mm respectively, which was mainly due to the massive improvement of fracture strain. The enhanced toughness induced by increased plastic deformation was noted to be a major reason for the significant improvement of fracture strain with thinner epoxy adhesives.

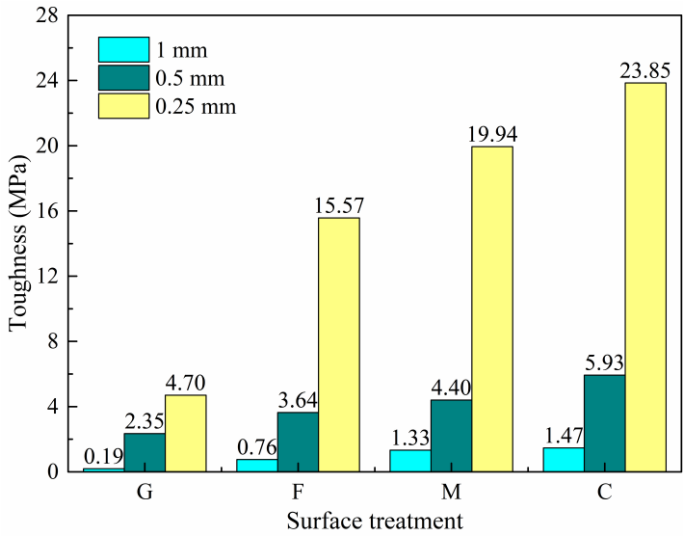

Figure 12. Comparisons of the toughness with different bondline thicknesses

Figure 13 only shows typical failure surfaces of neat epoxy resin with 0.25 mm bondline thickness, since the fracture surfaces of epoxy-based composites with 1 mm bondline thickness were very similar to those with 0.5 mm bondline thickness. As shown in Figure 11(a) and 13(a), on ground substrates, adhesion failure occurred for epoxy-based composites with the bondline thickness of both 0.25 mm and 0.5 mm. There was no pronounced difference of the surface conditions between those two different thick bondlines. However, better bonding performance was noted for epoxy-based composites with the bondline thickness of 0.25 mm, as seen in Table 4.

Fracture surfaces of neat epoxy resin with 0.25 mm bondline thickness on coarse-blasted substrates were totally different as shown in Figure 13(b). Compared with Figure 11(c), no visible epoxy remained the bottom surface, so the failure mode for the 0.5 mm thick bondlines was still

dominated by adhesion failure. However, as seen in Figure 13(b), when the bondline thickness was decreased to 0.25 mm, the epoxy adhesive was separated into two parts by a clear major crack occurred in the middle of the bondline, and the two parts remained on both surfaces of the sample separately. Although adhesion failure still existed on a large part of the bondline area for the 0.25 mm thick samples, the cracking area belonged to the cohesion failure, and the overall failure mode could be regarded as a combination of both two failure modes, which was more favorable than the complete adhesion failure. Furthermore, it was noticed that an evident discoloration took place inside the bondline layer as seen in Figure 13(b). Part of the epoxy was whitened in comparison with the rest, which was induced by the plastic behavior of epoxy resin. Higher surface roughness and thinner bondline thickness elevated the shear capacity and the toughness of the epoxy, which increased the capacity for the epoxy to deform plastically. Since the stress concentration always occurs in irregularities, the plasticity tends to happen near the edge of the overlap area at first. As the load continued to increase, more plastic deformations were generated, and the plastic zone spread from the edge toward the middle of the bondline, resulting in the large stress-whitened area indicted in Figure 13(b) [30,87].

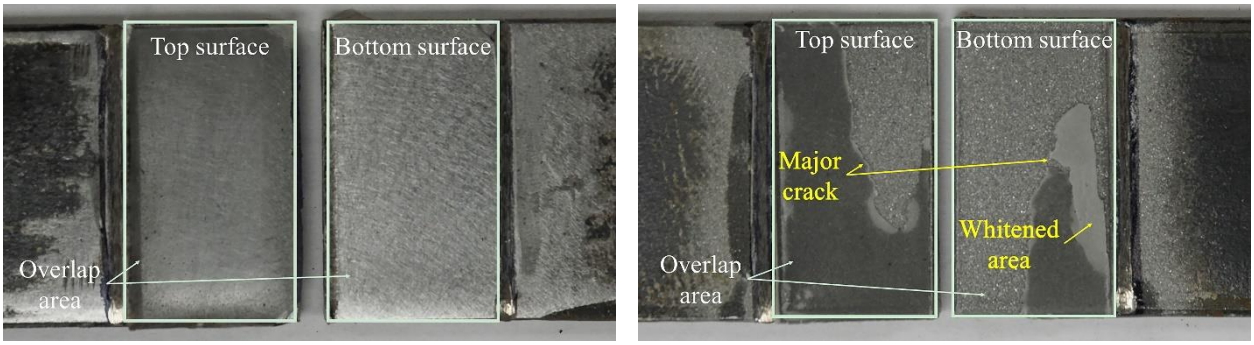

(a) (b)

Figure 13. Typical failure surfaces: (a) 0.25 mm ground samples and (b) 0.25 mm coarse-blasted samples

To further study the influence of bondline thickness as well as the plastic behavior of neat epoxy resin on the coarse-blasted substrate as shown in Figure 11(c) and Figure 13(b), SEM

analyses were conducted on the top surface of the 1 mm coarse-blasted sample, on non-whitened and the whitened areas of the 0.25 mm coarse-blasted sample, which are shown in Figure 14(a, c), respectively. As demonstrated in Figure 14(a, b), the fracture surface roughness on non-whitened area of 0.25 mm sample with more hill-, ridge- and valley-patterns, was much higher than that of 1 mm sample. The rougher fracture surfaces of the plastically deformed epoxy implied higher energy dissipation as a result of the enhanced toughness of the epoxy adhesive with the thinner bondlines. By comparing non-whitened and whitened areas in Figure 14(b, c), the surface morphology of the whitened area was apparently more featured and complex than that of the non-whitened area, revealing that more plastic deformations actually happened within the stress-whitened area of the 0.25 mm sample.

On the other hand, Figure 15(a, b) shows the SEM images of the major crack which was shown in Figure 13(b). Along the major crack, there were several voids inside the epoxy bondline, which could be air bubbles introduced during the process of mechanical mixing or some defects initiated during the curing process. It was also noted that the exposed epoxy interface was pretty smooth without any wrinkles as shown in Figure 15, indicating the rapid growth of the major crack with little energy consumption and plastic deformation. Porosity and number of voids are regarded as a critical reason for the weaker bonding performance of thicker epoxy bondlines [35,88]. Because cracks are prone to grow in the weakest path through voids, and thicker bondlines have more voids for the cracks to grow [89]. Although a lot of plastic deformations was generated, before the plastic zone covering the entire bondline area, the major crack penetrated the epoxy adhesive vertically through those voids and caused catastrophic rupture. Thus, a complete cohesion failure is more likely to happen when the bondline is uniformly distributed and free of any type of

imperfections. Under this circumstance, the plastic zone would possibly reach the end of the overlap area and the failure would occur within the epoxy adhesive layer.

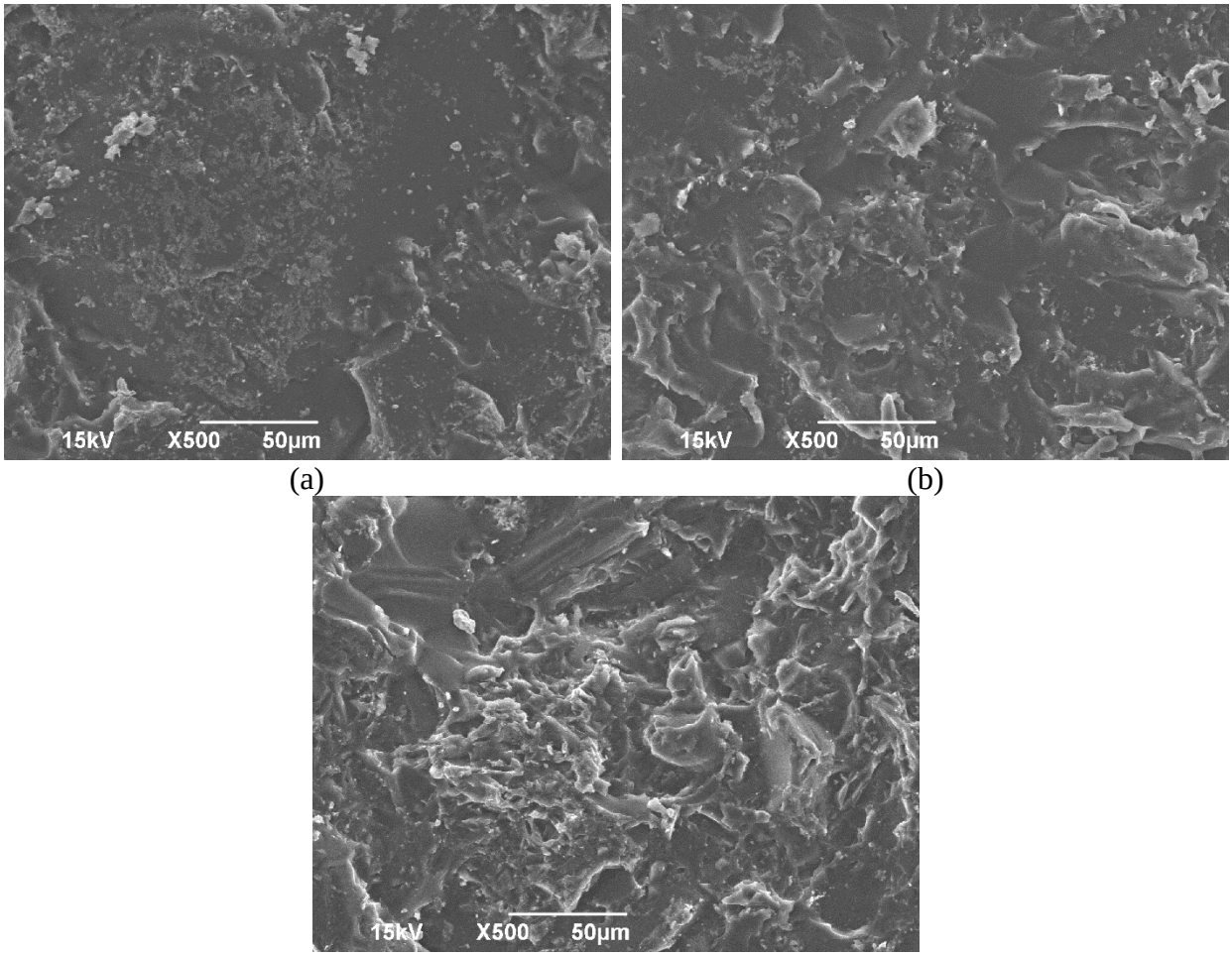

(a) (b)

(c)

Figure 14. SEM images of the fracture surfaces on the coarse-blasted substrate under 50 µm magnification: (a) top surface of the sample with 1 mm bondline thickness; (b) non-whitened area; and (c) whitened area of the sample of with 0.25 mm bondline thickness

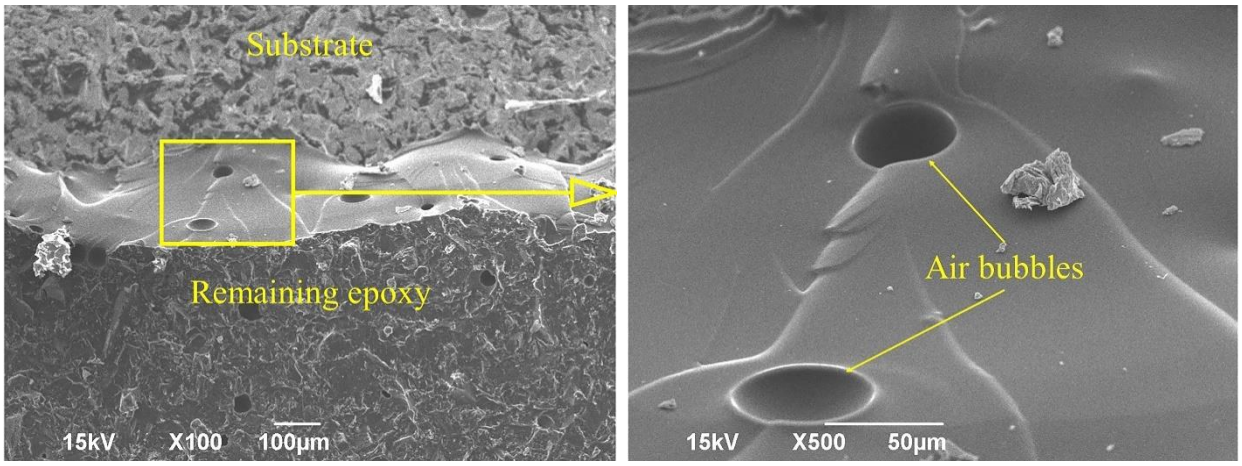

(a) (b)

Figure 15. SEM images of the major crack of 0.25 mm coarse-blasted sample: (a) under 100 μm magnification; (b) under 50 μm magnification

2.4. Summary

This chapter investigated the influences of surface roughness and bondline thickness on the bonding performance between epoxy resin and mild steel substrates. Based on the systematic experimental studies performed, the following general conclusions can be drawn:

1) Both bonding strength and fracture strain (fracture strain) of neat epoxy resin improved logistically with the increase of surface roughness on steel substrates. The influence of surface roughness was more significant on smoother substrates and became less efficient on over-roughing substrates.

2) Thinner bondlines provided better bonding performances in both bonding strength and fracture strain than thicker bondlines. The fracture strain of the epoxy adhesive on ground substrates could improve more than 400% when bondline thickness decreased from 1 mm to 0.5 mm and more than 600% for the reduction from 0.5 mm to 0.25 mm.

3) The reduction of bondline thickness could greatly improve the toughness of epoxy-based composites, resulting in more plastic deformations which were indicted in the stress-whitened area and rougher fracture surfaces (as shown in SEM images). The rapid crack growth with less energy

dissipation efficiency might have led to the premature adhesion fracture before a complete cohesion failure could occur.

4) Increasing the surface roughness or reducing the bondline thickness might be insufficient to completely modify the failure mode of neat epoxy resin, but a partial cohesion failure could be achieved on highly rough substrates (coarse-blasted) with thinner bondline thicknesses (0.25 mm).

Although a general-purpose epoxy resin was chosen as the epoxy adhesive with relatively large roughness and thickness ranges, the conclusions above might still not be universally valid because of the property differences among different types of epoxy resin or limited roughness or thickness ranges. However, this study could provide a general guidance on the investigation of the bonding performance of neat epoxy resin with different surface roughnesses and bondline thicknesses.

CHAPTER 3. INFLUENCES OF SURFACE ROUGHNESS ON THE BONDING PERFORMANCE OF CNT REINFORCED EPOXY COMPOSITES

Based on the findings in Chapter 2, this chapter systematically investigated the bonding performance of CNTs reinforced epoxy-based composites with four different surface roughnesses using SLS tests. Both bonding strength and fracture strain of epoxy-based composites were considered for bonding performance analysis. The surface morphology of the substrate before and after fracture was characterized using SEM image analysis to understand the reinforcing mechanisms of CNTs, and the wettability of water, neat epoxy and CNT reinforced epoxy droplets on four different substrates was also measured by the contact angle tests to evaluate the interfacial adhesion of each material on each surface roughness. In addition, a statistical analysis was performed on the experimental data to estimate the bonding strength and fracture strain of CNT reinforced epoxy composites under various surface roughnesses. Although the estimation may not be universal valid, it may provide some useful information on the bonding performances of CNT reinforced epoxy composites with any other surface roughness that was not tested in this study to cover a wide roughness range.

3.1. Experimental Setup

3.1.1. Materials

The steel substrate was still low carbon A36 steel, while the epoxy matrix used in this chapter was still the general-purpose epoxy resin. For the CNT reinforced epoxy composites, multiwalled carbon nanotubes with purity higher than 95%, diameter ranging from 50 nm to 100 nm, and length ranging from 5 μm to 20 μm length (supplied by Skyspring Nanomaterials Inc.) were used as CNTs reinforcement to modify neat epoxy resin. For the weight fraction of CNTs in

epoxy-based composites, literatures showed that the bonding strength of CNT reinforced epoxy composites would increase with higher CNTs weight fraction till a certain percentage followed by a decrease after that [52], and 0.75% by weight to the epoxy matrix was found to be the optimal CNTs percentage [51,56]. Therefore, in this chapter, to fabricate the CNT reinforced epoxy composites, 0.75% CNTs by weight were added into the epoxy and the mixture was mechanically stirred for 5 min, followed by ultrasonic mixing for 15 min to better disperse the CNTs into the epoxy matrix.

3.1.2. Surface preparation and roughness measurements

Surface preparation procedures are still the same as described in the last chapter, including the smooth, fine, medium, and coarse surface conditions. Right after all the surface treatments, the surface roughness of the steel substrates was measured using an PCE-RT 1200 roughness tester (supplied by PCE Instruments) following the ASTM D7127-17 standard. Three same roughness parameters (Rz, Ra, Rt) were also collected to evaluate the surface roughness. In addition, the surface morphology of the substrates with different roughness levels was also studied using the SEM image analysis.

3.1.3. Contact angle tests

Since the wettability of the steel substrates is an essential surface characterization for the bonding performance of epoxy-based composites, this chapter also studied the wettability of the steel substrates with different surface roughness using the contact angle tests. In total, twelve different combinations of contact angle tests from four different surface roughness levels (smooth, fine, medium, and coarse conditions) and three different liquid materials (water, neat epoxy, and CNT reinforced epoxy) were performed. Water droplets were used to estimate the surface energy which is a substantial property of different substrates, while neat epoxy resin and CNT reinforced

epoxy composites were used to evaluate their wettability on all the four different substrates. The contact angle tests were carried out by the FTA1000 Drop Shape Instrument B Frame Analyzer System (supplied by First Ten Angstroms, Inc.) following the ASTM D7334-08 standard. To be statistically valid, three drops of each liquid were placed on each substrate and two angle measurements were made on each edge of the droplets within 30 seconds after depositing the droplet.

3.1.4. SLS tests

The bonding performances of all epoxy-based composites was studied by SLS tests. The SLS test specimens were also designed according to the ASTM D3165-07 standard as shown in Figure 16. The bondline thickness in this chapter was controlled to be around 0.5 mm by using steel shims. Table 6 shows the test matrix for SLS tests. Eight testing groups were prepared, including two different adhesive materials (both neat epoxy and CNT reinforced epoxy composites) and four different surface roughnesses (smooth, fine, medium, and coarse levels). For each testing group, five valid specimens were made, resulting in a total of 60 specimens. The loading machine, testing procedures as well as load-displacement to stress-strain curves conversion are the same as described in the last chapter.

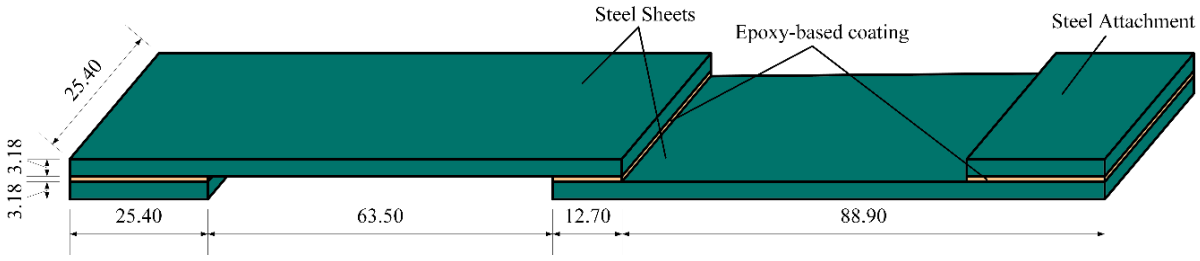

Figure 16. The detailed SLS specimen configuration (unit: mm)

Table 6. SLS test matrix in Chapter 3

Testing group	Specimen quantity	Surface roughness	Coating thickness	Coating material
SE	5	Smooth	0.5 mm	Epoxy
FE	5	Fine	0.5 mm	Epoxy
ME	5	Medium	0.5 mm	Epoxy
CE	5	Coarse	0.5 mm	Epoxy
SC	5	Smooth	0.5 mm	CNT reinforced epoxy
FC	5	Fine	0.5 mm	CNT reinforced epoxy
MC	5	Medium	0.5 mm	CNT reinforced epoxy
CC	5	Coarse	0.5 mm	CNT reinforced epoxy

3.2. Experimental Results

3.2.1. Surface characterizations

The average surface roughness (Ra) of the four different roughness levels of smooth, fine, medium, and coarse conditions achieved in this chapter, were 0.231 μm, 3.528 μm, 5.272 μm, and 8.457 μm, respectively. As expected, the surface roughness increased remarkably with higher roughness levels which were resulted from smaller girt size. The surface characterizations of the steel substrates can also be observed visually by surface morphology from the SEM analysis. Figure 17(a ~ d) show the SEM images of the four roughness levels at a magnification of 100X. The ground surface at the smooth roughness level was observed to be remarkably flat with minor interfacial scratches. The surface of the substrate at the fine level of roughness was densely filled with small bumps and holes, while at the medium roughness level the surface was majorly full of small irregularities except a few higher hills and deeper valleys and the coarse surface was clearly filled with more clearly visible hills and valleys. Higher bumps and deeper holes magnified the height difference of the profile leading to higher roughness values.

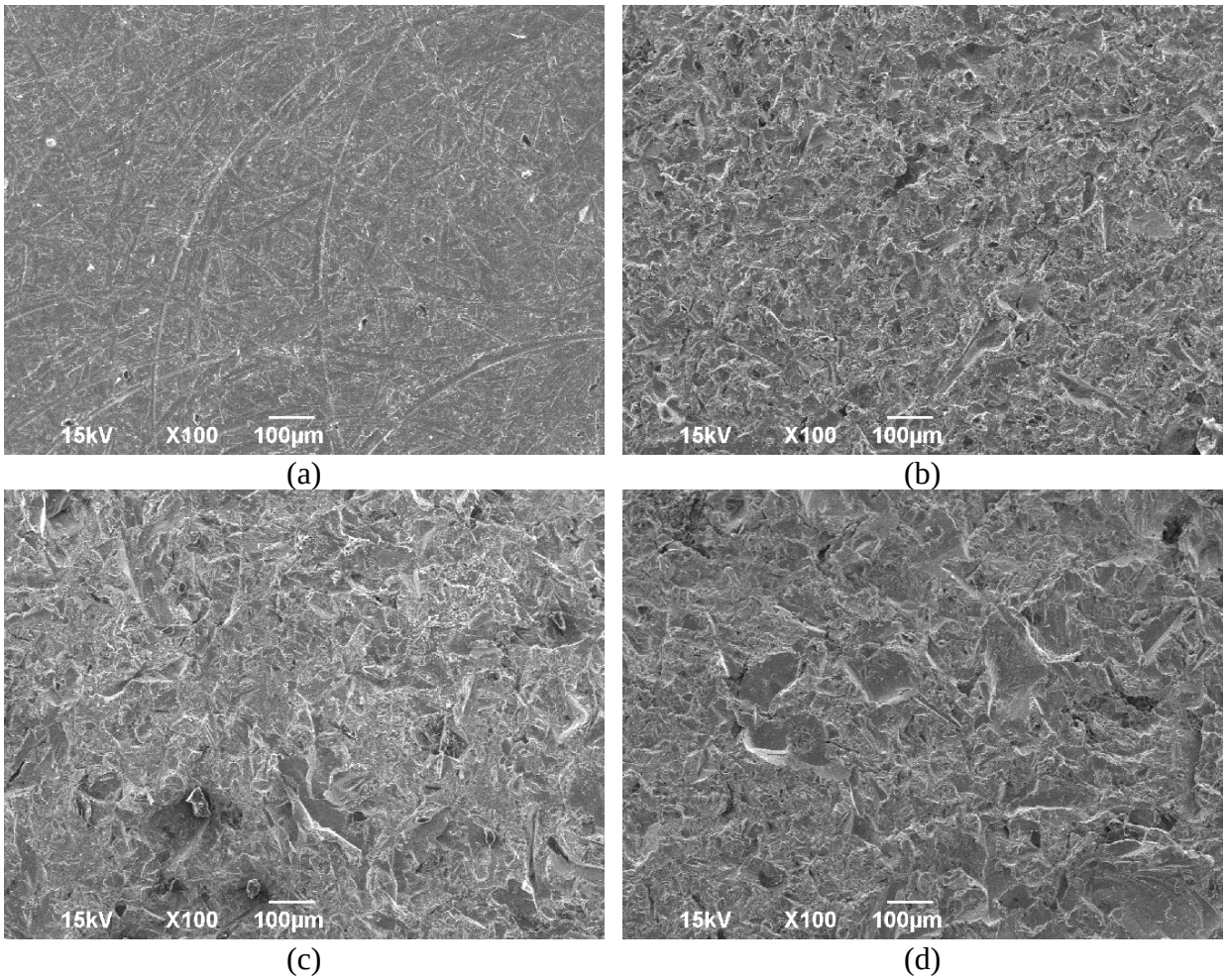

(a) (b)

(c) (d)

Figure 17. SEM images of steel substrates of four roughness levels at a magnification of 100X: (a) smooth; (b) fine; (c) medium; and (d) coarse substrates

For the wettability test results from the contact angle tests, Figure 18(a ~ d) show the typical appearances and contact angles of water droplets on four substrates with different roughness. Although all the four contact angles were less than 90º, indicating that all four substrates belonged to hydrophilic surfaces, the variation of the contact angles with four surface roughness levels shared the same trend as the roughness values increased. The contact angle of the smooth substrate was 74.72º which was apparently larger than those on the other substrates. Contact angles were noticed to be reduced from fine to medium and coarse substrates, of 59.84º, 55.67º and 48.11º, respectively. A smaller contact angle of water droplets with higher surface roughness indicated a higher wettability. Since the rougher substrates could have higher surface energy and more contact

areas for the coating materials to contact with, epoxy-based coatings on rougher substrates were expected to have better bonding performance than on smoother substrates.

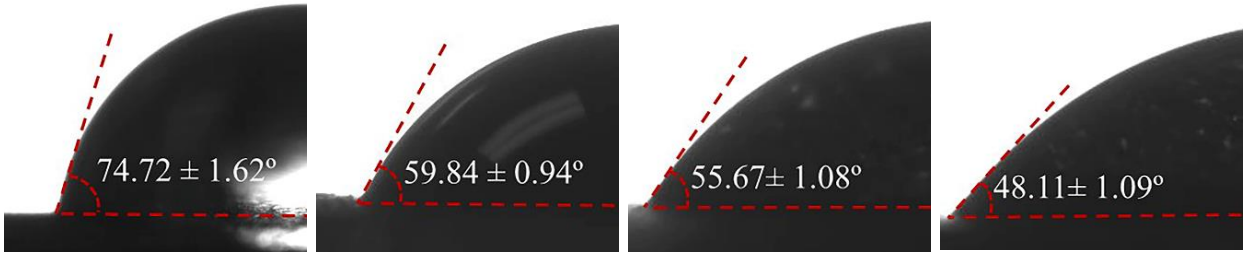

(a) (b) (c) (d)

Figure 18. Contact angles of water droplets on four different roughness substrates: (a) smooth; (b) fine; (c) medium; and (d) coarse substrates

3.2.2. SLS test results

Figure 19(a, b) plot all the average stress-strain curves of neat and CNT reinforced epoxy composites with regard to the four different surface roughness. Figure 19(a) shows that the stress and strain of neat epoxy resin exhibited evident linear relationship until a sudden failure occurred at the peak stress, regardless of the surface roughness levels. As for the CNT reinforced epoxy composites, similar to those of neat epoxy resin, the stress-strain curves went up approximately linearly before peak stress. But after the peak stress, only the curves of smooth surfaces followed the same pattern as the neat epoxy resin ended with a sudden failure. The curves of the rest three rougher surfaces dropped gradually from the peak stress to the failure, indicating an obvious nonlinear behavior. The three curves of CNT reinforced epoxy composites on the rougher surfaces showed typical stress-strain relation as for ductile materials with strain continually growing at a relatively stable stress level rather than a sharp failure for brittle materials. The nonlinearity illustrated in the curves was an indication of the plastic behavior of epoxy-based composites with the addition of CNTs on the rougher steel substrates.

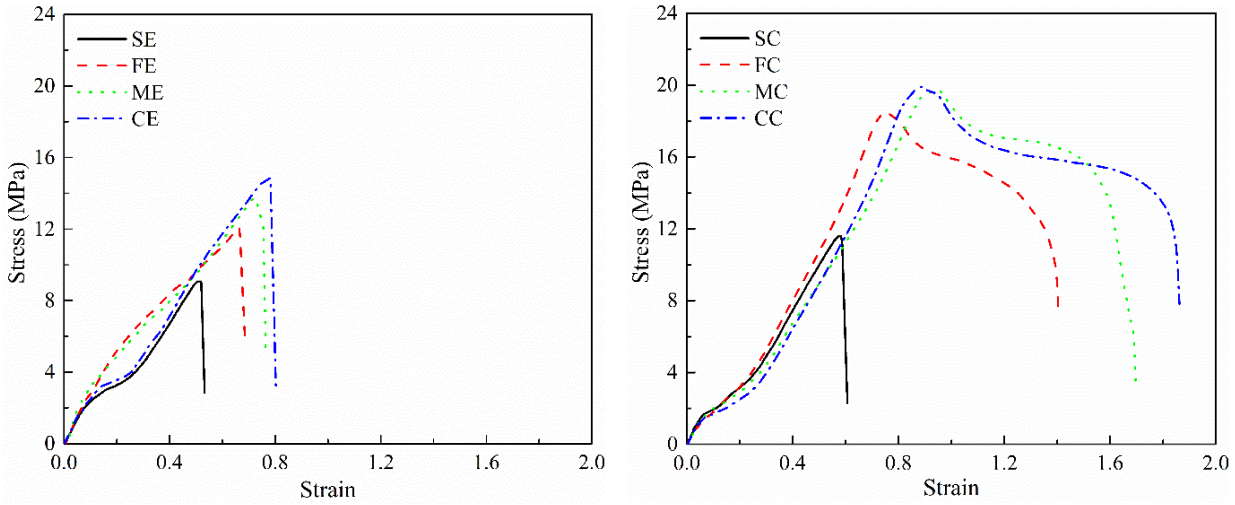

(a) (b)

Figure 19. Average stress-strain curves with different surface roughness: (a) the neat; and (b) the CNT reinforced epoxy composites

The average bonding strength and fracture strain were compared in details as shown in Table 7 for all eight testing groups. The bonding strengths were determined as the peak shear stresses from the stress-strain curves and the fracture strains were reflected by the fracture strains, which was identified as the strains when the curve experienced a rapid stress drop. As shown in Table 7, almost all the STDs in one testing group were smaller than 10% for both bonding strength and fracture strains, suggesting the consistency of the SLS tests.

Table 7. Results of SLS tests in Chapter 3

Group	Surface roughness, Ra (μm)	Bonding strength (MPa)	STD (%)	Fracture strain	STD (%)
SE	0.231	9.455± 0.699	7.39	0.534 ± 0.042	7.87
FE	3.528	12.234 ±0.765	6.25	0.692 ± 0.059	8.53
ME	5.272	14.764 ± 0.801	5.43	0.766 ± 0.068	8.88
CE	8.457	15.145 ± 0.776	5.12	0.805 ± 0.081	10.00
SC	0.231	11.595 ± 0.204	1.76	0.607 ± 0.031	5.11
FC	3.528	18.573 ± 0.409	2.20	1.416 ± 0.042	2.97
MC	5.272	19.475 ± 0.545	2.80	1.702 ± 0.100	5.88
CC	8.457	20.057 ± 1.053	5.25	1.876 ± 0.117	6.24

3.3. Data Analysis and Discussion

3.3.1. Influence of the addition of CNTs in epoxy-based composites

Figure 20(a, b) illustrate the bar chart comparison of bonding strength and fracture strain between the neat and CNT reinforced epoxy composites. The addition of CNTs (0.75%) showed greatly improvements of boning performances in both the bonding strength and fracture strain, but the improvements varied with different surface roughness levels. On the smooth substrate, compared to neat epoxy, the addition of CNTs increased the bonding strength and fracture strain by around 56% and 84%, while on the fine surfaces, while the enhancements of bonding strength and fracture e strain by adding CNTs were much more significant by around 123% and 382%, respectively. On the medium and coarse substrates, the enhancement of bonding strength by CNTs were around 70% compared to neat epoxy, but the CNTs reinforcement in epoxy improved the fracture strain significantly by around 280%. It is also worth mentioning that the increments in fracture strain were much more pronounced than those in bonding strength, which was largely due to the plastic deformation created by CNT reinforced epoxy composites.

Figure 20(c) demonstrates the toughness of the neat and CNT reinforced epoxy composites with the four different surface treatments. The toughness is defined as the ability of deforming plastically and absorbing energy before fracture, which could be evaluated by the area under the stress-strain curve as in Figure 15. From Figure 20(c), it can be seen that the CNTs in epoxy only increased the toughness slightly on the smooth substrate, but greatly on the other three rougher substrates. As a result of higher toughness, the CNT reinforced epoxy composites generated more plastic deformation resulting in higher increases in fracture strain and smaller increases in bonding strength, compared to neat epoxy.

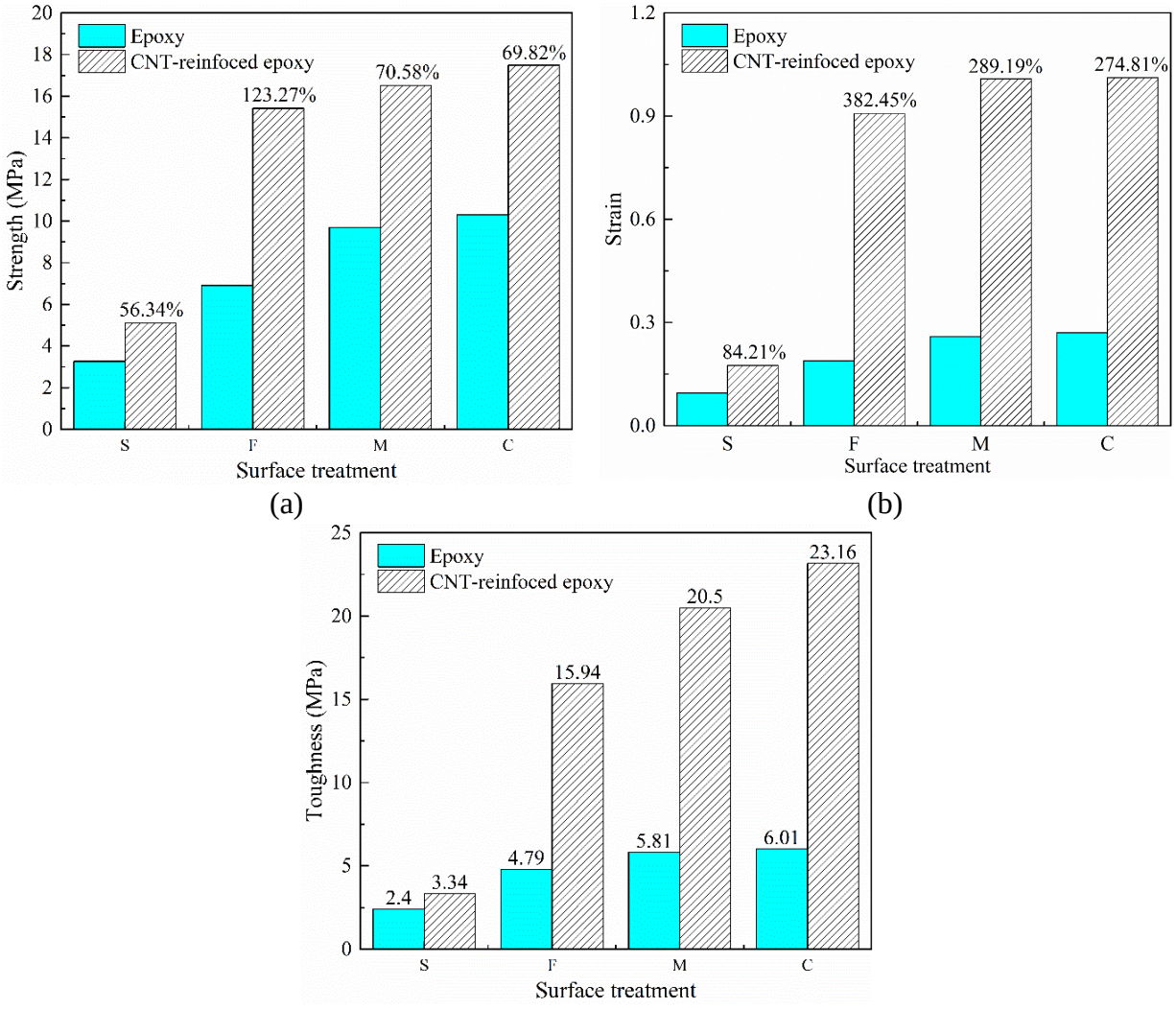

Figure 20. Increments between the neat and the CNT reinforced epoxy coatings: (a) bonding strength; (b) fracture strain; and (c) toughness

Figure 21(a, b) illustrate the typical fracture surfaces of SLS specimens with or without CNTs on the smooth substrates. No obvious differences were observed on the fracture surfaces between the neat and CNT reinforced epoxy composites on the smooth substrates. Both composites had fractures occurred at the adhesive-substrate interfaces with all the composites attached on the bottom surfaces of the specimens and no visible epoxy remaining on the other side, indicating a typical adhesive failure. For an adhesive failure, the interfacial adhesion instead of the adhesive mechanical properties played the dominating role for the bonding performance. Only the

composites near the adhesive-substrate interface contributed to the bond, while the rest large part of the composites did not contribute a lot to the bond before the catastrophic failure occurred on the interface. Therefore, on the smooth substrates, increasing the mechanical properties of epoxy-based composites (such as toughness) by adding CNTs had little influences on the failure mode. Although the failure modes remained the same for both the neat and CNT reinforced epoxy composites on smooth substrates as indicated in Figure 21, the bonding strengths and fracture strains of the CNT reinforced epoxy coatings on smooth surfaces were still moderately improved compared to CNT reinforced epoxy composites as shown in Figure 20(a, b). The resulted increases on the bonding performance might be benefited from the improvement of the interfacial adhesion between the adhesive and the substrates with the addition of the CNTs.

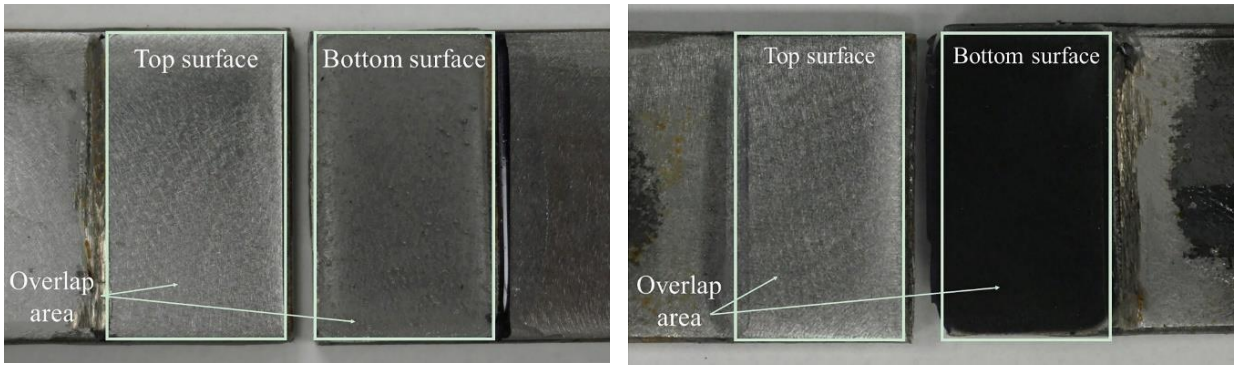

(a) (b)

Figure 21. Typical fracture surfaces on smooth substrates: (a) the neat; and (b) the CNT reinforced epoxy composites

To study the CNTs contributions to the interfacial adhesion between epoxy-based composites and steel substrates, Figure 22(a ~ h) display the contact angles of the neat and CNT reinforced epoxy composites on the steel substrates with the four different surface roughness levels. The contact angles on smooth substrates decreased from 53.42º for neat epoxy resin to 52.13 º for CNT reinforced epoxy composites, and similar reductions in contact angles were also observed in the other three rougher substrates, indicating a higher wettability by the CNTs reinforcement. Higher wettability by the addition of CNTs could increase the contact area between

CNT reinforced epoxy composites and the substrates. In addition, the epoxy which flowed into the irregularities of the substrate was also reinforced by the CNTs, which enhanced the connection of the epoxy and the substrate as well. The reductions of the contact angle for the CNTs reinforcement in epoxy-based composites confirmed with the findings from failure mode analysis in Figure 21(a, b) that the CNTs could improve the interfacial adhesion between the coatings and substrates, resulting in the improvements in the bonding performances as shown in Figure 20(a, b).

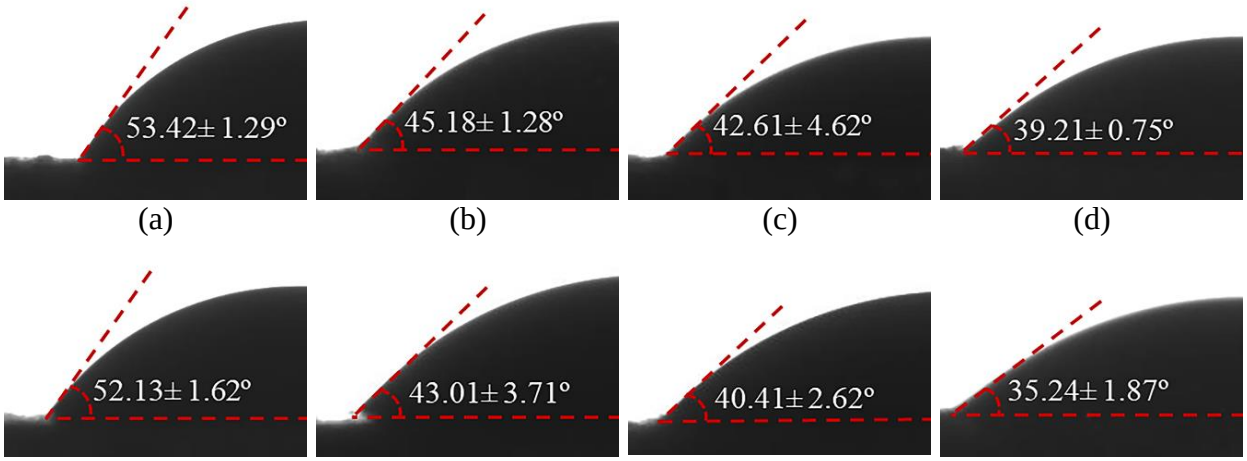

Figure 22. Contact angles of the neat and CNT reinforced epoxy droplets: (a) neat epoxy on the smooth substrates; (b) neat epoxy on the fine substrates; (c) neat epoxy on the medium substrates; (d) neat epoxy on the coarse substrates; (e) CNT reinforced epoxy on the smooth substrates; (f) CNT reinforced epoxy on the fine substrates; (g) CNT reinforced epoxy on the medium substrates; and (h) CNT reinforced epoxy on the coarse substrates

Figure 23(a, c) compare the overlap areas of the neat and CNT reinforced epoxy composites on coarse substrates after SLS tests. For the neat epoxy resin, similar as the fracture surfaces on the smooth surfaces, there was no sign of epoxy left on the top surface and all the epoxy-based composites on the bottom surface was free of any noticeable scars or cracks as shown in Figure 23(a), indicating that the adhesive failure was the dominant failure mode on the coarse substrates as well. However, for the CNT reinforced epoxy composites, as shown in Figure 23(c), a main crack was found in the middle of the coating and the coating material was left on both top and bottom surfaces. As fracture occurred within the bondline layer in the cracking area, partly

cohesive failure was achieved on the coarse-blasted substrates with the addition of CNTs. Figure 23(b, d) further compare the SEM images of bottom surfaces in the overlap areas with the neat and CNT reinforced epoxy composites on coarse substrates after testing. The fracture surface of the CNT reinforced epoxy composites was observed to be much rougher than that of the neat epoxy resin, indicating a sign of more plastic deformations and consequently more fracture energy consumption with the addition of CNTs.

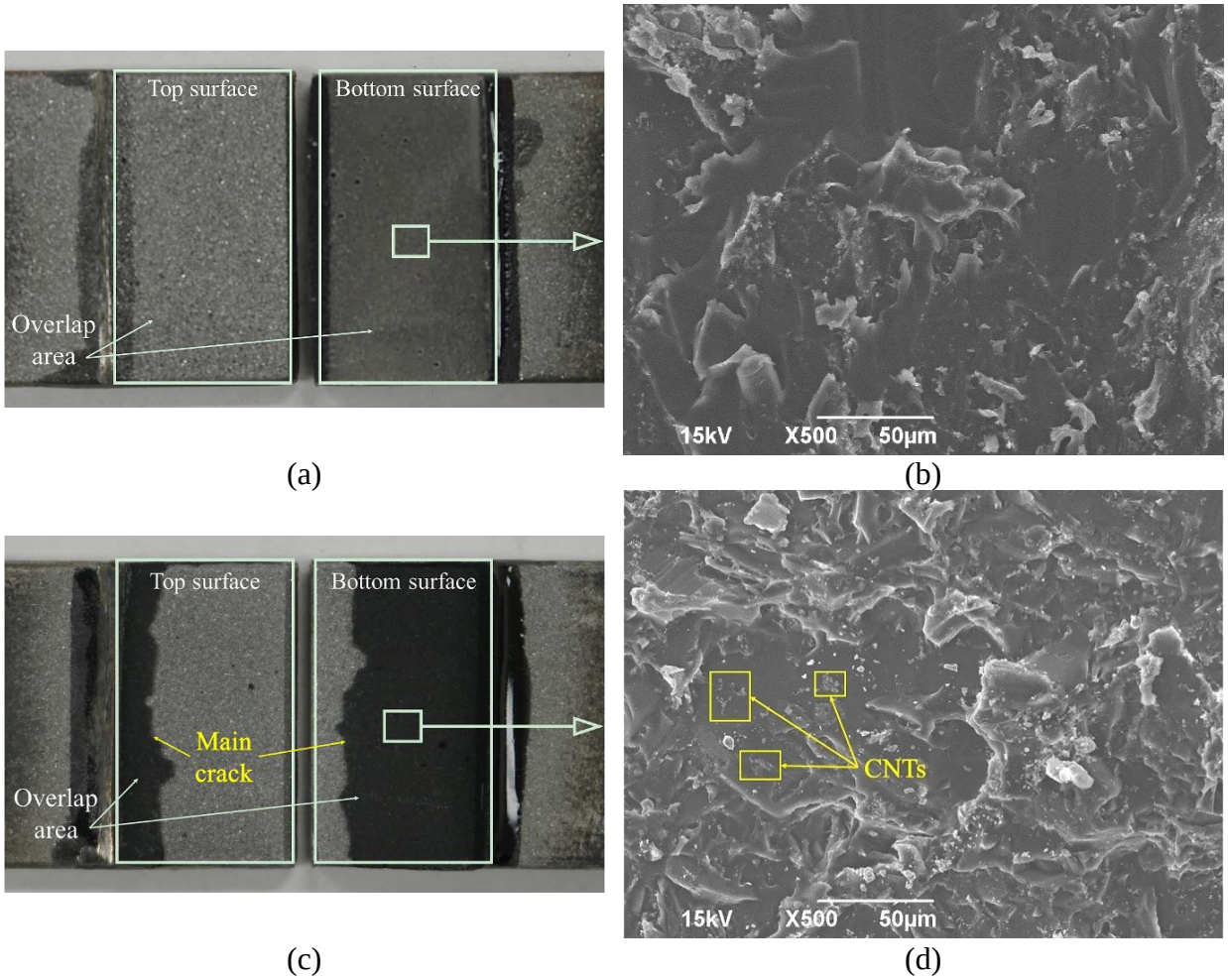

Figure 23. Typical fracture surfaces on coarse substrates: (a) neat epoxy coating; (b) SEM image of the fractured neat epoxy resin at a magnification of 500X; (c) CNT reinforced epoxy composites; (d) SEM image of the fractured CNT reinforced epoxy composites at a magnification of 500X

To further investigate the reinforcing mechanism of CNTs in epoxy-based composites, the SEM analysis under higher magnifications was conducted on the fracture surface and the main

crack in Figure 23(b) of the CNT reinforced epoxy composites, as shown in Figure 24(a ~ d). The pulling-out of CNTs as shown in Figure 24(a) and (b) was noticed as an important reinforcing mechanism, which could improve the bonding performance of epoxy-based composites. It required considerable energy to pull out the CNTs from the surrounding epoxy, leading to the higher toughness of the CNT reinforced epoxy composites than the neat epoxy resin. Figure 24(c) and (d) illustrate the CNT clusters on the main crack. Even though the weight fraction of CNTs was optimized and the ultrasonic mixing was used in mixing the CNTs in the epoxy matrix, the CNTs were still noticed to be not uniformly dispersed in the epoxy matrix with CNTs agglomerated into clusters as shown in Figure 24(c). The aggregation of CNTs was generated primly due to the high viscosity of epoxy and high surface energy of CNTs [49], which had a detrimental effect on the bonding performance. According to the literature [60], CNTs can be divided into three levels based on the unit structure, namely individual CNTs, CNT bundles (close-packed CNTs) and CNT fibers (an assembly of CNT bundles). The strength and toughness of the CNT clusters reduced significantly, as the aggregation of CNTs become larger. These CNTs clusters consisted of both CNT bundles and CNT fibers, which reduce the reinforcing mechanism of CNTs and also caused the local stress concentration. The adverse effect of CNT clusters as defects or imperfections led to the rapid growth of the main crack, which eventually restricted the improvement of CNTs on the bonding performances. On ideal condition when CNTs are uniformly dispersed in the epoxy matrix, CNT aggregation would not produce any defects and initial voids would be all mended by CNTs. It is foreseeable the bonding performance of CNT reinforced epoxy composites would get tremendously further improved if all the imperfections were eliminated within the bondline layer.

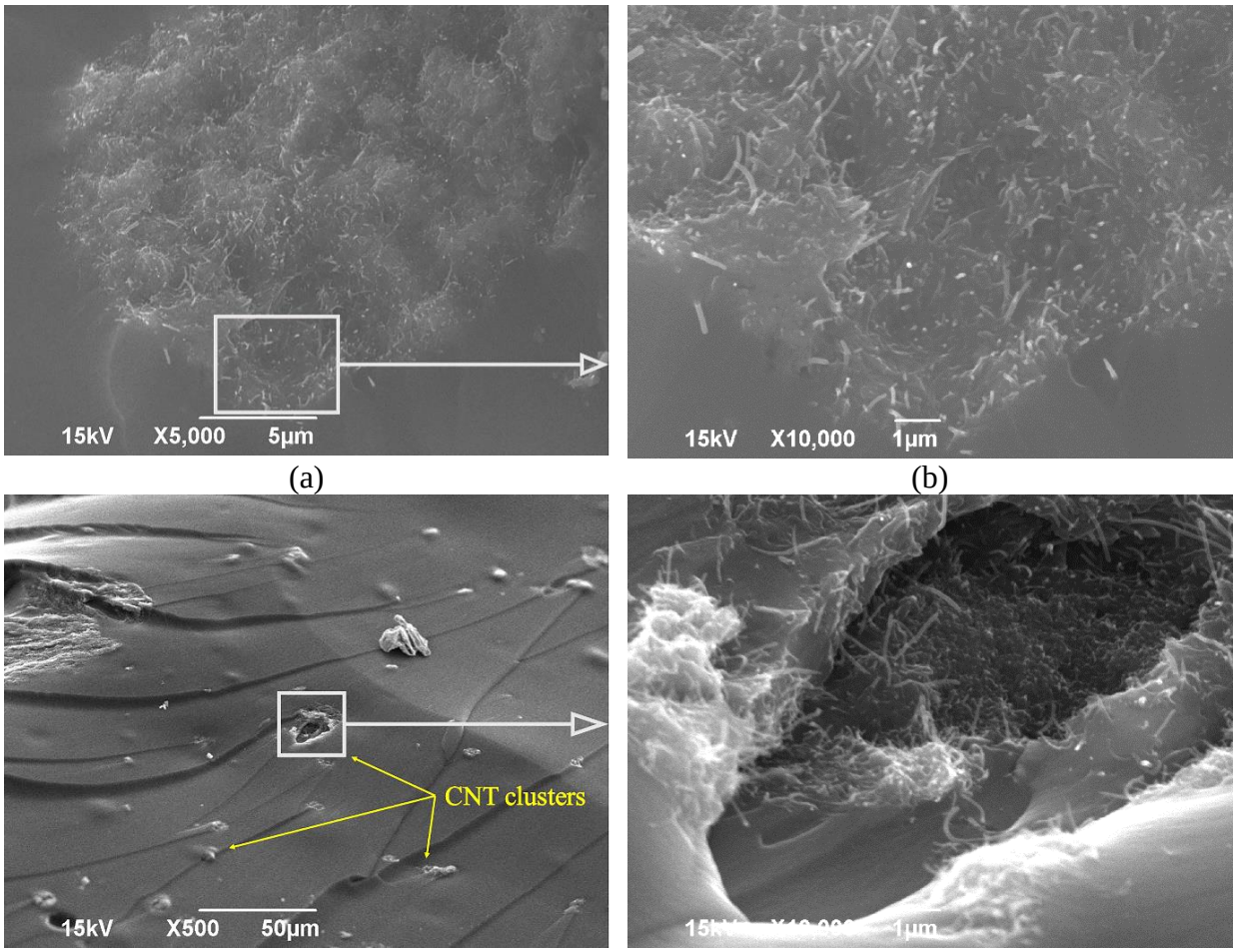

Figure 24. Detection of CNTs: (a) on fracture surfaces at a magnification of 5000X; (b) on fracture surfaces at a magnification of 10,000X; (c) on the main crack at a magnification of 500X; (d) on the main crack at a magnification of 10,000X

3.3.2. Influence of surface roughness for the CNT reinforced epoxy composites

Figure 22 showed that CNT reinforced epoxy composites on rougher substrates had lower contact angles, and the improvements of wettability resulted in the improvements in the interfacial adhesion to benefit the overall bonding performances. To further investigate the influences of surface roughness on the bonding performance of the CNT reinforced epoxy composites, Figure 25 plots the changes of the bonding strengths and fracture strains of the CNT reinforced epoxy composites with the changes of the surface roughness parameter, Ra. In general, the changing trends of the bonding strengths and fracture strains approximately followed a logarithmic pattern

as the increase of surface roughness, with both of the curves rising rapidly at lower surface roughness and then growing at a much slower rate at larger surface roughness. On the smooth substrates with the surface roughness of 0.231 μm, the bonding strengths and fracture strains were greatly lower than the other three rougher substrates owing to the lack of interfacial adhesion. Insufficient interfacial adhesion might result in the moderate improvements in the literature. As the surface roughness increased from 0.231 μm on smooth substrates to 3.528 μm on the fine substrates, significant increases in bonding strength and fracture strain were noted due to the improvement of the interfacial adhesion. Stronger interfacial adhesion could prevent premature adhesive failure and allow the epoxy-based composites to deform plastically as demonstrated in Figure 19 and 23. When the steel substrates were further roughened from 3.528 μm on the fine substrates to 5.272 μm on the medium substrates and 8.457 μm on the coarse substrates, the bonding strengths barely changed, but the fracture strains increased about 20% and 11%, from fine to coarse substrates, respectively. A much less significant changes were observed for both the bonding strengths and fracture strains, compared to changing the surface roughness from smooth to fine conditions, indicating that although the surface roughness was of vital importance to the bonding performances of the CNT reinforced epoxy composites, the influence was more crucial at lower roughness levels. When surface roughness was sufficient to provide a good interfacial adhesion, further increasing the surface roughness become much less effective.

To enable an estimation of bonding performances under all different surface roughness other than the values tested in this chapter, various fitting approaches were performed based on the obtained data in Figure 25 and Table 7. Although there were some differences between the changes of the bonding strengths and fracture strains for the CNT reinforced epoxy composites, the best fitted curves of both bonding strength and fracture strain could be expressed into a

logarithmic equation as Equation 3. The fitted curves using Equation 3 was also included in Figure 25. In addition, Table 8 shows the detailed fitted parameters in Equation 3 as well as the adjusted R-squared to evaluate the goodness of the fittings. With all the R2 being precisely close to 1 as shown in Table 8, Figure 25 also shows that all the traces of two fitting curves staying within the STDs of measured data points on original curves, indicating an effective fitting for the experimental data for future prediction use.

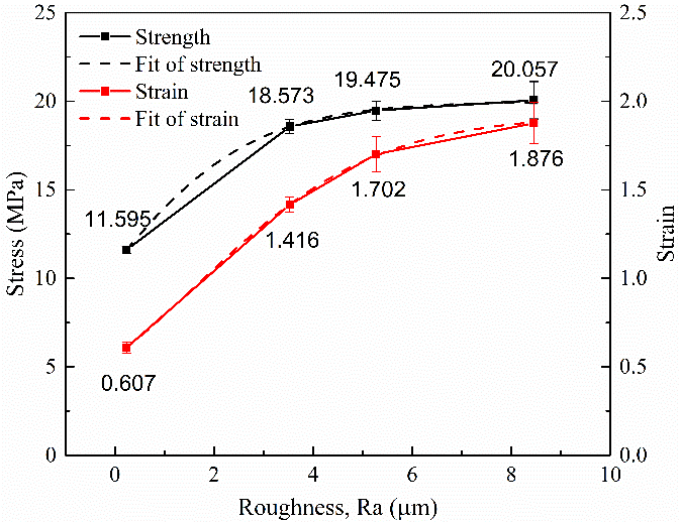

Figure 25. Changes of bonding strengths and fracture strains of the CNT reinforced epoxy composites with different surface roughness

Table 8. Fitting parameter values in Chapter 3

	Parameter value: a	Parameter value: Xc	Parameter value: k	R2
Strength	19.992	-0.244	0.679	0.999
Strain	1.928	1.656	0.546	0.999

In addition, Figure 26(a, b) further compare the SEM images of the top fracture surfaces for the CNT reinforced epoxy composites on smooth and coarse substrates. On the smooth substrates, there was no epoxy on the top surface and the fracture substrate after the SLS test was very similar to the substrate before applying the coatings. However, on the coarse substrates, it was evident that some of the CNT reinforced epoxy composites penetrated into the irregularities of the substrates. The stronger interfacial adhesion contributed to the improvements of the bonding

performances of the CNT reinforced epoxy composites on rougher substrates as shown in Figure 23.

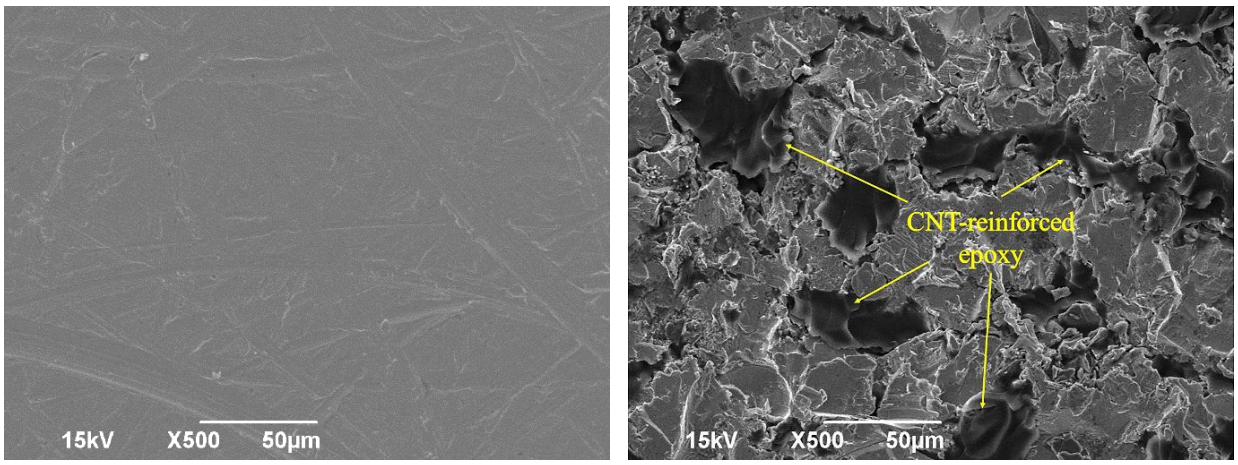

(a) (b)

Figure 26. Typical fracture surfaces of the CNT reinforced epoxy composites on top surfaces at a magnification of 500X: (a) on the smooth substrate; (b) on the coarse-blasted substrate

3.4. Summary

This chapter investigated the bonding performances of epoxy-based composites with and without CNT reinforcements on mild steel substrates fabricated with four different surface roughness. According to the experimental results, the following concluding remarks could be drawn:

(1) The addition of CNTs could significantly increase the bonding strengths and fracture strains as a result of great improvement in the toughness of epoxy-based composites. Higher ability of plastic deformation and pulling-out of CNTs with improved fracture energy consuming efficiency were the reinforcing mechanisms when interfacial adhesion between the epoxy-based composites and steel substrates was strong enough.

(2) When lacking sufficient interfacial adhesion due to low surface roughness, the bonding performance of the CNT reinforced epoxy composites could still be improved because the addition

of CNTs could improve the interfacial adhesion as indicated by the smaller contact angles of the CNT reinforced epoxy compared to the neat epoxy, although the improvement was less significant.

(3) The surface roughness had a positive influence on the bonding performances of the CNT reinforced epoxy composites by enhancing the interfacial adhesion. The positive influence of surface roughness was more significant on smoother substrates when lacking sufficient interfacial adhesion. When surface roughness was sufficient to provide a good interfacial adhesion, further increasing the surface roughness become much less effective.

(4) The failure mode could only be changed from adhesive failure of the neat epoxy resin to partly cohesive failure of the CNT reinforced epoxy composites on highly rough substrates due to the aggregation of CNTs even after mechanical stirring and ultrasonic mixing.

CHAPTER 4. INFLUENCES OF BONDLINE THICKNESS AND CNT WEIGHT FRACTION ON THE BONDING PERFORMANCE OF CNT REINFORCED EPOXY COMPOSITES

In this chapter, the bonding performance of CNT reinforced epoxy composites on steel substrates with different CNT weight fractions and bondline thicknesses were investigated using SLS tests. The following bonding performances of epoxy-based composites were evaluated included bonding strength, fracture strain, toughness, and failure mode. In addition, SEM image analysis was also performed on the fracture surfaces of epoxy-based composites to understand the reinforcing mechanisms of the CNTs in the epoxy-based composites and reveal the potential effectiveness of the CNT reinforcement.

4.1. Experimental Setup

The steel substrates are made of mild A36 steel, the neat epoxy adhesive in this chapter was still the genera-purpose epoxy resin, while the CNTs were still the multi-walled carbon nanotubes with the same mixing method. Epoxy-based composites with three different weight fractions of 0%, 0.375%, and 0.75% were fabricated to investigate the influence of CNT weight fractions on the bonding performances of epoxy-based composites when different bondline thicknesses were considered. The SLS sample configurations and loading protocols were still the same, except all the surfaces were only fine-blasted and three different bondline thicknesses of 1 mm, 0.5 mm, and 0.25 mm were considered for each CNT fraction. Table 9 (Column 1 ~ 4) shows the test matrix for the SLS tests in this chapter. 9 testing conditions were considered covering three different bondline thicknesses (0.25 mm, 0.5mm, and 1 mm) and three different CNT weight fractions (0%, 0.35%, 0.75%). For each testing condition, to restrict random error, five samples were made, resulting in a total of 45 samples.

Table 9. Results of SLS tests in Chapter 4

Testing condition	Sample quantity	Bondline thickness (mm)	CNT addition (%)	Toughness (MPa)	Bonding strength (MPa)	Fracture strain
E1	5	1	0	0.78	6.54 ± 0.43	0.195 ± 0.007
E0.5	5	0.5	0	3.41	11.72 ± 0.82	0.614 ± 0.037
E0.25	5	0.25	0	15.36	17.66 ± 1.35	1.474 ± 0.107
HC1	5	1	0.375	5.01	12.26 ± 1.04	0.699 ± 0.037
HC0.5	5	0.5	0.375	10.41	17.31 ± 1.60	1.210 ± 0.072
HC0.25	5	0.25	0.375	21.89	18.48 ± 1.23	1.982 ± 0.145
C1	5	1	0.75	7.50	15.56 ± 1.13	0.853 ± 0.041
C0.5	5	0.5	0.75	16.65	18.27 ± 1.45	1.372 ± 0.095
C0.25	5	0.25	0.75	32.45	19.25 ± 1.87	2.079 ± 0.165

4.2. Results and Discussions

4.2.1. Stress-strain curve

Figure 27 (a ~ i) show the original experimental stress-strain curves in each testing condition with three different bondline thicknesses and three different CNT weight fractions following the termination of the test matrix as shown in Table 9. To clearly compare the stress-strain curves in different testing conditions, the five-individual stress-strain curves from the five samples in each testing condition were fitted mathematically into one average stress-strain curve as also illustrated in Figure 27 (a ~ i). The applied fitting algorithm was called trace interpolation which was able to compute the average curves whose shapes were similar to those of the five experimental curves in the same testing conditions. From Figure 27, it can be seen that the five individual curves and the corresponding average curve in each testing condition followed the same traces with similar peak stresses and fracture strains. Therefore, in the further analysis, the typical stress-strain curves in each testing condition were represented by the corresponding average curves.

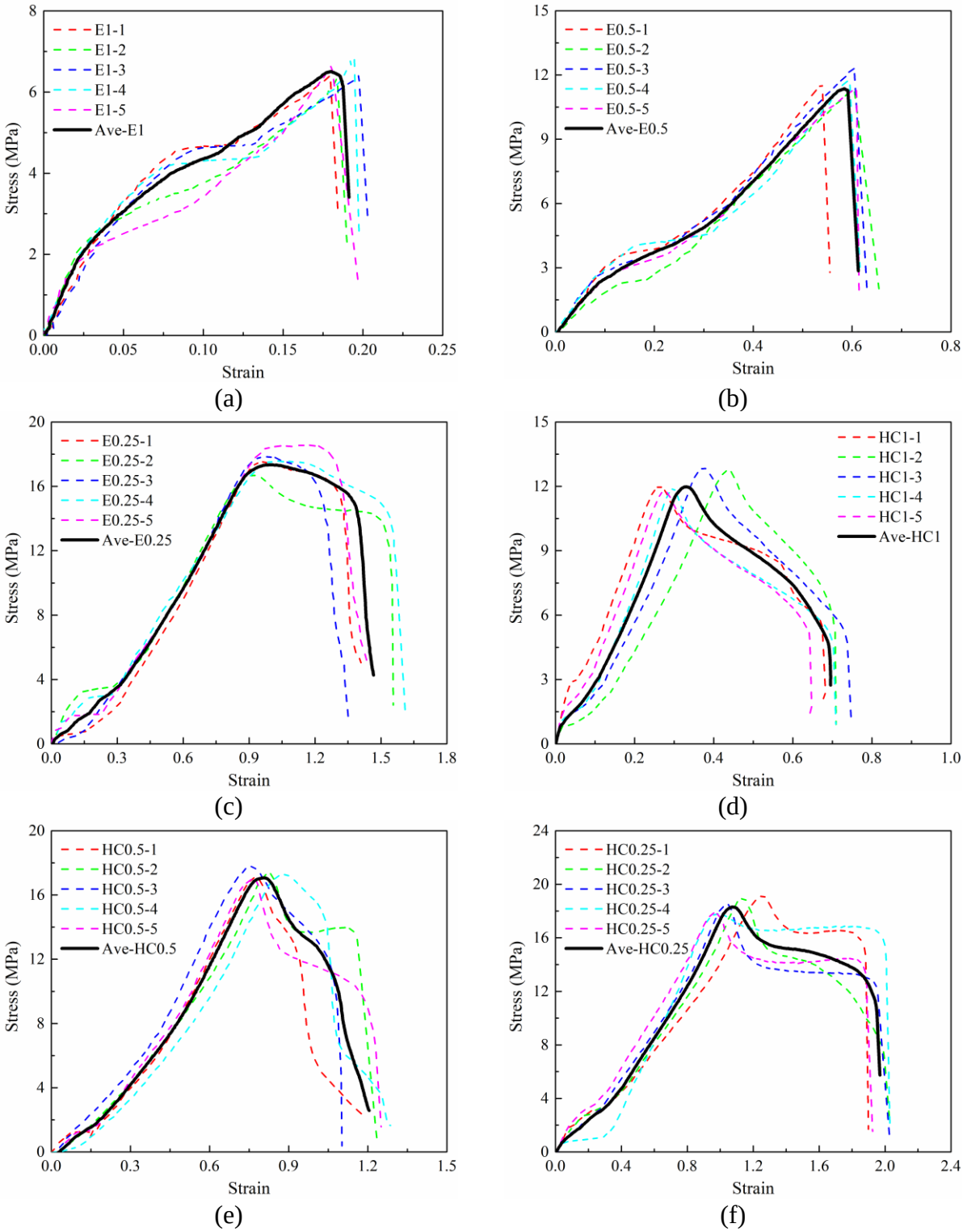

Figure 27. Comparisons between original experimental stress-strain curves and the average fitting curves in each testing conditions: (a) E1; (b) E0.5; (c) E0.25; (d) HC1; (e) HC0.5; (f) HC0.25; (g) C1; (h) C0.5; (i) C0.25

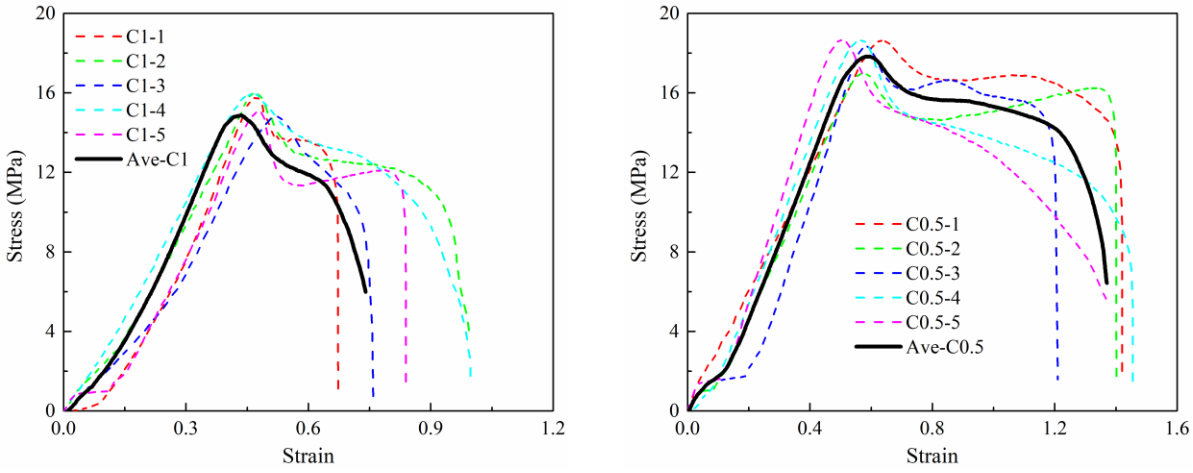

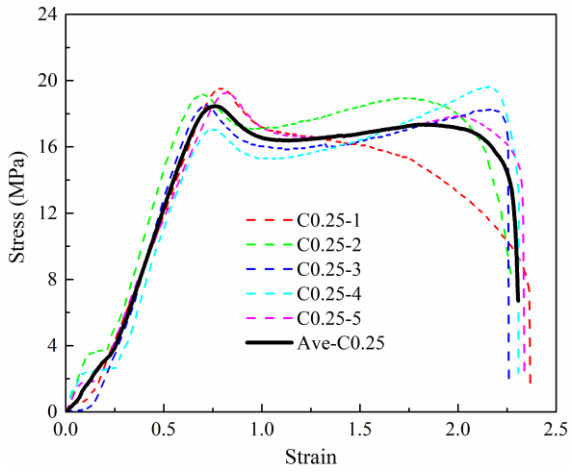

Figure 27. Comparisons between original experimental stress-strain curves and the average fitting curves in each testing conditions: (a) E1; (b) E0.5; (c) E0.25; (d) HC1; (e) HC0.5; (f) HC0.25; (g) C1; (h) C0.5; (i) C0.25 (continued)

Figure 28(a ~ c) plot the average stress-strain curves of 0%, 0.35% and 0.75% CNT reinforced epoxy composites with the three different bondline thicknesses of 0.25 mm, 0.5 mm, and 1 mm. As shown in Figure 28(a), the stress-strain curves of neat epoxy resin (0% CNT addition) with different bondline thicknesses showed significantly different changing traces. For the neat epoxy resin with the bondline thicknesses of 1 mm and 0.5 mm, the shear stress increased almost linearly with the increase of strain, and then decreased suddenly after reaching the peak stress, ending up with a sudden failure. However, when the bondline thickness was reduced to 0.25 mm, the average stress-strain curve showed a typical nonlinear pattern, with the stress dropping

gradually after the peak stress. For the CNT reinforced epoxy composites with 0.35% and 0.75% CNT additions, as shown in Figure 28(b) and 4(c), respectively, the shapes of the stress-strain curves were not obviously affected by neither CNT weight fractions nor bondline thicknesses. All the stress-strain curves exhibited nonlinear patterns which were very similar as the neat epoxy resin with a bondline thickness of 0.25 mm. However, the degrees of nonlinearity varied with different bondline thicknesses and CNT weight fractions. In general, a higher level of nonlinearity of the curves was observed with higher CNT additions and thinner bondline thicknesses, indicating more plastic deformations generated by the epoxy-based composites.

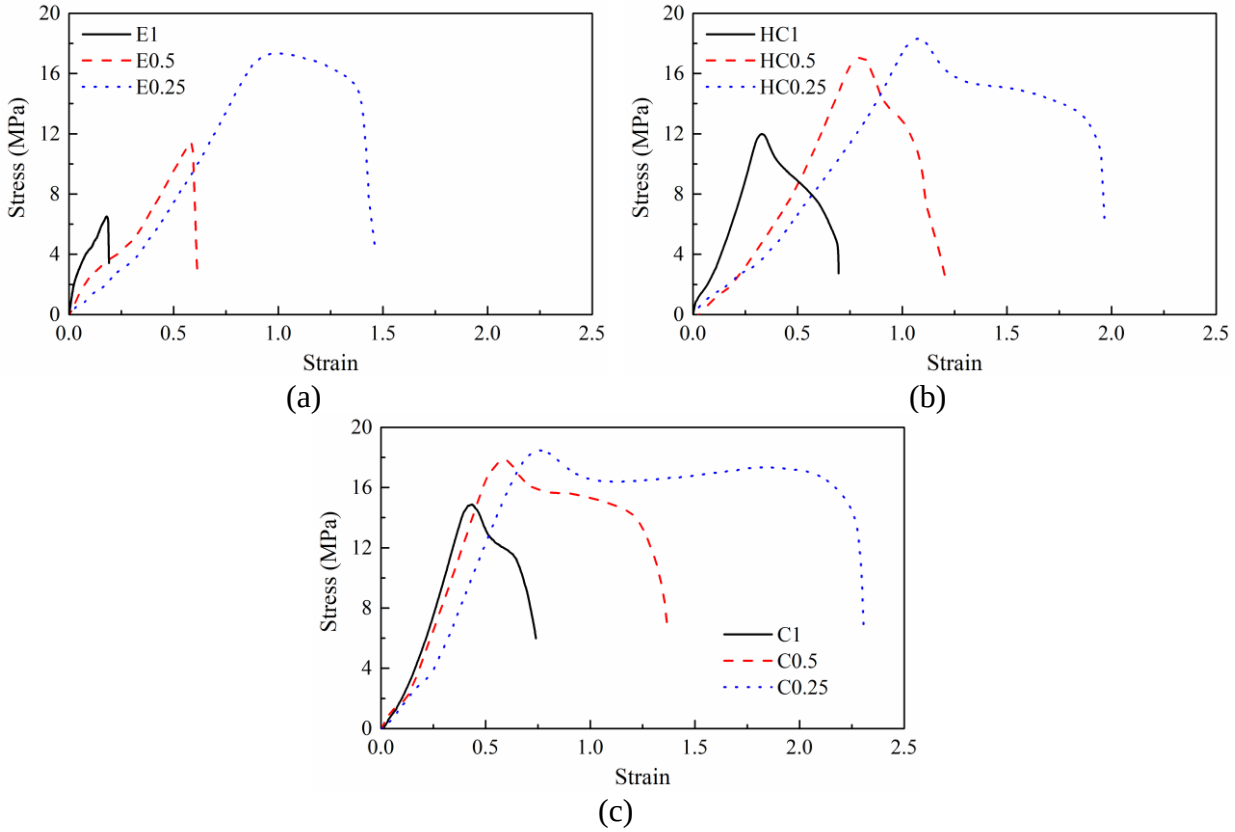

Figure 28. Average stress-strain curves of epoxy-based composites: (a) neat epoxy; (b): 0.375% CNTs; (c) 0.75% CNTs

The plastic behaviour of the neat and CNT reinforced epoxy composites could quantitively be reflected by the area under the stress-strain curve, which is an indication of the toughness as the ability of plastically deforming and absorbing energy. Epoxy-based composites with higher

toughness could generate more plastic deformations and consume more energy while deforming, indicating the improved bonding performances. Based on the average stress-strain curve in each testing condition as shown in Figure 28, the toughness of epoxy-based composites among the different bondline thicknesses with each CNT addition can be calculated and the values of the toughness are presented in Table 9 (Column 5) and compared in Figure 29. According to Figure 29, the reduction of bondline thickness could remarkably improve the toughness of epoxy-based composites with the same CNT fractions. For the neat epoxy resin, as the bondline thickness decreased from 1 mm to 0.5 mm and from 0.5 mm to 0.25 mm, the toughness increased by 337% and 350%, respectively. However, for the CNT reinforced epoxy composites, the improvements of toughness by the same decreases of bondline thicknesses reduced to 108% and 110% with 0.375% CNT addition, and 122% and 95% with 0.75% CNT addition, respectively. Compared to neat epoxy resin, the increments of the toughness among CNT reinforced epoxy composites with different bondline thicknesses became smaller and smaller due to the increase of CNT fractions.

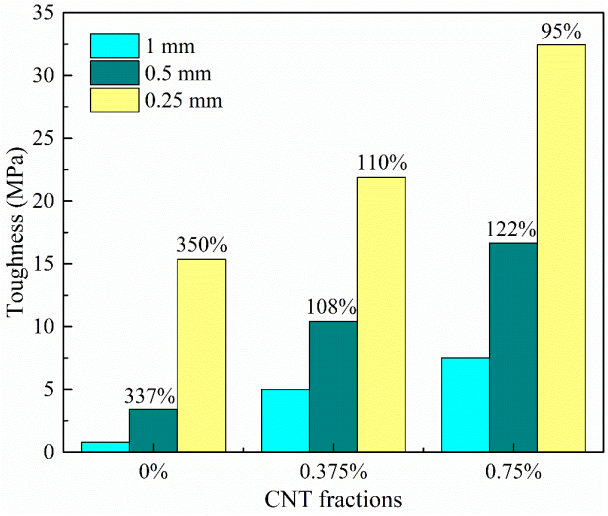

Figure 29. Comparisons of toughness between different bondline thickness (including increments from 1 mm to 0.5 mm and 0.5 mm to 0.25 mm) with each CNT addition

Moreover, it was clearly indicated Table 9 (Column 5) that when comparing epoxy-based composites with the same bondline thicknesses, the toughness appreciably increased as the

increase of CNT fractions. According to Table 9, as the CNT fraction increased from 0% to 0.375%, the toughness of epoxy-based composites with the bondline thickness of 1 mm and 0.5 mm increased by 542% and 205%, respectively. For the rest epoxy-based composites with different bondline thicknesses and CNT fractions, the increments of the toughness were only around 43% ~ 60%. The improvements were more significant by increasing the CNT fractions from 0% to 0.375% when the bondline thicknesses were 1 mm and 0.5 mm compared to further increasing the CNT fractions from 0.375% to 0.75% or when the bondline thickness was 0.25 mm. The influence of the CNT addition was more effective on the epoxy-based composites with thicker bondline thicknesses.

4.2.2. Bonding strength and fracture strain

Table 9 (Columns 6-7) also includes the influence of bondline thickness and CNT fraction on the bonding strength and fracture strain of the epoxy-based composites. Figure 30(a, b) displays the increments of bonding strength and fracture strain with standard deviations of epoxy-based composites among different bondline thicknesses with various CNT weight fractions. It was found that both bonding strength and fracture strain of neat epoxy resin increased significantly as the decrease of bondline thickness, which is the agreement with findings in Chapter 2. The similar trend was also seen for both 0.375% and 0.75% CNT reinforced epoxy composites among different bondline thicknesses.

Specifically, as shown in Figure 30(a), for the neat epoxy resin, when the bondline thickness was reduced from 1 mm to 0.5 mm and from 0.5 mm to 0.25 mm, the bonding strength increased by 79% and 51%, respectively. For the CNT reinforced epoxy composites, the corresponding increments of bonding strength improved by 41% and 7% for 0.375% CNT reinforcement, and 17% and 5% for 0.75% CNT reinforcement, respectively. The increments in

fracture strain also showed a similar trend as those in bonding strength, as shown in Figure 30(b). For the neat epoxy resin, by reducing the bondline thickness from 1 mm to 0.5 mm and from 0.5 mm to 0.25 mm, the fracture strain increased 215% and 140%, respectively. For CNT reinforced epoxy composites, the corresponding improvements were restricted to 73% and 64% with 0.375% CNT addition, and to 61% and 52% with 0.75% CNT addition, respectively. It was worth noticing that the improvement of both bonding strength and fracture strain became less significant from 0% to 0.75% CNT reinforced epoxy composites, indicating that the impact on the bonding performances of epoxy-based composites by bondline thickness was restricted with the addition of CNTs. The restricted impact of bondline thickness with the addition of CNTs could be possibly related to the reinforcing mechanism of CNTs on the epoxy-based composites. Existing studies found that voids and micro-cracks inside the bondline layer could be deflected, pinned and bridged with the incorporation of CNTs [53, 90, 91]. In terms of the influence of bondline thickness, porosity is one of the most critical reasons for thicker bondlines yielding weaker bonding performance [88]. The voids and micro-crack could be possibly cured by the added CNTs, so that the adverse impact of bondline thickness might be mitigated or even minimized with the addition of CNTs. Thus, the increments of bonding strength and fracture strain became smaller among CNT reinforced epoxy composites with the reduction of bondline thickness.

On the other hand, previous researches [9, 45, 54, 92] found out that the bonding strength of CNT reinforced epoxy composites increased as the CNT fractions increased to around 0.75%, and then decreased gradually with further additions of CNTs owing to the aggregation of CNTs [52, 56, 91]. The experimental results in Table 9 (Columns 6-7) confirmed that for epoxy-based composites with the same bondline thicknesses, as the CNT fraction increased from 0% to 0.75%, both bonding strengths and fracture strains increased continuously. By increasing the CNT

fractions from 0% to 0.75%, more CNTs were incorporated to reinforce the epoxy bondlines, which could surely improve the bonding performances of the epoxy-based composites.

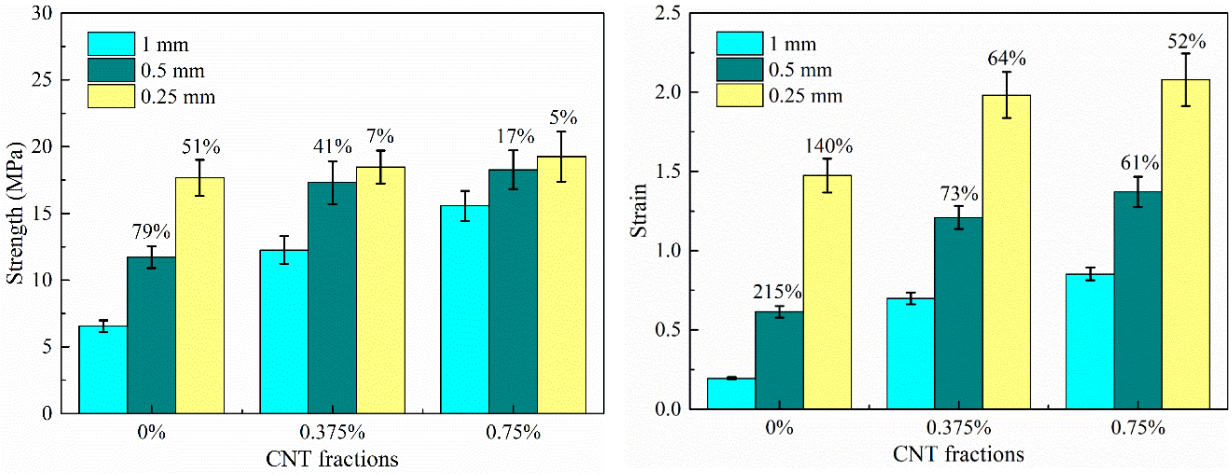

(a) (b)

Figure 30. Comparisons between different bondline thickness (including increments from 1 mm to 0.5 mm and 0.5 mm to 0.25 mm) with each CNT addition: (a) bonding strength; (b) fracture strain

To further investigate the influence of CNT fractions on the bonding strength and fracture strain of epoxy-based composites with different bondline thicknesses, it was noted that when the bondline thickness was 1 mm, adding the CNT fraction from 0% to 0.375%, the bonding strength and fracture strain increased by 87% and 258%, respectively. and further increasing the CNT fraction from 0.375% to 0.75%, the improvements of bonding strength and fracture strain were 27% and 22%, respectively. When the bondline thickness was 0.5 mm, the corresponding improvements reduced to 48% and 97% from 0% to 0.375% CNT additions, and 6% and 13% from 0.375% to 0.75% CNT additions. When the bondline thickness was 0.25 mm, except the fracture strain increased by 34% with the increase of CNT addition from 0% to 0.375%, the other increments were only around 5%. It was observed that the increments of bonding strength and fracture strain by increasing CNT fractions were reduced with the decrease of bondline thicknesses. The literature showed that thicker epoxy bondlines are prone to have more voids and

micro-cracks than thinner bondlines [89]. Thus, more imperfections in thicker bondlines could be fixed by the CNTs, resulting in more significant improvements of the bonding performances.

4.2.3. Failure mode analysis

Figure 31(a, b) compare the fracture surfaces of the neat and the 0.75 % CNT reinforced epoxy composites with the bondline thickness of 1 mm. As shown in Figure 31(a), a complete adhesive failure occurred for the neat epoxy resin with 1 mm bondline thickness because the epoxy bondline was completely attached on the top surface of the neat epoxy, and there was no visible epoxy remaining on the bottom surface. For the 0.75% 1 mm thick CNT reinforced epoxy composite, adhesive failure was also the dominant failure mode with most of the epoxy remaining on one fracture surface. However, as shown in Figure 31(b), some spots of CNT reinforced epoxy could be found on the bottom surface indicating the existence of cohesive failure. Then the overall failure mode turned into a combination of both adhesive and cohesive failure. It could also be noticed that there were several visible small cracks on the CNT reinforced epoxy bondline on the top surface. These cracks might be generated due to the plastic behaviour of CNT reinforced epoxy. Given that the addition of CNTs increased the shear capacity and toughness of the epoxy-based composites, it indicated that adding CNTs into the epoxy could improve the failure mode of epoxy-based composites.

In addition, Figure 31(a, c) and (b, d) compare the typical fracture surfaces of the neat and 0.75% CNT reinforced epoxy composites with bondline thicknesses of 1 mm and 0.25 mm, respectively. Specially, for the CNT reinforced epoxy composites with the bondline thickness of 0.25 mm, the bondline was penetrated by a big crack thoroughly, and the two separated parts of epoxy remained on both fracture surfaces. Although a large part of the bondline area still belonged to adhesive failure, cohesive failure occurred on the cracking areas including the big crack and

some smaller cracks inside the adhesive area. The similar failure mode modification was also observed between the neat epoxy resin with the bondline thicknesses of 1 mm and 0.25 mm. The preferred partial cohesive failures were achieved for both the neat and CNT reinforced epoxy composites with the bondline thickness of 0.25 mm, indicating that the change of failure mode was more pronounced between the neat epoxy resin compared to the change between the CNT reinforced epoxy composites with those different bondline thicknesses.

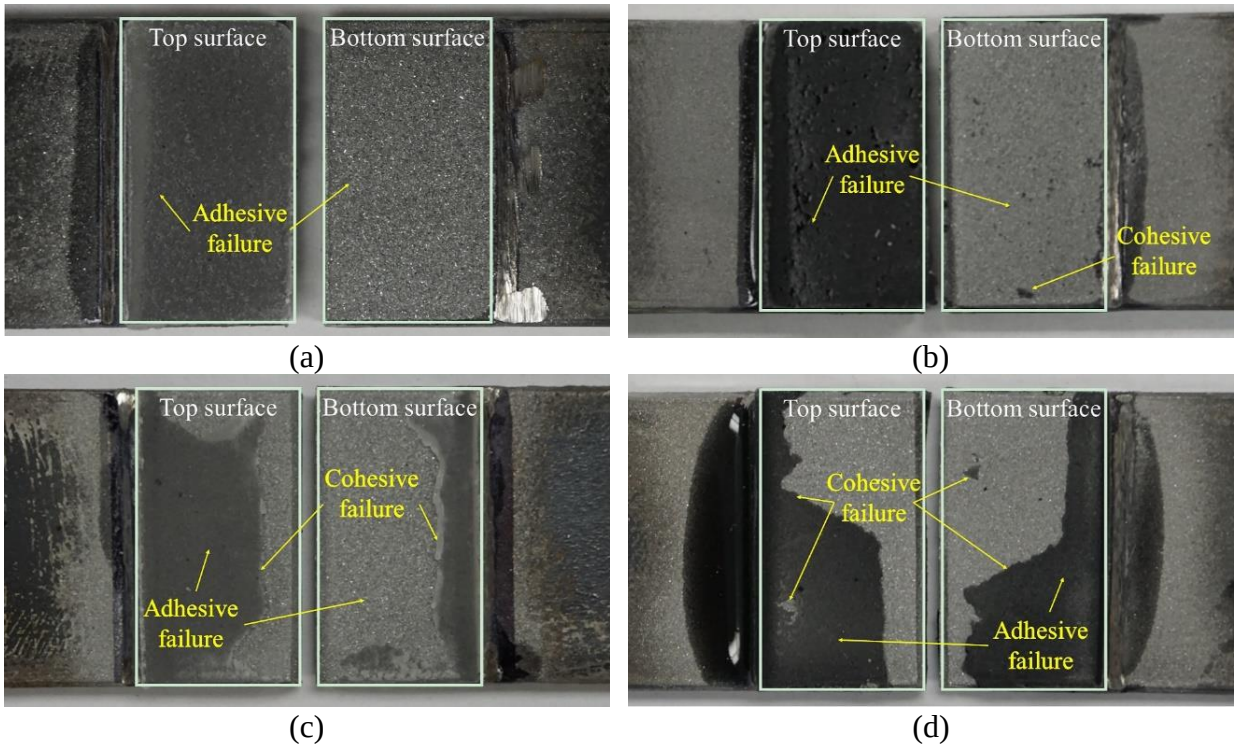

Figure 31. Typical fracture surfaces of epoxy-based composites: (a) 1 mm neat epoxy; (b): 1 mm 0.75% CNT reinforced epoxy; (c) 0.25 mm neat epoxy; (d) 0.25 mm 0.75% CNT reinforced epoxy

4.2.4. SEM image analysis

To further analyse the fracture surfaces of the neat and CNT reinforced epoxy composites shown in Figure 31, SEM image analysis at a magnification of ×1000 was conducted on the top surfaces of those epoxy-based composites, which are illustrated in Figure 32(a ~ d). As shown in Figure 32(a, b), the typical fracture surface of neat epoxy resin with 1 mm bondline thickness was comparatively smoother and flatter than the fracture surface with the 0.75% CNT reinforcement.

Adding CNTs into the 1 mm thick adhesive bondlines could visibly increase surface roughness of the fracture surfaces.

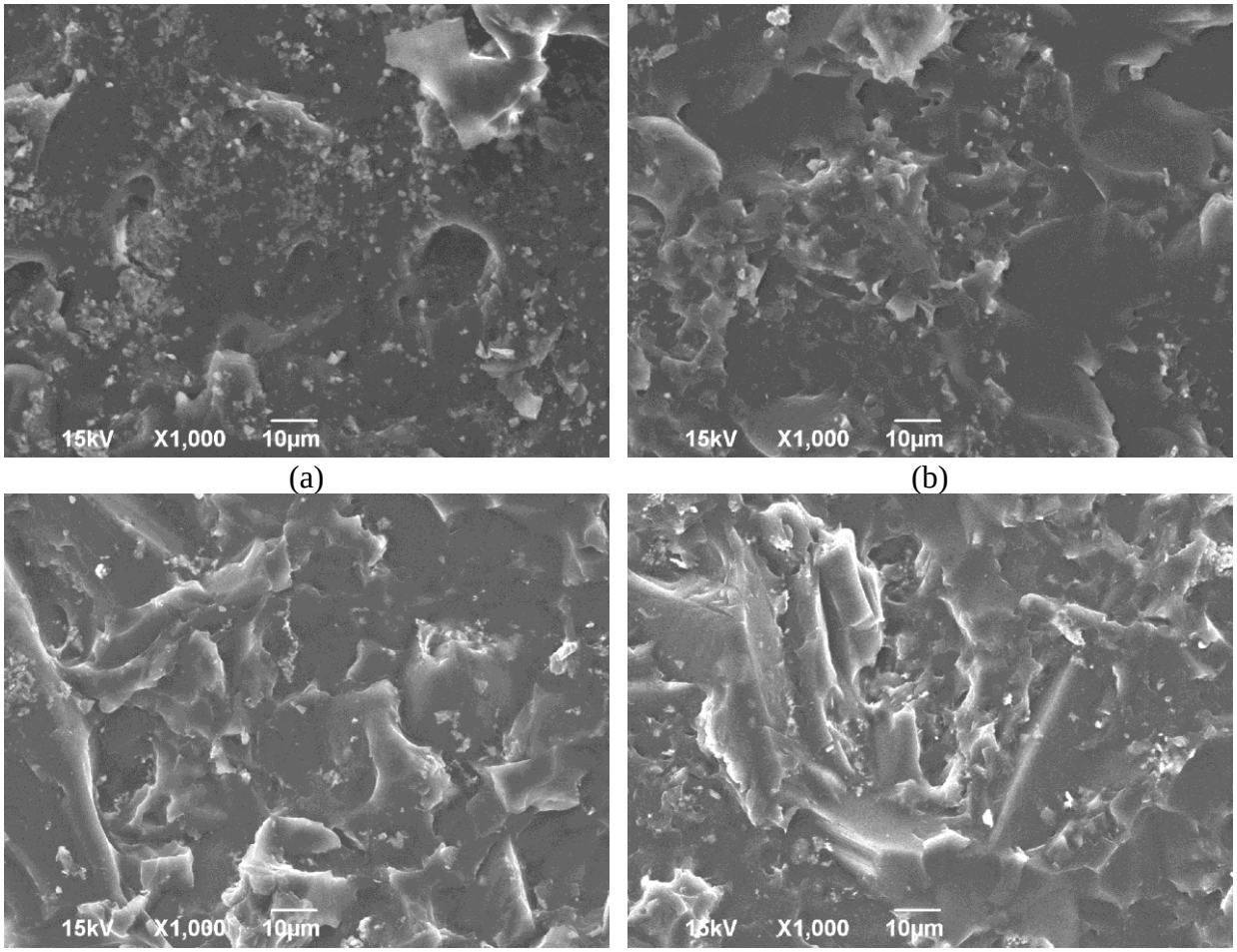

(a) (b)

(c) (d)

Figure 32. SEM images of the typical fracture surfaces: (a) 1 mm neat epoxy; (b): 1 mm 0.75% CNT reinforced epoxy; (c) 0.25 mm neat epoxy; (d) 0.25 mm 0.75% CNT reinforced epoxy

Additionally, for the neat epoxy resin as shown in Figure 32(a, c), the reduction of bondline thickness apparently increased the surface roughness of the fracture surfaces by introducing more hills, ridges and valleys on the surfaces. The similar roughness improvement was also seen on the fracture surfaces of the CNT reinforced epoxy composites between 1 mm and 0.25 mm bondline thicknesses, while it was less obvious than the improvement between neat epoxy resin. The influence of bondline thickness on surface roughness of fracture surfaces became less significant with the increase of CNT additions, which was also echoed with the previous findings in the last

section. Rougher fracture surfaces revealed more plastic deformations of epoxy bondlines, resulting in more complex fracture mechanisms with higher energy dissipation and toughness. But when comparing the fracture surfaces of the neat and CNT reinforced epoxy composites with 0.25 mm bondline thickness as in Figure 32(c, d), there was no big difference between the surface morphologies of the neat and CNT reinforced epoxy composites, the improvement of surface roughness between them was rather limited.

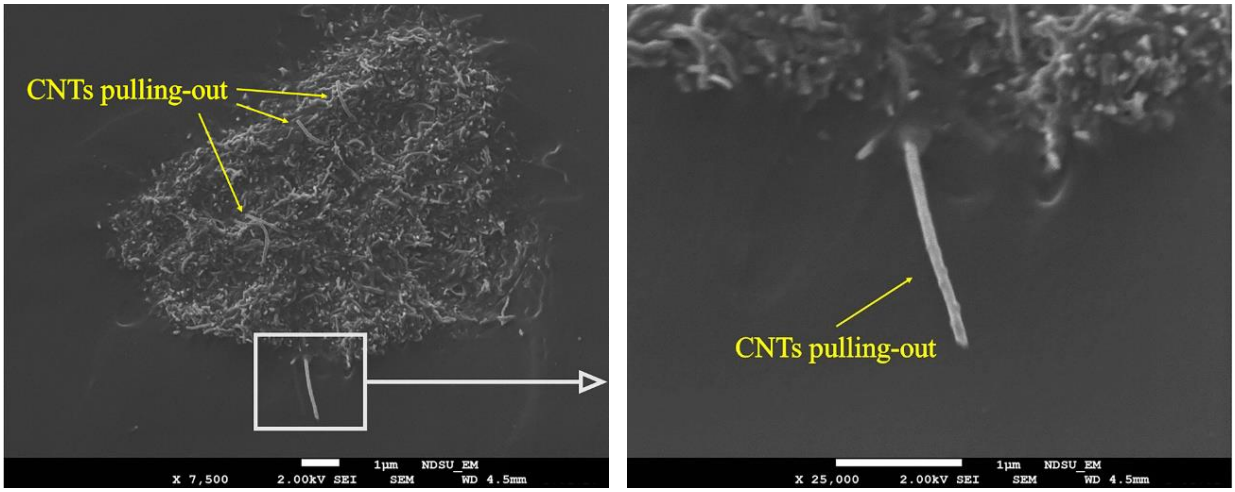

(a) (b)

Figure 33. SEM images of the presence of CNTs in the epoxy bondlines at higher magnifications: (a) the presence of CNTs; (b): CNT pulling-out from epoxy bondlines

Figure 33(a, b) present the SEM images of the presence of CNTs in the reinforced epoxy bondlines at higher magnifications, showing that several CNTs were pulled out from the surrounding epoxy bondline, which can be regarded as one of the important reinforcing mechanisms of CNTs. In terms of the CNTs pulling-out, CNTs and the surrounding epoxy matrix are tightly bonded together at the beginning until CNTs started to debond owing to the increase of the pull-out force. During debonding, a part of the CNTs moved along the interface against a friction force between CNTs and the epoxy matrix, with the rest part remaining well-bonded. When the debonding part extended to the whole length of CNTs, slipping occurred and CNTs were

pulled out [93]. A lot of energy was consumed during this process, leading to the increase of the toughness and improvement of the bonding performances of epoxy-based composites [49].

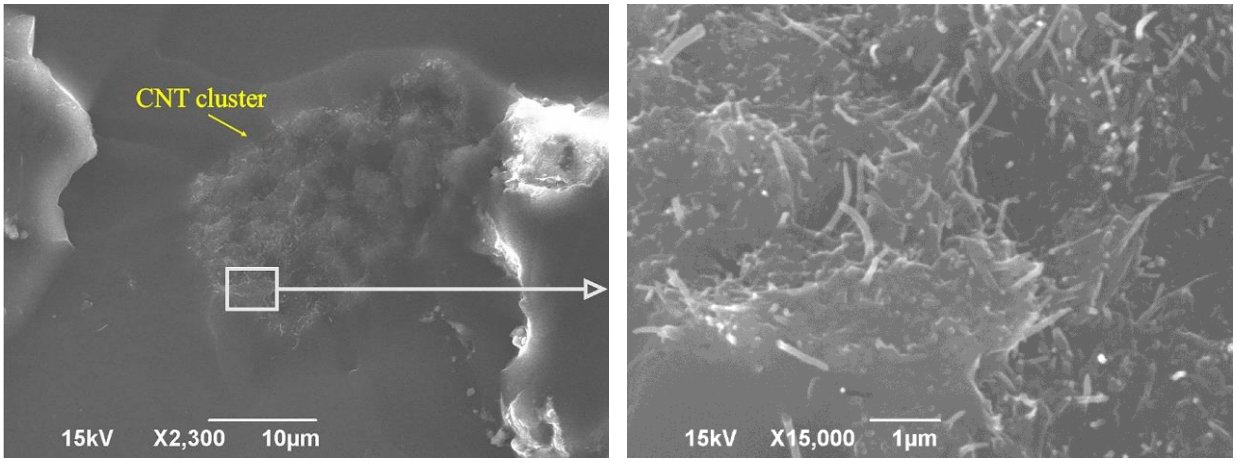

(a) (b)

Figure 34. SEM images of a CNT cluster on the fracture surface of 0.75% CNT reinforced epoxy composites: (a) a CNT cluster at a magnification of ×2300; (b): enlarged view of (a) at a magnification of ×15000

Although the CNT reinforcement could lower the influence of bondline thickness on the bonding performance of reinforced epoxy-based composites, it still could not eliminate the influence of bondline thickness, not to mention reverse the influence. This might be induced by the CNT clusters generated in the bondlines, as illustrated in Figure 34(a, b). According to Figure 34(a), the CNTs were not uniformly dispersed in the epoxy matrix even the optimal CNT weight fraction of 0.75%. The CNTs were agglomerated together into a CNT cluster which was restricted in a certain area as evidently shown in Figure 34(b). No recognizable CNT was found in the other area outside the CNT clusters. The CNT cluster played a negative role in the bonding performance improvement of the CNT reinforced epoxy composites, acting as defects or imperfections in the bondline layer. The aggregation of CNTs imposed local stress concentration, accelerated the damage process and eventually reduced the bonding performances of CNT reinforced epoxy composites. In addition, since CNTs were not uniformly dispersed with the CNT clusters, it might be challenging for the CNTs to cure all the imperfections in the epoxy bondline. The improvement

of the CNT reinforcement was reduced due to the presence of some unfixed imperfections, resulting in that CNT reinforced epoxy composites with thicker bondlines still yielded a little weaker bonding performance compared to thinner ones. The influence of bondline thickness was expected to be further restricted or even minimized with a more uniform CNT dispersion.

4.3. Summary

In this chapter, the neat and CNT reinforced epoxy composites with three bondline thicknesses of 1 mm, 0.5 mm, and 0.25 mm and three CNT weight fractions of 0%, 0.375%, and 0.75% were fabricated and their bonding performances were studied using the SLS tests and SEM image analysis. Based on the experimental results, it was found that the increase of CNT weight fraction (from 0% to 0.75%) and the reduction of bondline thickness (from 1 mm to 0.25 mm) could significantly improve the bonding strength, the fracture strain, and the toughness of epoxy-based composites. The failure mode could be changed from complete adhesion failure for neat epoxy resin with the bondline thickness of 1 mm to partial cohesive failure for CNT reinforced epoxy composites with the bondline thickness of 0.25 mm. However, the influence of bondline thickness on the bonding performances of epoxy-based composites become less significant as the increase of CNT weight fractions, which could be explained by the reinforcing mechanism of CNTs. The SEM image analysis also indicated that the addition of CNTs could not eliminate the influence of bondline thickness, which was induced by the non-uniform dispersion and the aggregation of CNTs.

CHAPTER 5. INFLUENCES OF CNT GEOMETRIES ON THE DISPERSION CHARACTERIZATIONS AND BONDING PERFORMANCE OF CNT REINFORCED EPOXY COMPOSITES

In this chapter, effects of CNT geometries on the dispersion characterizations and bonding performance of CNT reinforced epoxy composites were systematically investigated for the first time. CNTs with three different diameters, two different lengths and three different weight fractions were used and compared regarding dispersion characterizations and bonding performance respectively. Specifically, Particle size analyses were carried out to directly display the dispersion degree of CNTs. The bonding performance of CNT reinforced epoxy composites including bonding strength, fracture strain and toughness was examined by SLS tests. TEM and SEM analyses were conducted on CNTs aqueous solution and fracture surfaces of CNT reinforced epoxy composites to actual reveal CNT distribution within the epoxy matrix.

5.1. Experimental Setup

5.1.1. Materials

Multi-walled CNTs with six different geometries including three different diameter ranges (10-12nm, 20-30nm, 50-100nm) and two different length ranges (normal-length range between 5 to 20μm, and short range between 0.5 to 2μm) were used in this chapter (supplied by Skyspring Nanomaterials Inc, Houston, TX, USA), labeled as N10, N20, N50, S10, S20, and S50. Table 10 shows the detailed geometries and other details of the six different types of CNTs according to the manufacturer's specification. Pure acetone supplied by Sunnyside Corporation was used as solvent to disperse CNTs, since acetone is more volatile than ethanol or deionized water. Moreover, it is easier and faster to get rid of the acetone solution after mixing with epoxy resin. Besides, the general-purpose epoxy and low carbon A36 steel were still used in this chapter.

Table 10. CNT geometries and other properties

Type	CNT Length (μm)	CNT Diameter (nm)	Specific surface area (m^2/g)	Purity (%)	Bulk density (g/cm^3)
N10	5-20 (Normal)	10-12	500	95	0.27
N20	5-20 (Normal)	20-30	110	95	0.28
N50	5-20 (Normal)	50-100	60	95	0.28
S10	0.5-2 (Short)	10-12	350	98	0.27
S20	0.5-2 (Short)	20-30	90	98	0.25
S50	0.5-2 (short)	50-100	70	98	0.18

5.1.2. Preparation of CNT suspensions

Although the most prevalent method of mixing CNTs is ultrasonic processing, it was found that the ultrasonic mixing may often induce the shortening of tube length and aspect ratio, which lead to differences in mechanical properties and other performances [68,71]. Thus, in order to accurately investigate the effect of CNT geometries, ultrasonication was avoided during the mixing process. In this chapter, a new mixing protocol using a magnetic stirrer was developed to minimize alterations in CNT geometries and keep the CNTs intact. First of all, a conical flask filled with acetone was placed on the magnetic stirrer (supplied by Across International) and stirred by a magnetic rod at a speed of 1600 rpm, while CNTs with different geometries were gently added into the solvent. A commercially available surfactant called Sodium dodecylbenzene sulfonate (SDBS, obtained from Sigma-Aldrich Corp) with a constant weight fraction of 0.5% was also added into the solvent along with at least 2h mechanical stirring to make sure that CNTs were thoroughly dispersed. For each CNT geometry, suspensions with three different weight fractions (0.5%, 1%, and 2%) were examined to further investigate the effect of weight fractions on the dispersion characterizations of CNTs with different geometries.

5.1.3. Preparation of CNT reinforced epoxy composites

To prepare the CNT reinforced epoxy composites, the mechanical stirring CNT/acetone suspension was firstly mixed with the curing agent since the curing agent had less viscosity than

the resin, followed by continually mechanical stirring on the stirrer for 2h to ensure a sufficient mixing between CNTs and curing agent. Then the whole mixture was placed in a vacuum at 80℃ for at least 4h to thoroughly remove the acetone. At last, the CNT/curing agent mixture was mechanically mixed with the resin. The complete mixing protocols of CNT acetone suspensions and CNT reinforced epoxy composites adopted in this chapter are illustrated in Figure 35.

5.1.4. Testing

Particle size analysis is the most commonly used analytical testing method to directly reveal the particle size distribution of CNTs in a wide range. In this chapter, the dispersion characterizations of CNTs with different geometries were investigated by particle size analysis using Particle Sizing Systems SPOS 780. The SLS test set-up were still the same while the thickness of the epoxy layer between the two sheets was all controlled at 0.5 mm. Table 11 demonstrates the experimental matrix to clearly present all the testing conditions.

Table 11. Experimental matrix in Chapter 5

Testing condition	CNT Length	CNT Diameter (nm)	CNT fraction (%)
N10-0.5	Normal	10-12	0.5
N10-1	Normal	10-12	1
N10-2	Normal	10-12	2
N20-0.5	Normal	20-30	0.5
N20-1	Normal	20-30	1
N20-2	Normal	20-30	2
N50-0.5	Normal	50-100	0.5
N50-1	Normal	50-100	1
N50-2	Normal	50-100	2
S10-0.5	Short	10-12	0.5
S10-1	Short	10-12	1
S10-2	Short	10-12	2
S20-0.5	Short	20-30	0.5
S20-1	Short	20-30	1
S20-2	Short	20-30	2
S50-0.5	Short	50-100	0.5
S50-1	Short	50-100	1
S50-2	Short	50-100	2

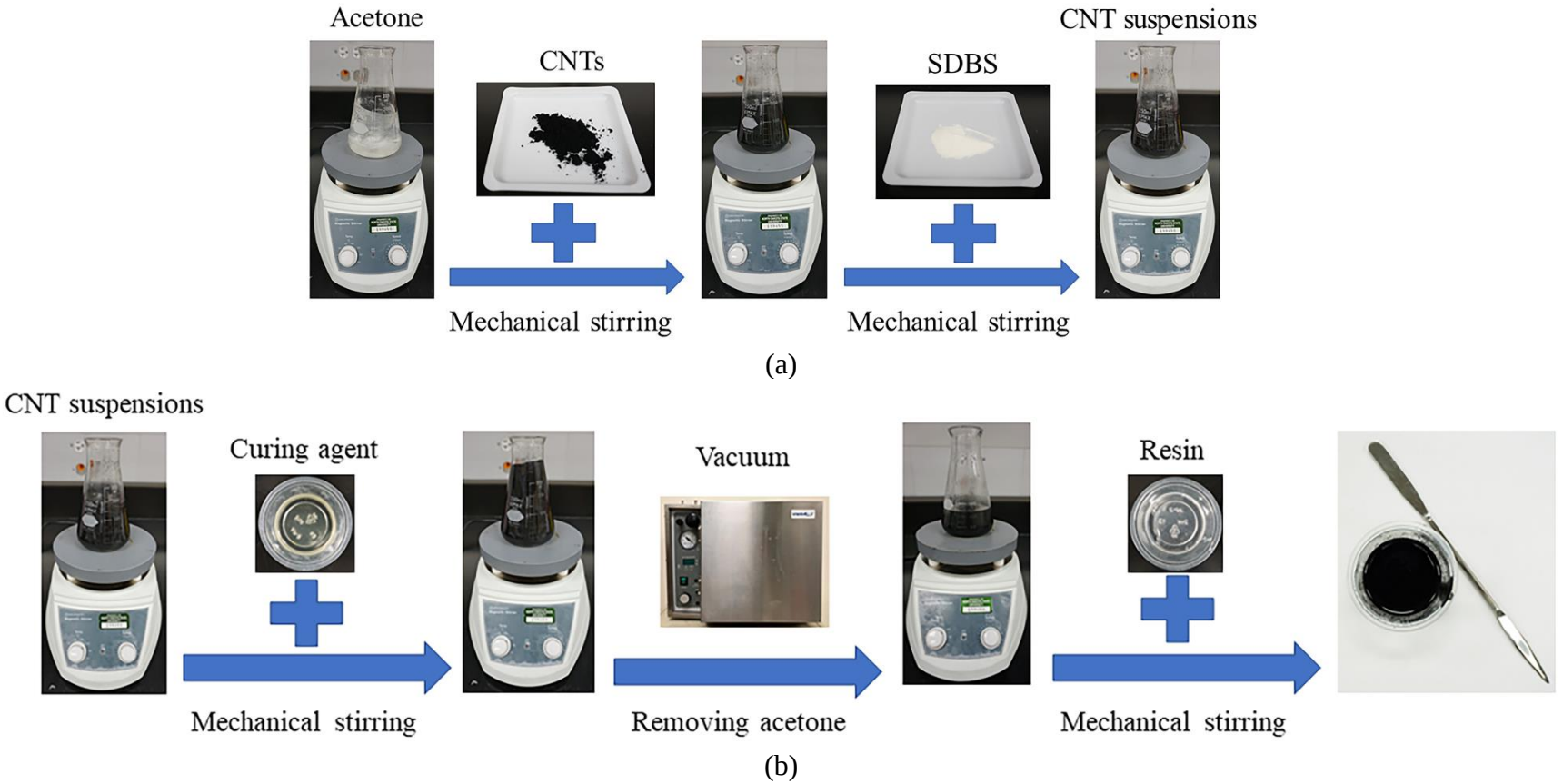

Figure 35. The complete mixing procedures: (a) CNT suspensions; (b) CNT reinforced epoxy composites

5.2. Results and Discussions

5.2.1. Validation of CNT geometries with a new mixing protocol

Before discussing the dispersion characterizations of CNT reinforced epoxy composites with different CNT geometries, it is indispensable to find out if CNTs remained their initial geometries after the newly-developed mixing procedures, even though ultrasonication was not involved in the mixing protocol. Figure 36(a ~ c) and Figure 37(a, b) display typical TEM images of CNTs suspensions from different testing groups visualizing the diameters and lengths, respectively. The average diameters of CNTs from different testing groups (N10, N20, and N50) were around 10.1 nm, 24.4 nm, and 58.5 nm, respectively, which precisely matched the diameter range of the corresponding testing groups and similar to the values in Figure 36. Furthermore, as for the comparison of CNT lengths, it is clearly illustrated in Figure 37 that CNTs from N20 group were generally much longer than CNTs from S20 group. Although it is quite difficult and time-consuming to accurately measure the length of all the individual CNTs, it is feasible to roughly estimate the average length of most CNTs in each Figure by taking a few visible CNTs with most frequently lengths as representatives. The estimated average length of CNTs in N20 and S20 group were around 10.4 μm and 1.4 μm, respectively, according to Figure 37. The average lengths of CNTs in those two testing groups were coincident with the corresponding original length range as well as the ratio between the two CNT geometries. Thus, both diameters and lengths of CNTs were not evidently affected by the mechanical stirring or the surfactant in the mixing protocol, indicating the validity of this new mixing protocol and experimental results in this chapter.

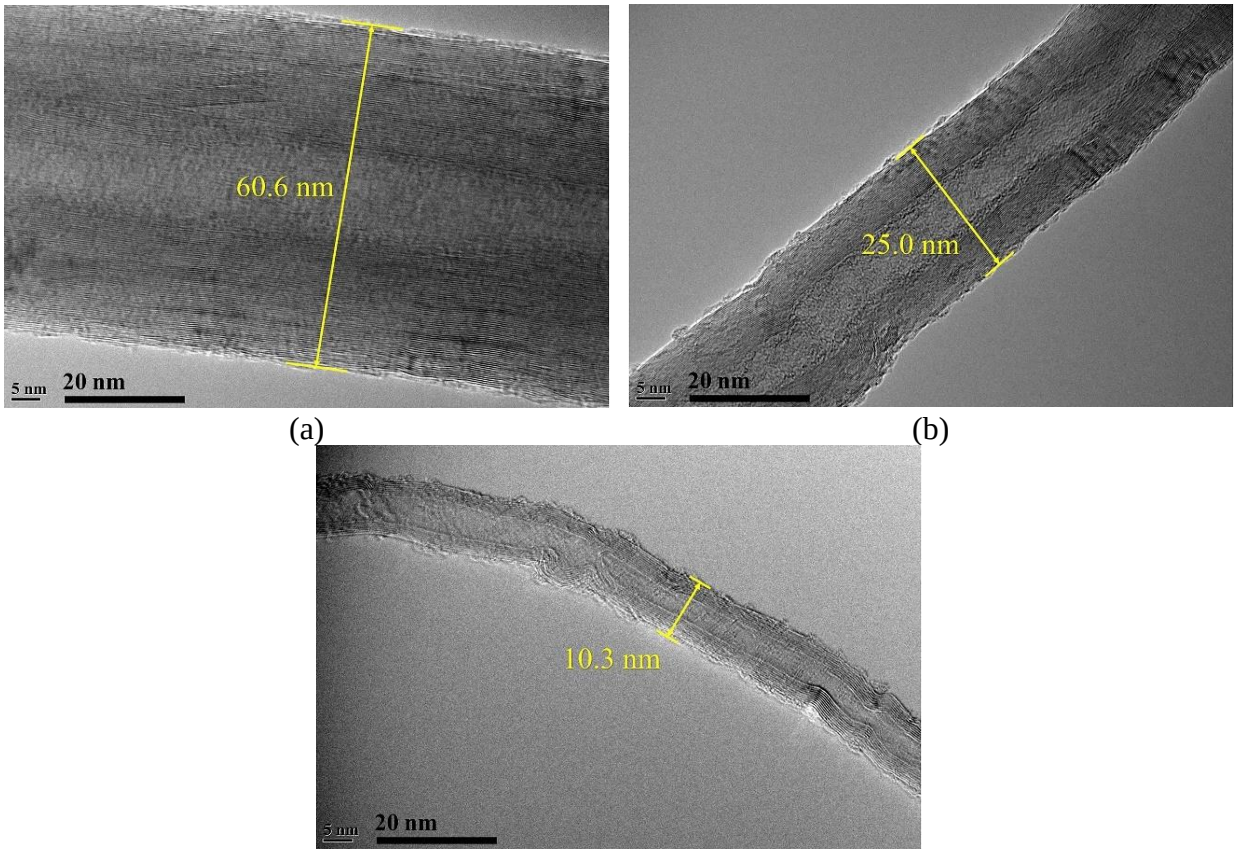

(a) (b)

(c)

Figure 36. TEM images showing the diameters of CNTs: (a) N10; (b) N20; (c) N50

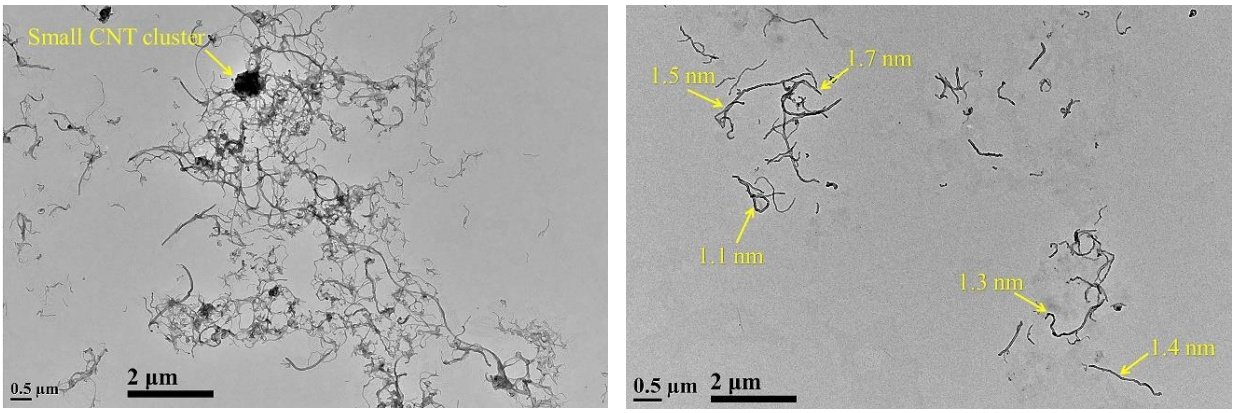

(a) (b)

Figure 37. TEM images showing the lengths CNTs: (a) N20; (b) S20

5.2.2. Dispersion characterizations

Figure 38(a ~ c) illustrate the volume weighted particle size distributions of CNT suspensions of different CNT geometries with 0.5%, 1%, and 2% CNT fractions, respectively. The particle size corresponding to the peak in the distribution curve is called ‘mode’ describing the size

with the highest frequency. As shown in Figure 38, for CNT suspensions with all the testing conditions, two particle size distribution types were observed, namely unimodal distribution with only one mode and bimodal distributions with two modes [34]. For example, as shown in Figure 38(b), S10-1 (short CNTs with the diameter around 10 nm in 1% CNT fraction) showed a distribution type of unimodal since there was only one mode located at approximately 64 μm. While the distribution type of S20-1 (short CNTs with the diameter around 20 nm in 1% CNT fraction) belonged to bimodal distribution, with two modes occurring at around 12 μm and 33 μm, respectively. Table 12 summarizes the distribution types of all the testing conditions. In order to clearly and quantitatively demonstrate and compare the size distributions or dispersion with different CNT geometries and fractions, in Table 12, the statistical analysis of the particle distribution in each testing condition was also presented, including the mode and geometric mean. The geometric means were calculated using the equation below [71]:

$$D_{mean} = \sum_{i=1}^{n} (V_i \cdot D_i). \tag{4}$$

where, n is the number of particle size classes, Vi is the volume in percentage with class i, and Di is particle size of class i. It is generally believed that particle size distributions with smaller mode sizes or smaller geometric means yield better dispersion. Because larger particles confirm the existence of bigger CNT clusters as the result of non-uniform dispersion.

When comparing the particle size distributions of CNT suspensions with different diameters, it is found that CNTs with larger diameters always had smaller mode sizes and smaller geometric means, indicating the better dispersions of thicker CNTs, holding CNT length and fraction the same. For instance, according to Figure 38(a), N10-0.5, N20-0.5 shared a same bimodal distribution. For N10-0.5, the volumes of 1st and 2nd mode were about less than 2% and 6%, respectively, implying that a larger proportion of CNTs had larger sizes. While for N20-0.5,

the volumes of 1st and 2nd mode were about 5% and 3%, respectively. This volume change of the modes indicated that as the increase of CNT diameter, CNTs were more likely to exist in the form of smaller particles or clusters rather than larger ones.

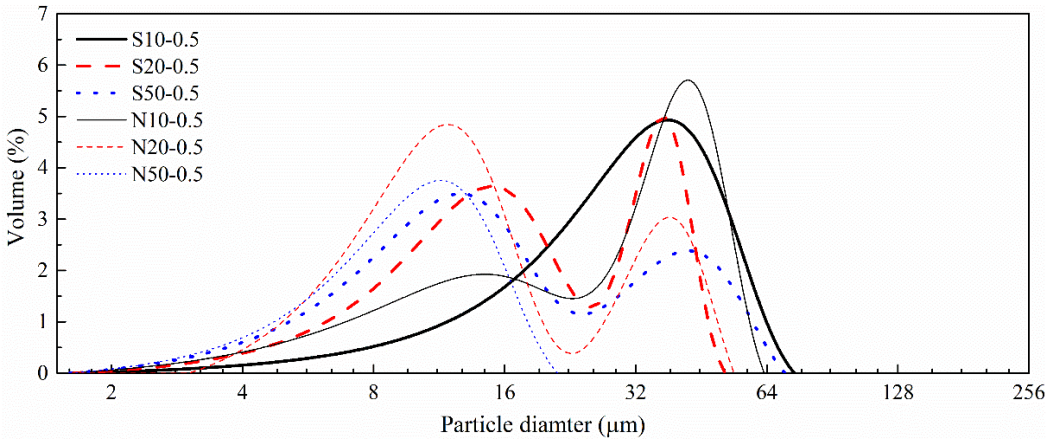

(a)

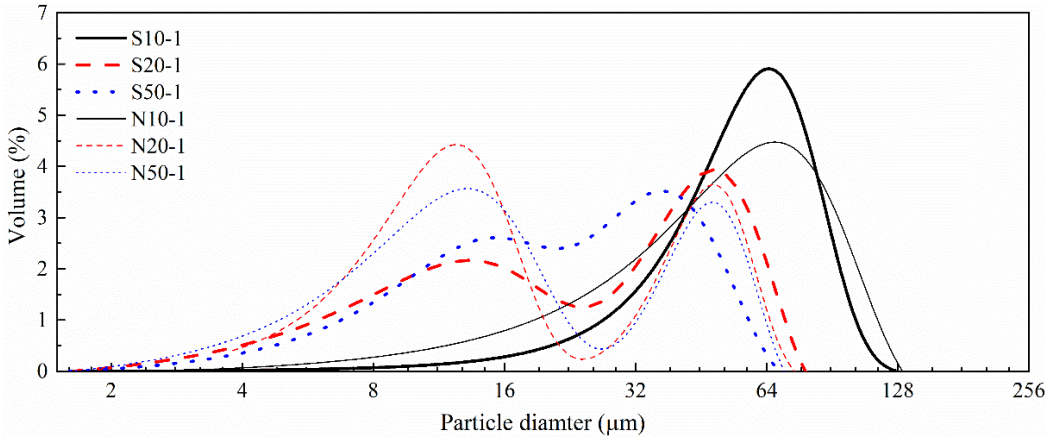

(b)

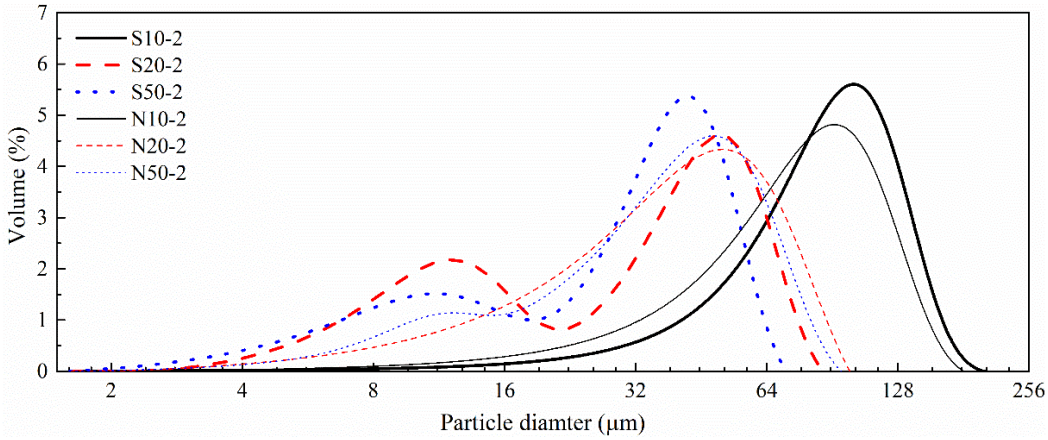

(c)

Figure 38. Volume weighted particle size distributions of CNT suspensions of different CNT geometries: (a) 0.5%; (b) 1%; (c) 2% CNT fractions

Table 12. Particle size distribution and its statistical analysis

Testing condition	Distribution type	1st Mode (μm)	2nd Mode (μm)	Geometric mean (μm)
S10-0.5	Unimodal	37.93	/	31.29
S10-1	Unimodal	64.56	/	56.93
S10-2	Unimodal	101.43	/	87.78
S20-0.5	Bimodal	14.94	36.86	20.34
S20-1	Bimodal	13.32	48.23	28.46
S20-2	Bimodal	12.09	50.20	33.00
S50-0.5	Bimodal	12.65	41.81	20.26
S50-1	Bimodal	15.28	36.86	24.31
S50-2	Bimodal	11.09	42.05	29.95
N10-0.5	Bimodal	14.43	42.05	27.78
N10-1	Unimodal	66.82	/	52.06
N10-2	Unimodal	91.51	/	76.30
N20-0.5	Bimodal	11.81	38.15	14.10
N20-1	Bimodal	12.37	48.19	28.72
N20-2	Unimodal	50.78	/	38.36
N50-0.5	Unimodal	11.40	/	10.10
N50-1	Bimodal	13.09	47.96	20.67
N50-2	Bimodal	12.19	48.23	37.55

Moreover, from Table 12, the 1st and 2nd modes as well as the geometric mean of N20-0.5 were 11.81 μm, 38.15 μm, and 14.10 μm, which were all smaller than the corresponding values of N10-0.5 (14.43 μm, 42.05 μm, and 27.78 μm), respectively. For N50-0.5, when further enlarging the diameter of CNTs, the dispersion was continually improved. As shown in Figure 38(a) and Table 12, the distribution type of N50-0.5 was converted into unimodal distribution with all the particles concentrating near the mode of 11.40 μm, and there was no larger particles or clusters to form the 2nd mode. It was evident that as the increase of CNT diameter, the particle size of CNTs in the suspension became smaller resulting in more uniform particle size distribution and dispersion. The same findings could also be drawn from CNTs with other lengths or fractions based on Figure 38 and Table 12.

According to comparisons of particle size distributions between different lengths, the mode sizes and geometric means of CNTs with normal length were often smaller than short CNTs, holding the same CNT diameters and fractions. Take the comparisons between N20-1 and S20-1

as example as shown in Figure 38(b). Both of them had bimodal distributions, but the mode sizes and geometric mean of S20-2 were 13.32 μm, 48.23 μm, and 28.46 μm which were precisely close to those of N20-2 (12.37 μm, 48.19 μm, and 28.72 μm), respectively as shown in Table 12. Regarding most of the other testing conditions with the same CNT diameters and fractions, the distribution parameters of normal-length CNTs were moderately smaller than short CNTs. On the contrary, there were also some cases that short CNTs had better particle size distribution than long CNTs, such as S20-2 and N20-2. In general, the differences of particle size distributions between normal-length and short CNTs were not significant enough to provide evident relationship between the dispersion states of CNTs with different lengths.

In addition to the effect of CNT geometries, the CNT fractions also had a considerable influence on the particle size distribution and dispersion of CNTs. By comparing CNTs with the same geometries but different percentages of additions, it was obvious that as the increase of CNT fractions, CNTs tended to have less uniform particle size distributions resulted from apparently larger distribution parameters. Because higher CNT fraction means more CNTs in a certain volume of solvent, leading to that CNTs are more likely to entangled together into larger CNT clusters.

The effects of CNT geometries and fractions on the dispersion characterizations could be verified by TEM images. Figure 39(a ~ f) show the TEM images for the dispersion states of N10-2, N20-2, N50-2 (different diameters), S20-2 (different lengths), N20-0.5, and N20-1 (different fractions). According to Figure 39(a) of N10-2, almost all the CNTs were entangled with each other into huge CNT clusters, and there were very few individual CNTs apart from those clusters. With the increase of CNT diameter as shown in Figure 39(c) of N20-2, not only the size of cluster significantly reduced, but also many CNTs were separated from the medium-sized cluster, indicating a more uniform dispersion compared to N10-2. When further enlarging the CNT

diameter to 50 nm as shown in Figure 39(e) of N50-2, most of CNTs were relatively well dispersed with only two smaller clusters within the image area. Comparisons among CNTs with different diameters in the TEM images confirmed that thicker CNTs were prone to have better dispersion characterizations than thinner CNTs. With the same CNT additions, the reduction of CNT diameter increased the surface area and aspect ratio of the tubes leading to stronger interaction among each CNT. Thus, CNTs with small diameter are expected to aggregated tightly with each other yielding non-uniform dispersion.

By comparing the TEM images of CNTs with different lengths as shown in Figure 36(b) and 39(e), N20-2 and S20-2 had similar dispersion characterizations with a CNT cluster surrounded by many separate CNTs. However, the cluster size of N20-2 was fairly larger than of S20-2 indicating the better dispersion of short CNTs, which was consistent with the results from particle size analysis. The effect of CNT length on the dispersion was not pronounced because the variation of length did not significantly change the surface area, so that the attraction forces among each CNT nearly remained the same level. Therefore, the dispersion characterizations of CNTs with different lengths were very similar.

Moreover, the comparisons of dispersion characterizations among CNTs with different fractions were revealed by Figure 39(b ~ d). It was evident that N20-0.5 and N20-1 were free of any clusters showing a more preferable dispersion than N20-2. Although there was no noticeable difference between 0.5% and 1% CNT fractions, the dispersion characterization of N20-0.5 seemed to be slightly better than that of N20-1. Since CNTs with higher addition have higher possibility to interact or entangle with each other, it was understood that higher CNT fractions normally exhibit non-uniform dispersion.

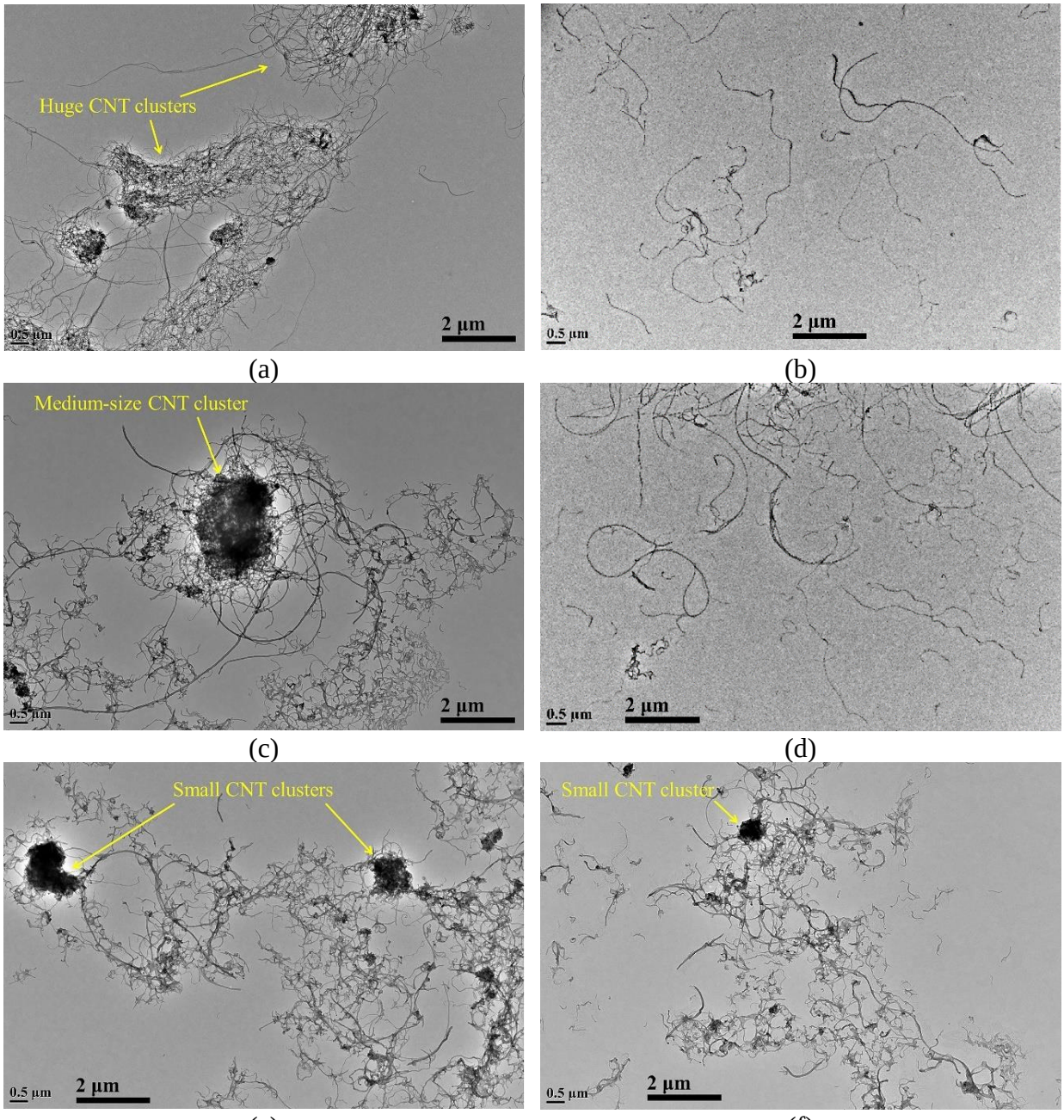

Figure 39. TEM images showing the real dispersion states of CNTs with different geometries and fractions: (a) N10-2; (b) N20-0.5; (c) N20-2; (d) N20-1; (e) N50-2; (f) S20-2

5.2.3. Bonding performances

Bonding performances are of top priority to the overall performance of epoxy composites. Figure 40(a ~ c) illustrate the average stress-strain curves of CNT reinforced epoxy composites among different CNT geometries with 0.5%, 1%, and 2% CNT fractions, respectively. According

to Figure 40, all the curves shared a similar changing trend regardless of CNT geometries and fractions. As the increase of strain, the stress went up with a sharper slope at the beginning. After the strain reached at over 0.5, an inflection point was observed with the stress increasing remarkable slower and obviously dropping at the end.

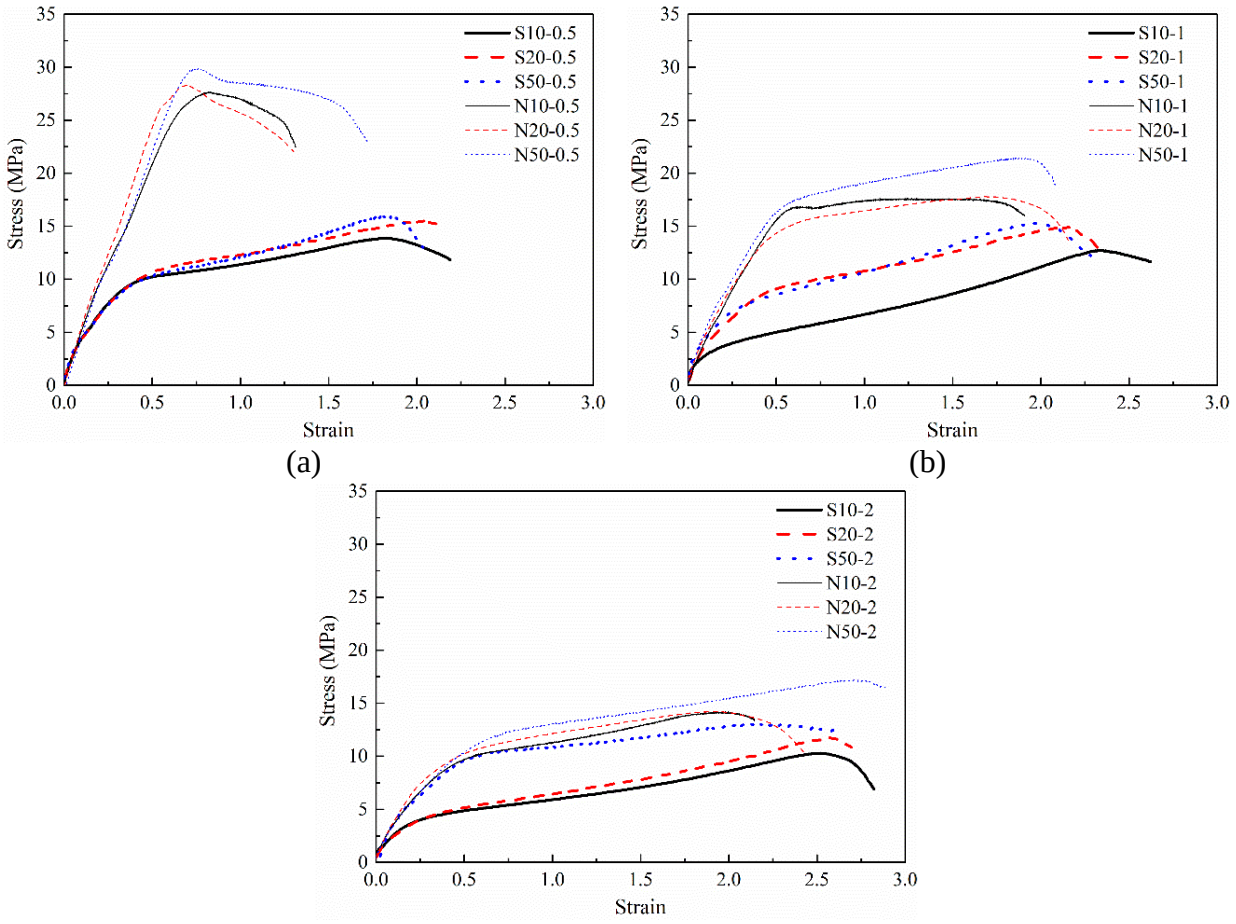

Figure 40. Average stress-strain curves of CNT reinforced epoxy composites with different CNT geometries: (a) 0.5%; (b) 1%; (c) 2% CNT fractions

The shape of the stress-strain curves could be interpreted by pulling-out of the CNTs which is widely believed as one of the major reinforcing mechanisms of CNTs. At the beginning when the epoxy composites and CNTs were firmly bonded, they worked together as a strong integrity to bear the external loading. Owing to different moduli between epoxy and CNTs, when the strain increased to the ultimate shear strain of epoxy, the epoxy matrix was fractured and deactivated,

which reduced the overall shear modulus. Although a part of CNTs started to be pulled-out from the surrounding epoxy matrix, the rest part kept well bonded and continually worked to bear the loading. As the pulling-out part extended, the remaining CNTs were not able to bear the loading, catastrophic fracture occurred and CNT reinforced epoxy composites failed [52, 93].

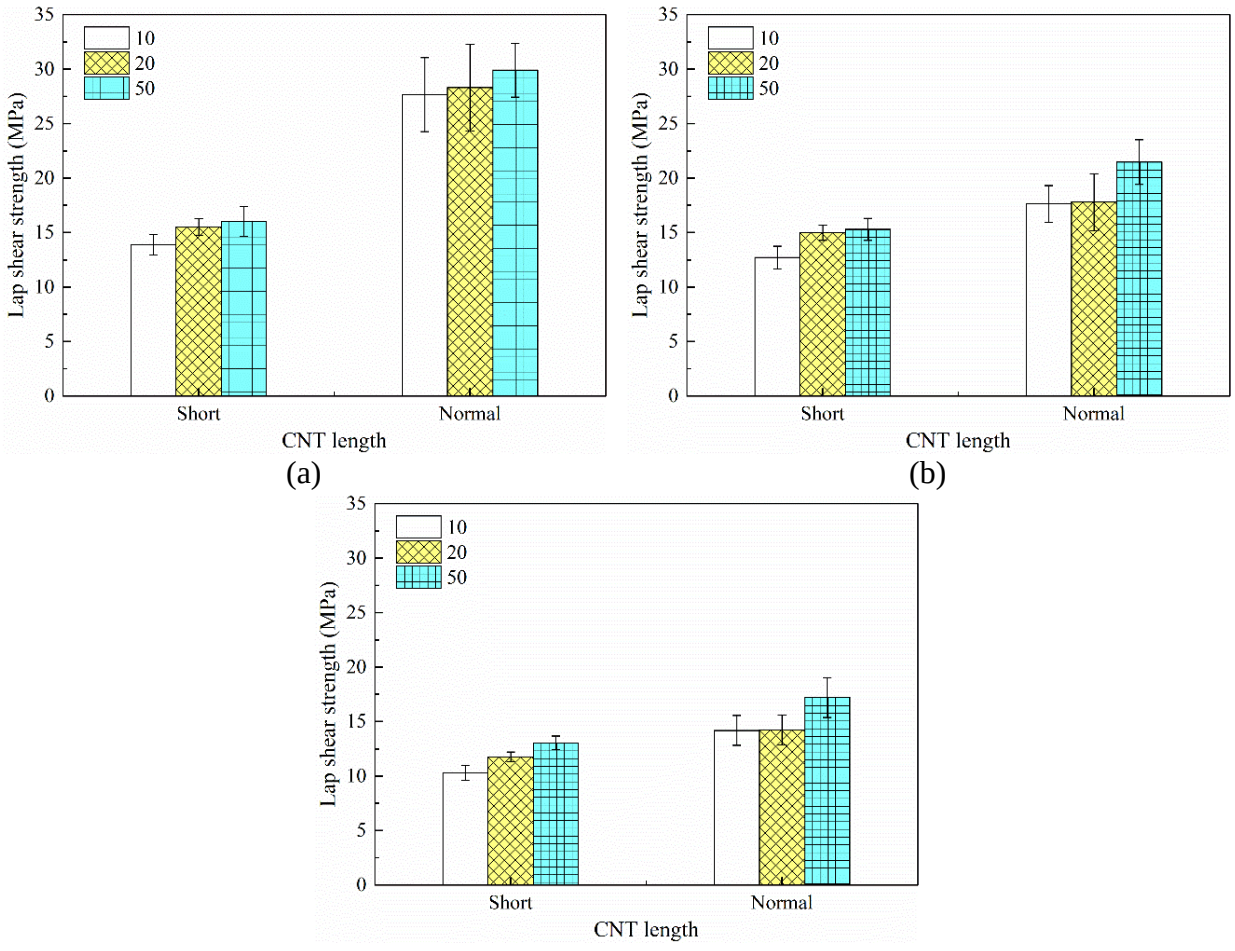

Figure 41. Bonding strenths of CNT reinforced epoxy composites with different CNT geometries: (a) 0.5%; (b) 1%; (c) 2% CNT fractions

The bonding strength was identified as the highest stress in the stress-strain curves. Figure 41(a ~ c) show the bonding strengths of CNT reinforced epoxy composites among different geometries with 0.5%, 1%, and 2% CNT fractions, respectively. As shown in Figure 41(a), the bonding strength of N20-0.5 (normal length, 20 nm diameter and 0.5% CNT fraction) was 28.30 MPa which was slightly higher than that of N10-0.5. After further increasing the diameter to 50

nm, the bonding strength reached 29.90 MPa with about 8% increase compared to N10-0.5. For CNT reinforced epoxy composites with the other lengths and fractions, similar increasing trends were observed. The most noteworthy improvement was obtained by N50-1, with increase of around 22% compared to N10-1. It was known that the dispersion characterization of CNTs had a decisive effect on the bonding strength and bonding performances of CNT reinforced epoxy composites, and CNTs with larger diameters normally have better dispersion characterizations [56]. Therefore, epoxy composites reinforced by thicker CNTs tend to have higher bonding strength due to the more uniform dispersion.

As for the influence of CNT length on the bonding strength of CNT reinforced epoxy composites, it was obvious in Figure 41 that with the same CNT diameters and fractions, the bonding strengths of epoxy composites reinforced by normal-length CNTs were much higher than those reinforced by short CNTs. Especially, the lap strength of N10-0.5 was almost twice as much as that of S10-0.5. Furthermore, it was noted that the bonding strength of N10-0.5 was even a little higher than that of S50-0.5, and this trend was valid for the other CNT fractions of 1% and 2%. Given that the dispersion characterizations of S50-0.5, S50-1, and S50-2 were much better than those of N10-0.5, N10-1, and N10-2 respectively as shown in Figure 38 and Table 12, epoxy composites reinforced by longer CNTs yielding stronger bonding strengths cannot be simply explained by the effect of dispersion characterization. It was reported in the literature [95, 96] that CNTs with very small lengths were difficult to accomplish a sufficient stress transfer between them and the surrounding epoxy matrix. When lacking interfacial bonding and anchoring on the CNT-epoxy interface, short CNTs were expected to have the similar detrimental effect as imperfections which reduced the stiffness and continuity of the epoxy matrix [97]. On the other hand, by comparing the bonding strength of CNT reinforced epoxy composites with different CNT

fractions, as the increase of CNT addition, the bonding strength kept dropping due to more non-uniform CNT dispersion.

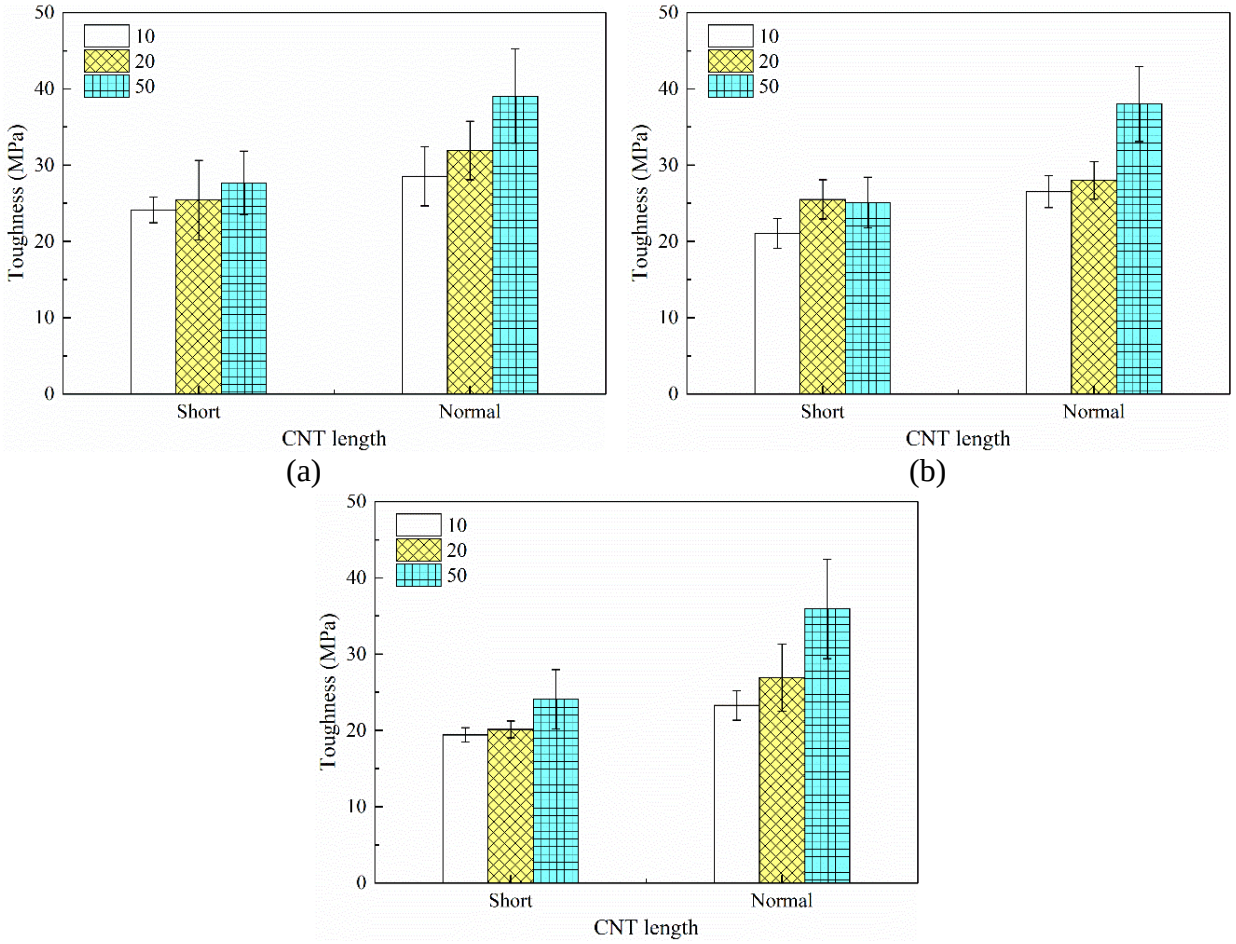

Figure 42. Toughness of CNT reinforced epoxy composites with different CNT geometries: (a) 0.5%; (b) 1%; (c) 2% CNT fractions

In addition to bonding strength, the area under the stress-strain curve could be integrated as toughness which is another important adhesion parameter describing the ability of energy absorption and plastic deformation. Based on Figure 40, Figure 42(a ~ c) show the comparisons of toughness among CNT reinforced epoxy composites with different geometries and fractions. Similar as the changing trend of bonding strength, as the increase of CNT diameter, the toughness of CNT reinforced epoxy composites also improved. As shown in Figure 42(a), the toughness of N50-0.5 was 36% and 22% higher than those of N50-0.5 and N50-1, respectively. The most

tremendous enhancement was also achieved by N50-1, with the increments reaching 54% compared to N10-1. It was worth noting that nearly all the increments in toughness with the same testing conditions were more significant than those in bonding strength. Considering toughness is determined by both strength and ductility, the increase of CNT diameter not only improved the bonding strength, but also enhanced the deformability and ductility of CNT reinforced epoxy composites.

When comparing CNT reinforced epoxy composites with the same CNT diameter and fractions but different lengths, Figure 42 demonstrates that the toughness of epoxy composites reinforced by normal-length CNTs was always markedly better than those by short CNTs. The improvement in toughness of N50-1 was as much as 52% higher compared to S50-1 in particular. The variation in toughness between epoxy composites reinforced by normal-length and short CNTs was attributed to the same mechanism in bonding strength as discussed above. Since insufficient stress transfer between short CNTs and epoxy leading to discontinuity and imperfections of the matrix as a whole, undoubtedly the toughness of short CNT reinforced epoxy composites was rather limited. Moreover, the changing trend of CNT fractions in bonding strength was still valid in toughness. As the increase of CNT fraction, the toughness of CNT reinforced epoxy composites decreased as a results of non-uniform CNT dispersion.

5.2.4. SEM analysis on fracture surfaces

To further investigate the dispersion state of CNTs into the epoxy matrix as well as understanding the mechanisms of CNT geometries behind the experimental data, SEM images were also taken on the fracture surfaces of epoxy composites as illustrated in Figure 43(a ~ f) including N10-0.5, N20-0.5, N50-0.5 (different diameters), S50-0.5 (different length), N50-1 and N50-2 (different fractions). It was found in Figure 43(a) for N10-0.5 that there was a huge CNT

clusters with the estimated diameter of 28.0 μm, along with several small clusters. With the increase of CNT diameter for N20-0.5 as shown in Figure 43(c), the size of the biggest CNT cluster reduced significantly to around 14 μm, and further reduced to around 10.0 μm for N50-0.5 as shown in Figure 43(e). It was confirmed that epoxy composites reinforced by thicker CNTs had better dispersion which contributed to better bonding strength and toughness.

Figure 43(e, f) compare the typical SEM images of CNT reinforced epoxy composites with different lengths. The sizes of CNT clusters of N50-0.5 were visibly smaller than those of S50-0.5 indicating the better dispersion characterizations and bonding performances of epoxy composites reinforced by normal-length CNTs. By comparing N50-0.5, N50-1, and N50-2 as shown in Figure 43(b, d, e), CNT reinforced epoxy composites with lower CNT fraction had smaller clusters leading to more uniform CNT dispersion and stronger adhesion. In general, the sizes of CNT clusters demonstrated in each SEM image were consistent with the measurements in particle size analysis, which proved the validation and accuracy of the experimental results. Except those CNT clusters, there was also a great deal of individual CNTs as demonstrated in Figure 43(b) as well as other figures. Although those thoroughly and homogeneously dispersed CNTs overnumbered CNT clusters a lot, the global dispersion characterization was still dominated by CNT clusters.

The SEM images of N10-0.5 and N50-0.5 as shown in Figure 43(a) and 43(c) were further scanned at high magnification as shown in Figure 44(a, b). It was observed in Figure 44(a) that the phenomenon of CNT pulling-out was not significant. For most visible CNTs, the main part of the length was still buried into the epoxy with only a tip exposed above the matrix surface. However, as shown in Figure 44(b), a large part of CNTs had been considerably pulled out from the epoxy matrix, although the pulled-out length varied with each individual CNT. The process of CNT pulling-out was discussed in the last section. Since a lot of energy was consumed by the pulled out

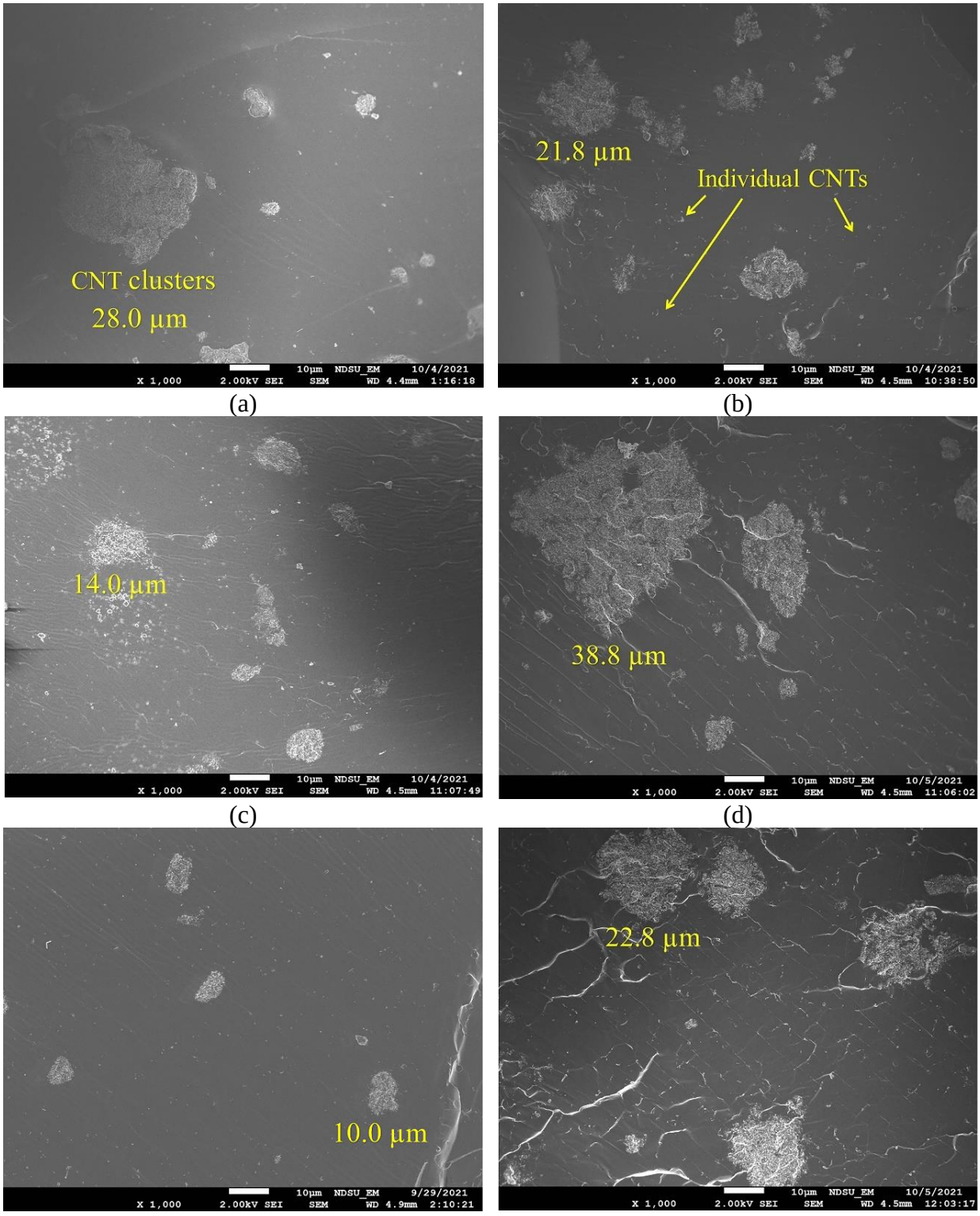

(a) (b)

(c) (d)

(e) (f)

Figure 43. SEM images on the fracutre surfaces of CNT reinforced epoxy composites: (a) N10-0.5; (b) N20-1; (c) N20-0.5; (d) N20-2; (e) N50-0.5; (f) S50-0.5

CNTs, this comparison verified that the toughness of CNT reinforced epoxy composites with larger CNT diameters was higher than that with thinner ones, and similar phenomena could also be found between CNT reinforced epoxy composites with different CNT lengths and fractions. It was noted that more CNT pulling-outs prompted the energy consumption, improved the toughness and eventually resulted in better bonding performances.

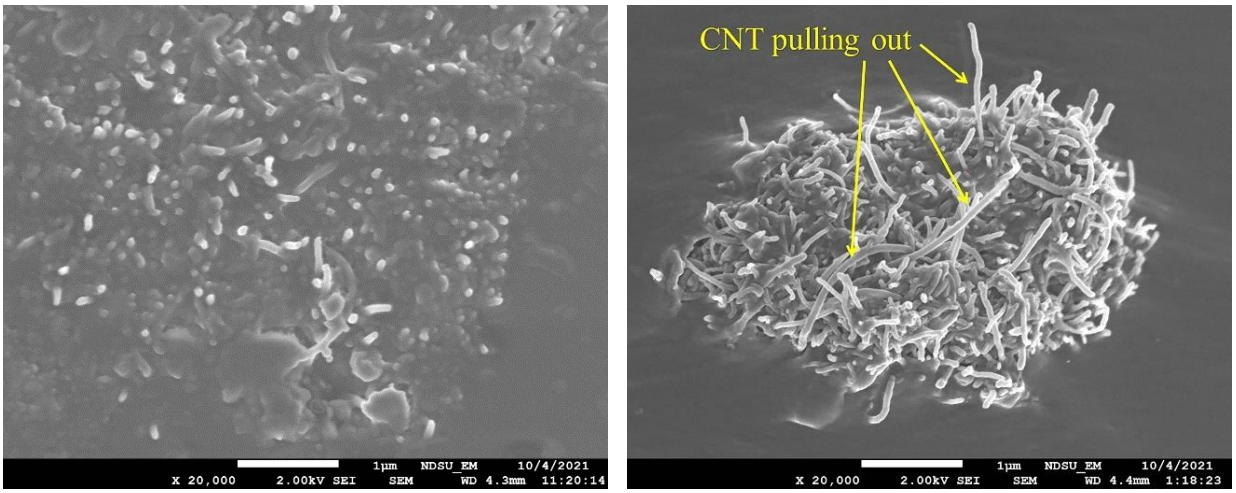

(a) (b)

Figure 44. SEM images at high magnification: (a) N10-0.5; (b) N50-0.5

5.3. Summary

The main objective of this chapter was to investigate the effects of CNT geometries on the dispersion characterizations and bonding performances of CNT reinforced epoxy composites. CNTs with different geometries were dispersed into pure acetone solution by a new mixing protocol, and dispersion characterizations of the CNT suspensions were studied by particle size analysis and TEM. The bonding performances of CNT reinforced epoxy composites were exanimated by SLS tests and SEM. Based on the findings, following conclusions can be drawn:

(1) The TEM analysis confirmed that the diameter and length of CNTs were not evidently affected by newly-developed mixing protocol. After the mixing process, CNTs were able to keep their original diameters and lengths.

(2) CNT suspensions with larger CNT diameters were more likely to have smaller particle size as a result of better dispersion characterizations. This was because smaller CNTs exhibited larger surface area and aspect ratio which normally resulted in stronger interaction to entangle CNTs together as CNT clusters.

(3) Due to the more uniform dispersion of CNTs, epoxy composites reinforced by thicker CNTs had better bonding performances not only in the higher bonding strength but also higher toughness implying better ductility and deformability.

(4) For the effect of CNT length, according to both particle size and TEM analysis, there was no evident difference between the dispersion characterizations of CNT suspensions with normal-length and short CNTs. Since the variance of CNT length did not significantly change the surface area of CNTs, so that the attraction forces among each CNT nearly remained the same level. However, the bonding performances of CNT reinforced epoxy composites with normal-length CNTs were much better than those with short CNTs, with the increments could reach as much as 100% in bonding strength and 52% in toughness. In addition, as the increase of CNT fractions, both dispersion characterizations and bonding performances deteriorated owing to severe CNT agglomeration.

CHAPTER 6. CNT REINFORCED EPOXY COMPOSITES USING CMC SURFACE TREATMENT AS A NOVEL MIXING METHOD

In this chapter, a new CNT physical surface treatment method using carboxymethyl cellulose (CMC) was proposed to improve the dispersion effectiveness of CNTs in epoxy matrix-based composite. The dispersion characterizations and bonding performance of CNTs reinforced epoxy composites treated with CMC were systematically investigated. For dispersion characterizations, Raman spectroscopy was carried out to prove the effectiveness of CMC treatment on the surface of CNTs. Particle size analysis was also conducted to directly reflect the dispersion state of CNTs with and without CMCs. The wettability and bonding performance of pristine CNTs and CNTs/CMCs reinforced epoxy-based composites were examined by contact angle test and SLS tests respectively. In addition, TEM and SEM analyses were also performed on the individual CNTs, CNT aqueous solution and CNTs reinforced epoxy composites to reveal the dispersion-modifying mechanism and result of CMCs.

6.1. Experimental Setup

6.1.1. Materials

Same epoxy resin and steel substrates were used in this chapter. For CNTs, because of the test results in the last chapter, the diameter and length of the tubes were selected optimally as 50-100 nm and 5-20 μm respectively. The surfactant used in physical surface treatment was a water dispersible sodium salt of carboxymethyl ether of cellulose (sodium CMC 419273) obtained from Sigma-Aldrich Corp with formula of C28H30Na8O27 and an average mole weight around 90,000.

6.1.2. CMC surface treatment to CNTs

To prepare the CMC surface treated CNTs, CMCs with a constant weight fraction of 0.5% [98] were gradually added into deionized water (DI) while the solution was mechanically stirred

by a magnetic rod on a magnetic stirrer at a speed of 1600 rpm. After CMCs were thoroughly dissolved in the DI water, CNTs were dispersed in the CMC solution with the same mechanical stirring. To ensure a good dispersion as well as sufficient interact between CNTs and CMCs, the aqueous suspensions were further mechanically mixed on a tube rotator for 24h at a speed of 30 rpm. The whole mixing procedures of CNT aqueous suspensions are shown in Figure 45. The CMC surface treatment method did not involve any ultrasonic process to avoid reducing the CNT geometry and keep CNTs intact. Three different CNT fractions (0.5%, 1% and 2%) were considered to study the effect of CMCs on slightly-, mediumly- and highly-aggregated CNTs. For each CNT fraction, CNT suspensions without the CMC treatment were also prepared as the control groups.

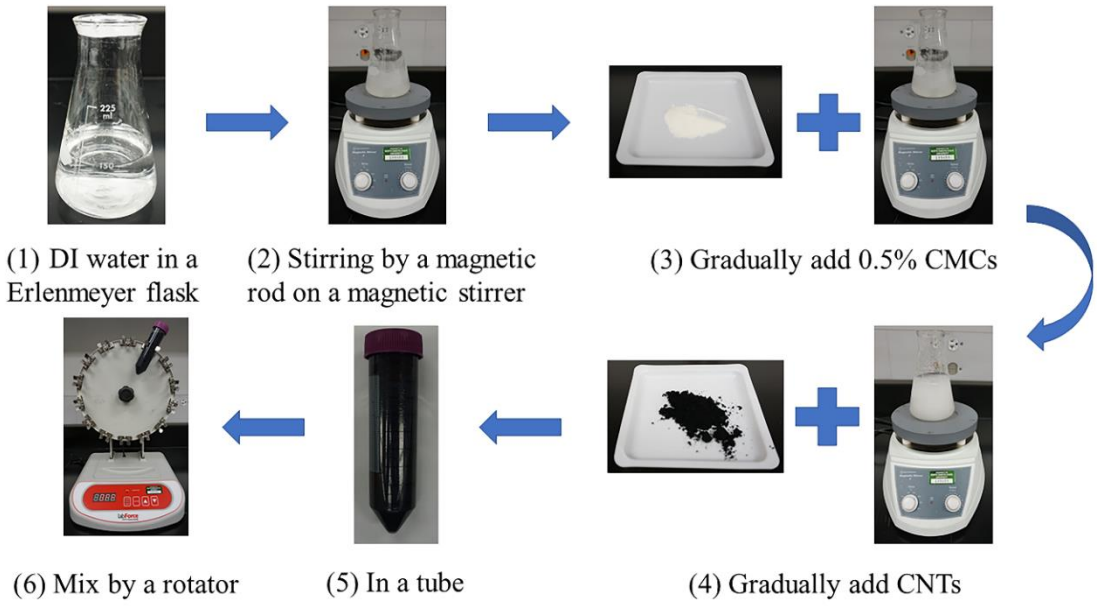

Figure 45. CMC and CNT mixing procedures

6.1.3. Dispersion characterizations

The dispersion characterizations of pristine CNTs and CMC treated CNTs prepared in last section were evaluated by Raman spectroscopy and particle size analysis. Raman spectroscopy was performed using Aramis Confocal Raman Imaging Raman System, Horiba Jobin Yvon's

Raman spectrometer equipped with a 532 nm laser and a 10X magnification objective lens. The recorded region was from 800 cm-1 to 2400 cm-1. Particle size analysis was conducted using Particle Sizing Systems SPOS 780 which is capable of detecting particle sizes from 0.5 nm to 400 μm. Using DI water instead of epoxy resin as the solution for dispersion characterizations was because resin and curing agent could severely contaminate the test instruments.

6.1.4. Bonding performance

Bonding performances are the top priorities of the epoxy composites, especially when they are used in adhesive joints. The experimental set-up and testing protocols are the same as described in the previous chapters. For a clear presentation of the testing conditions, the test matrix is displayed in Table 13. In total, six different testing conditions including three CNT weight fractions (0.5%, 1%, and 2%) and two adhesive materials (pristine CNTs and CMCs treated CNTs), were involved in this chapter.

Table 13. Results of SLS tests in Chapter 6

Testing condition	Adhesive material	CNT fraction (%)	Bonding strength (MPa)	STD (%)	Fracture strain	STD (%)
C0.5	Pristine CNTs	0.5	16.57± 1.12	6.76	1.11 ± 0.084	7.57
CC0.5	CMC treated CNTs	0.5	20.12 ± 1.74	8.65	1.55 ± 0.100	6.45
C1	Pristine CNTs	1	19.21 ± 1.31	6.82	1.40 ± 0.083	5.85
CC1	CMC treated CNTs	1	25.43 ± 1.87	7.35	1.85 ± 0.149	8.01
C2	Pristine CNTs	2	15.85 ± 1.29	8.13	0.91 ± 0.085	9.34
CC2	CMC treated CNTs	2	22.44 ± 1.71	7.62	1.76 ± 0.116	6.59

6.2. Experimental Results and Discussions

6.2.1. Raman spectroscopy

Raman spectroscopy was used in this chapter to show the structural differences between pristine CNTs and CMCs coated CNTs. Normalized Raman spectra of pristine CNTs and CMCs coated CNTs with different CNT fractions are illustrated in Figure 46(a ~ c). As shown in Fig 45, all the spectra exhibited two main typical peaks referring to D band around 1345 cm-1 and G band

around 1373 cm-1. The locations of those two brands were consistent with the results in the literature [99,100].

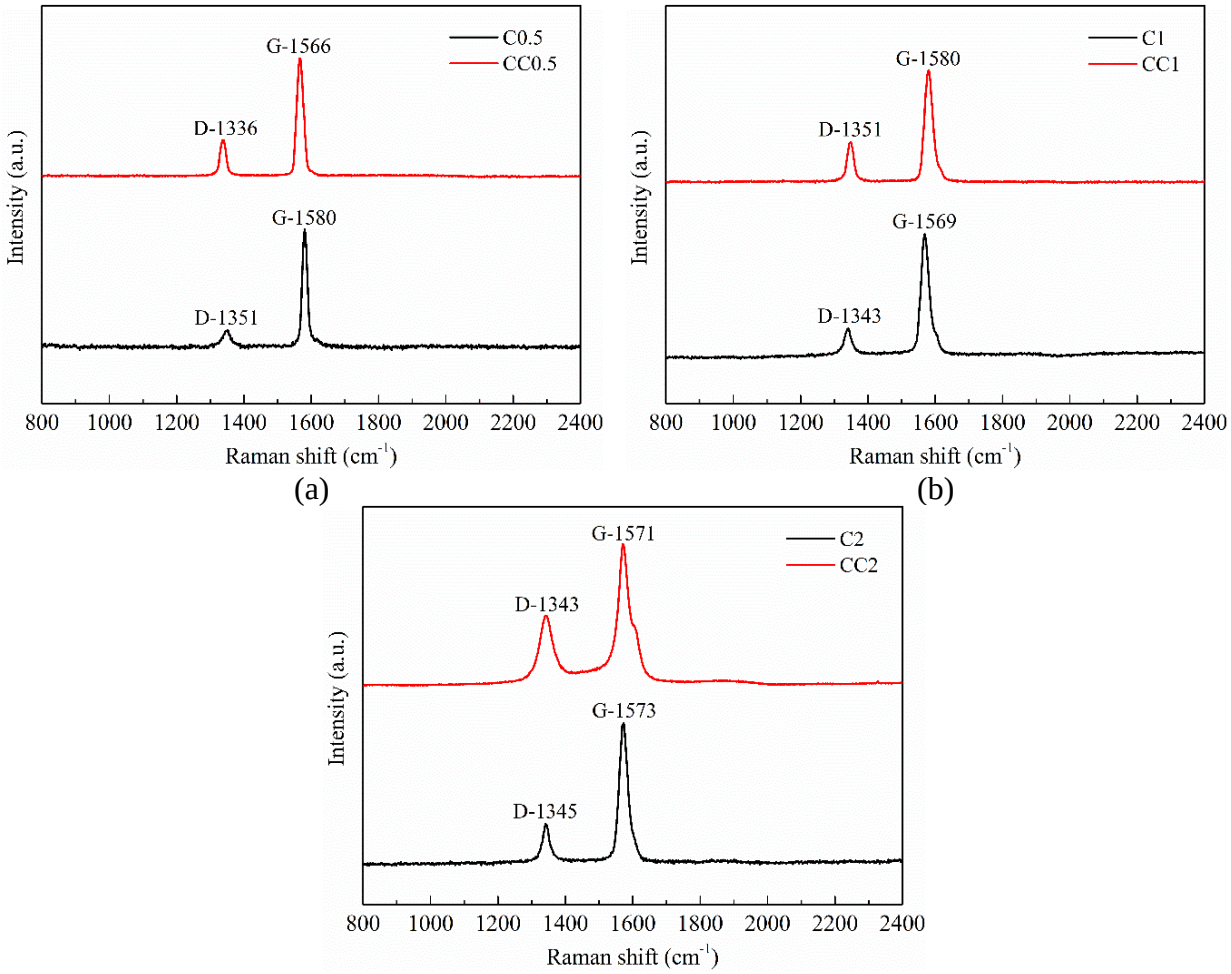

Figure 46. Raman spectra of pristine CNTs and CMCs coated CNTs with different CNT fractions: (a) 0.5%; (b) 1%; (c) 2%

It is noted that D band reflects the existence of defects, while G band represents the normal C-C bond of the carbon system [101], and the intensity ratio between D and G band, ID/IG is able to indicate the density of disordered structures due to any surface treatments on the CNTs [102]. The ID/IG ratios of pristine CNTs were 0.15, 0.24, and 0.3 for three CNT fractions of 0.5%, 1%, and 2%, respectively. After CMC treatments, the corresponding ratios increased to 0.3, 0.36 and 0.5, respectively. In terms of all CNT fractions, the increases of ID/IG ratios proved the

effectiveness of CMC treatment indicating that CMCs were attached on the surface of CNTs and changed the physical and chemical structures of the CNTs. The attached CMCs were expected to help achieve a better CNT dispersion.

6.2.2. Particle size analysis

The dispersion state of CNTs depends on various factors such as type, geometry, shape and surface condition. Among all those methods to evaluate the dispersion state of CNTs, particle size analysis is the most direct ways to quantitively demonstrate the size and the distribution of CNT agglomeration. Figure 47(a ~ f) presents the particle size distributions of pristine CNTs and CMCs coated CNTs with different CNT fractions. It is obviously shown that all the particle size distributions followed an approximate normal distribution pattern, so that the average diameter is equal to the median diameter with the highest volume. As shown in Figure 47(a, c, e), The average diameters of pristine CNTs with three CNT fractions (0.5%, 1%, and 2%) were 9.4 μm, 16.3 μm, and 19.5 μm, respectively, implying that the agglomerations were more severe with higher CNT fractions. According to Figure 47(b, d, f), the average diameters of CMC treated CNTs were 7.2 μm, 8.6 μm, and 10.3 μm for the three CNT fractions, respectively. By comparing pristine CNTs and CMC treated CNTs for each fraction, the average diameters reduced significantly by 23%, 47%, and 47%, correspondingly. The results clearly indicated that large CNT clusters were broken up into smaller one with CMC surface treatment which greatly improved the dispersion states of CNTs. The particle size reduction was less significant for slightly-aggregated (0.5%) CNTs because CNTs were less likely to form CNT agglomerations with the lower fraction.

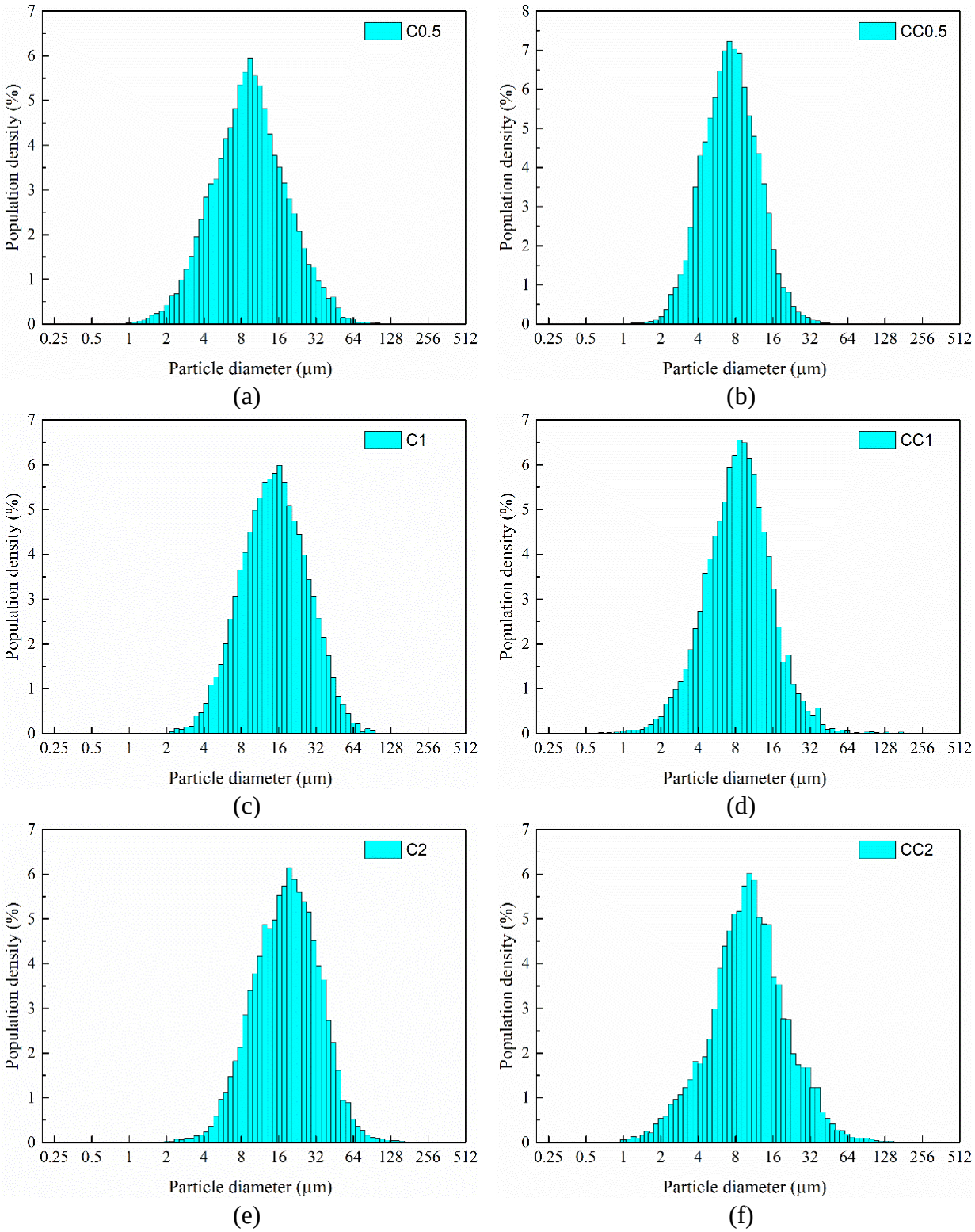

Figure 47. Particle size distributions of pristine CNTs and CMCs coated CNTs with different CNT fractions: (a) C0.5; (b) CC0.5; (c) C1; (d) CC1; (e) C2; (f) CC2

6.2.3. TEM analysis

The effectiveness of CMCs treatment was further illustrated by TEM analysis. The TEM observations of pristine CNTs and CMCs coated CNTs with different CNT fractions are displayed in Figure 48(a ~ f). A relatively low magnification of 0.5 μm was used to show the overall dispersion states. According to Figure 48(a, c, e), without any special dispersion methods, the dimension of those CNT clusters become larger as the increase of CNT fractions. 0.5% CNTs were only slightly aggregated, while almost all visible CNTs were entangled with 2% CNT addition. Moreover, Figure 48(a, d), (b, e) and (c, f) compare the dispersion states of pristine CNTs and CMC coated CNTs with the same fractions. For pristine CNTs, almost all of the CNTs were entangled into CNT clusters without the presence of any individual CNTs. While for CMCs coated CNTs some agglomerated CNTs were broke up into individual CNTs and the dimension of the rest CNT clusters were apparently reduced resulting in more uniform CNT distribution states. Thus, it was evidently confirmed that CMC treatment was effective in mitigating CNT agglomerations and eventually improving the dispersion of CNTs.

To further reveal the dispersion modifying mechanism of CMCs treatment, Figure 49(a, b) present the typical TEM images of individual pristine CNTs and CMCs coated CNTs at a higher magnification. The sidewall of the pristine CNT was sharp and clear in Figure 49(a). For the CMCs coated CNTs, a thin layer was observed outside the sidewall of the CNT as shown in Figure 49(b). The boundary of pristine CNT was obviously smoother than the boundary of CMCs coated CNTs. It was directly proved that CMCs were attached on the sidewall of the CNTs forming an amorphous layer which helped build up a better CNT dispersion state.

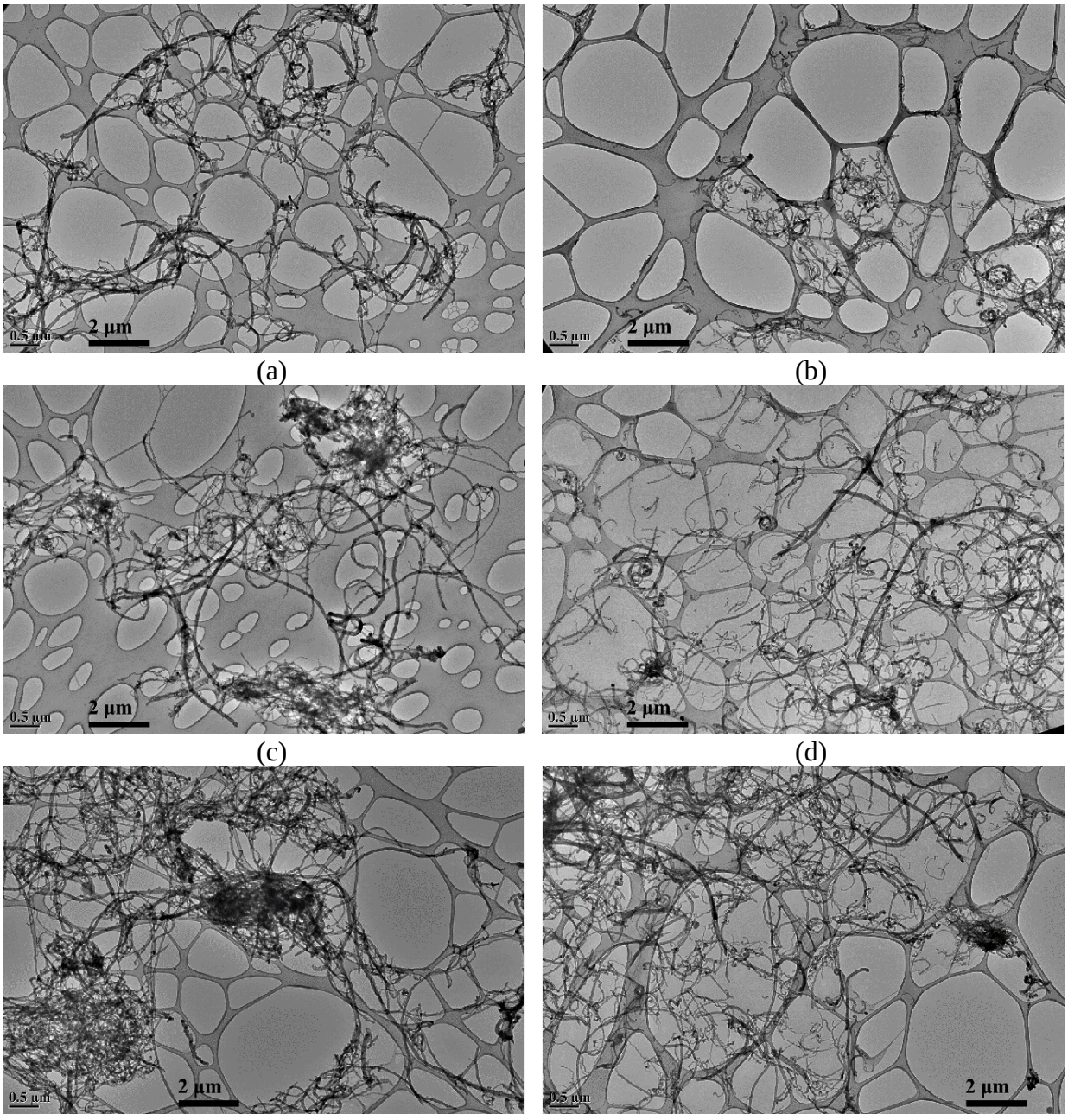

Figure 48. TEM observations of pristine CNTs and CMCs coated CNTs with different CNT fractions: (a) C0.5; (b) CC0.5; (c) C1; (d) CC1; (e) C2; (f) CC2

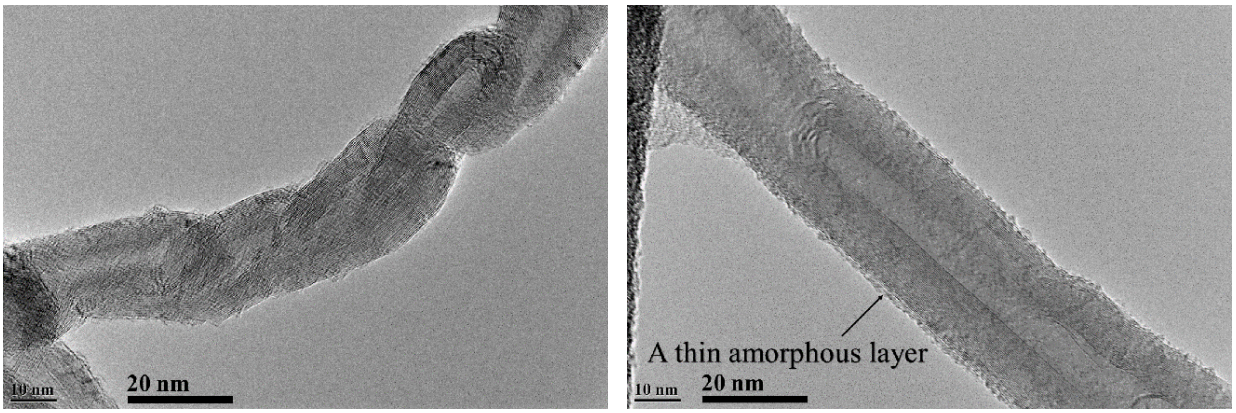

(a) (b)

Figure 49. Typical TEM images of individual pristine CNTs and CMCs coated CNTs at a higher magnification: (a) pristine CNTs; (b) CMCs coated CNTs

6.2.4. Contact angle test

As for CNTs reinforced epoxy composites, wettability is of vital importance on the bonding performances especially the interfacial adhesion. It is found that epoxy composite is unable to gain a solid bond without sufficient interfacial adhesion between adhesives and substrates [50]. Figure 50(a ~ f) display the appearance of CNTs reinforced epoxy droplets and their contact angles on steel substrates. As shown in Figure 50(a, b, c), the contact angle of 0.5% pristine CNTs reinforced epoxy was 44.9º. With the increase of CNT fractions to 1%, the contact angle was lowered to 43.0º indicating higher wettability and interfacial adhesion. While further adding the CNT addition to 2%, the contact angle increased to 45.1º which was even higher than the contact angle of 0.5% pristine CNTs reinforced epoxy. The CNT agglomeration led to the further increase of contact angle from 1% to 2% CNT fractions. CMCs/CNTs reinforced epoxy showed a similar trend with the increase of CNT fractions as shown in Figure 50(d, e, f). The contact angle of 0.5% pristine CNTs reinforced epoxy came to be the highest, although epoxy composites with 1% CNT addition still yielded the best. Regarding pristine CNTs and CMCs/CNTs reinforced epoxy with the same CNT additions, it is clearly observed in Figure 50(a, d), (b, e) and (c, f) that CMCs/CNTs reinforced epoxy had smaller contact angles than pristine CNTs reinforced epoxy. This finding

showed that CMC treatments improved the wettability of CNT reinforced epoxy composites, and the deterioration of CNT dispersion state also had a negative influence on the wettability of the composites and interfacial adhesion at the adhesive-substrate interface.

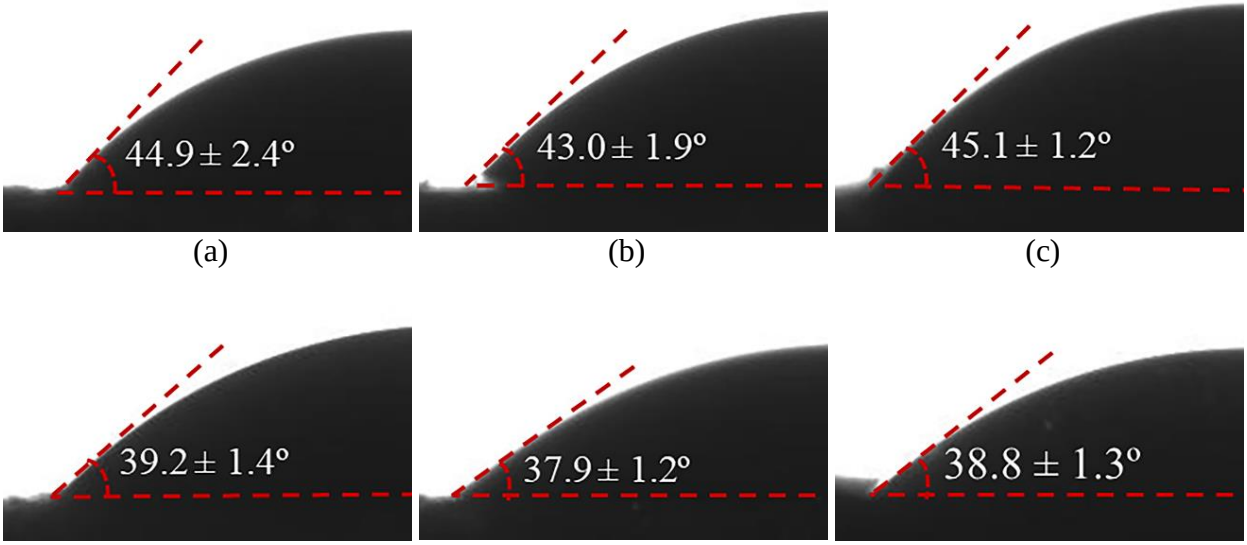

(a) (b) (c)

(d) (e) (f)

Figure 50. CNTs reinforced epoxy droplets and their contact angles: (a) C0.5; (b) C1; (c) C2; (d) CC0.5; (e) CC1; (f) CC2

6.2.5. SLS test

Figure 51(a) presents the typical stress-strain curves of all the SLS specimens tested in this chapter. All the curves shared a similar pattern with a practically linear stage followed by a nonlinear stage, while the degrees of nonlinearity varied among each curve. To compare the nonlinearities quantitively, Figure 51(b) demonstrates the areas under all the curves which are regarded as the toughness indicating the ability of plastic deformation and energy consumption. The toughness of 0.5% pristine CNTs reinforced epoxy composite was 11.56 MPa. As the CNT fractions increased to 1%, the toughness also increased to 16.58 MPa. Then when the CNT fraction continually increased to 2%, the toughness decreased to 7.3 MPa which was even lower than pristine CNTs reinforced epoxy composites with 0.5% addition. The significant decrease of toughness from 1% to 2% CNTs reinforced epoxy composites was mainly due to the formation of

CNT clusters with a poor dispersion state. On the other hand, by comparing SLS specimens with same CNT fractions but different adhesive materials, the toughness of the specimens with CMC treatments increased approximately 100%, 112%, and 338% for 0.5%, 1%, and 2% CNT fractions, respectively. It was very obvious that CMC treatments improved the toughness of CNTs reinforced epoxy composites by improving the CNT dispersion. As for the toughness of CMCs/CNTs reinforced epoxy composites, although the highest value still lied in the specimens with 1% CNT addition, the lowest value went to the specimens with 0.5% addition instead of 2% addition. Since CNTs have more agglomerations with more additions, the improvements were more significant with highly aggregated CNTs.

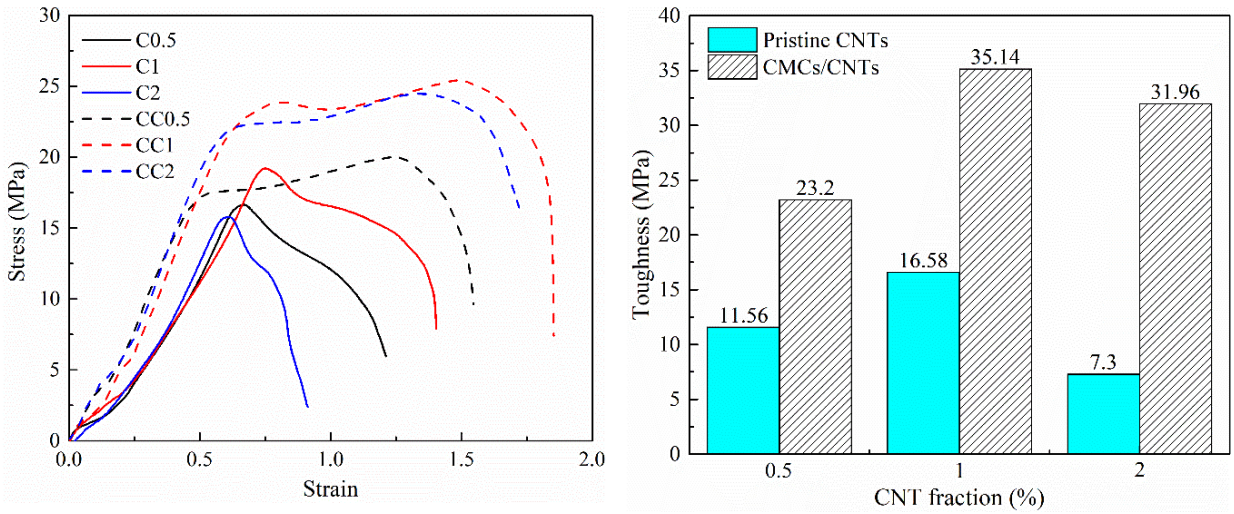

(a) (b)

Figure 51. SLS test results: (a) stress-strain curves of SLS specimens; (b) toughness of SLS specimens

Among all the bonding performances of epoxy composites, the most important parameters are bonding strength and fracture strain which can be obtained from the stress-strain curve. Figure 52(a, b) illustrate increments of the bonding strength and fracture strain between pristine CNTs and CMCs/CNTs reinforced epoxy composites with different CNT fractions. As for pristine CNTs reinforced epoxy composites, the specimens with 1% CNT fractions gained the highest bonding strength, while the lowest strength belonged to the specimens with 2% fractions. This was because

1% addition appears to be the optimal fraction, and severe CNT agglomerations are more prone to occur with higher CNT fractions. However, regarding CMCs/CNTs reinforced epoxy composites, the bonding strength of the specimens with 2% CNT fraction was only slightly lower that the highest value of the specimens with 1% fraction, making 0.5% fraction the worst case. The reason could be interpreted by comparing the increments of CMCs/CNTs reinforced epoxy composites compared to pristine CNT reinforced epoxy composites. It was clearly shown in Figure 52(a) that CMC treatments considerably improved the bonding strength of CNTs reinforced epoxy composites, with the increments of three CNT fractions being 21%, 32%, and 42%, respectively. As the increase of CNT fractions, the improvements of bonding strength by CMC treatments were more and more significant. In addition, according to Figure 52(b), the variations of fracture strain were very similar to those of bonding strength, which was also consistent with the findings of toughness. The results of SLS tests clearly showed that better dispersion states by CMC treatments had a remarkably positive effect on the bonding performances of CNTs reinforced epoxy composites.

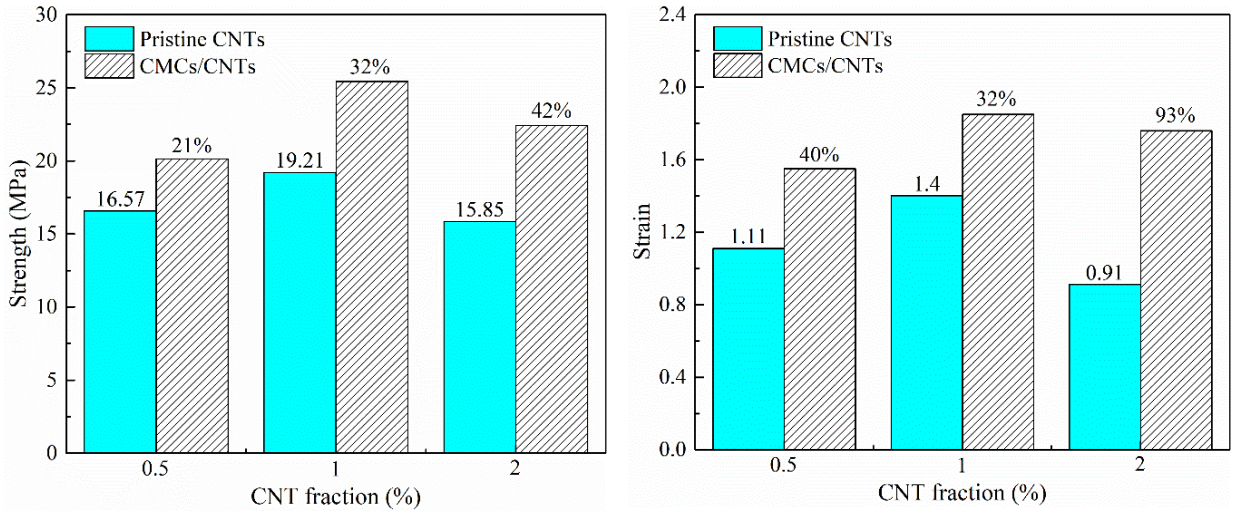

(a) (b)

Figure 52. Increments of the bonding strength and fracture strain between pristine CNTs and CMCs/CNTs reinforced epoxy composites with different CNT fractions: (a) bonding strength; (b): fracture strain

6.2.6. SEM analysis

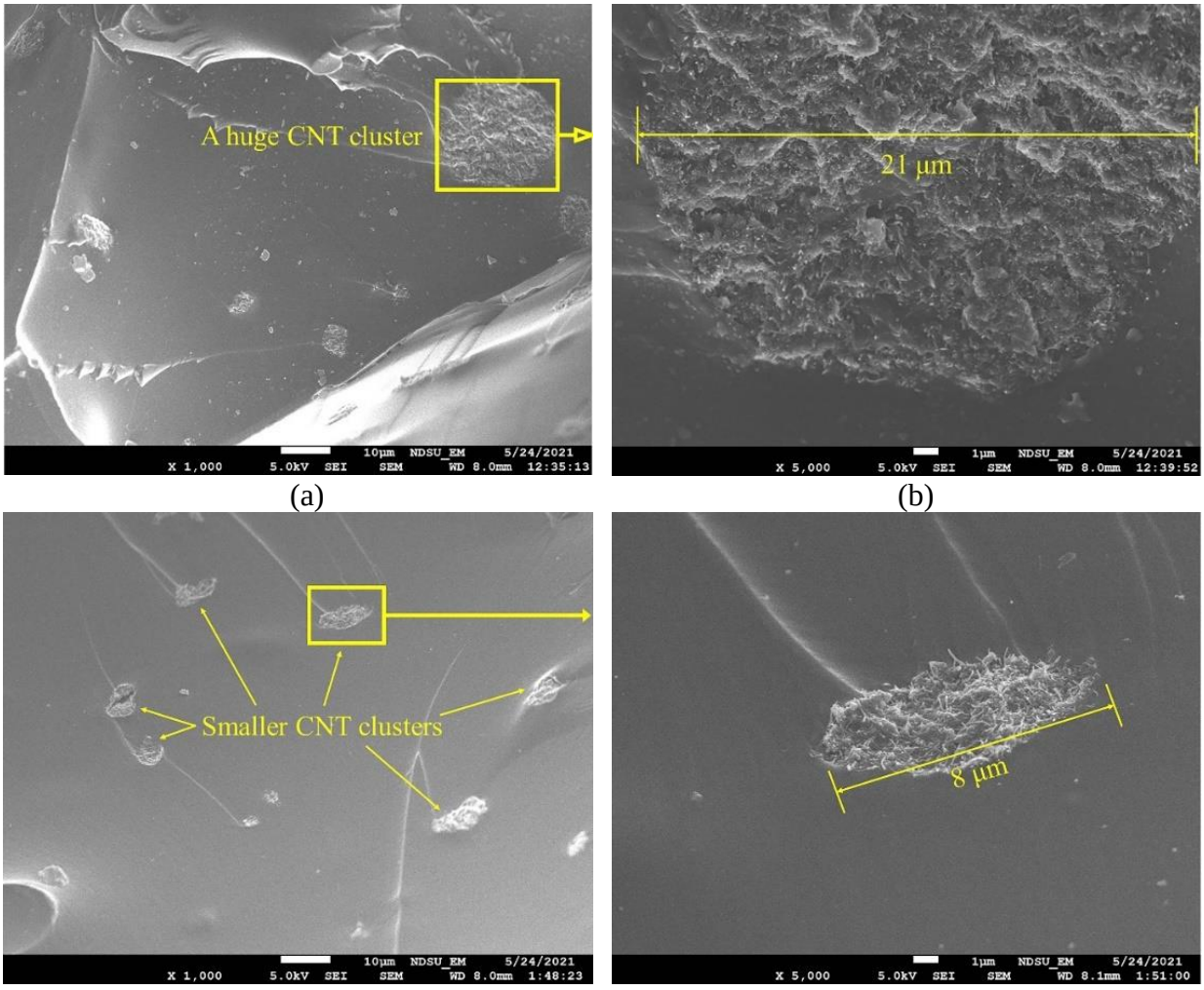

(a) (b)

(c) (d)

Figure 53. Typical CNT clusters on the fracture surfaces of 2% pristine CNTs and CMCs/CNTs reinforced epoxy composites: (a) C2; (b) close-view of the CNT cluster of C2; (c); CC2; (d) close-view of the CNT cluster of CC2

The dispersion states of epoxy composites were further evaluated using SEM analysis to show the size of CNT clusters on the fracture surfaces. Figure 53(a ~ d) demonstrates the typical CNT clusters on the fracture surfaces of 2% pristine CNTs and CMCs/CNTs reinforced epoxy composites, since most apparent differences was seen with the 2% CNT addition. For pristine CNTs reinforced epoxy composites as shown in Figure 53(a, b), there was a huge CNT cluster with a diameter of more than 21 μm on the fracture surface. The existence of that huge CNT cluster

was due to that CNTs tended to form larger CNT clusters and highly aggregate with higher CNT fractions. However, for CMCs/CNTs reinforced epoxy composites as shown in Figure 53(c, d), although CMC treatments did not eliminate the CNT clusters, most of the CNT clusters yielded a similar diameter around 8 μm. The remarkably smaller CNT clusters after CMC treatments were in agreement with the results of particle size analysis. Although CMC treatments did not completely break up CNT clusters into individual CNTs, it did improve the dispersion state of CNTs in the epoxy matrix by reducing the size of clusters and mitigating CNT agglomeration.

6.3. Summary

This chapter introduces the use of CMC surface treatment to improve the dispersion of CNTs in epoxy-CNTs composite and investigated the dispersion characterizations and bonding performances of the epoxy composites reinforced by CMC surface treated CNTs for three different CNTs fractions (0.5%, 1%, and 2%). The results of Raman spectroscopy and TEM analysis proved the effectiveness of CMC treatments that CMCs were attached on the surface of CNTs forming a thin amorphous layer. It was found by particle size analysis, TEM, and SEM analysis that although CMC treatments did not completely break up all the CNT clusters into individual CNTs, CNT dispersion states were improved by reducing the size of CNT clusters after CMC treatments. For 1% and 2% CNT addition, the CNT agglomerations were significantly mitigated with average diameter reductions of 47%. While the dispersion improvement was less significant for 0.5% CNT addition, since CNTs were less likely to agglomerate with a low fraction. The improved CNT dispersion state by CMC treatments also had a positive influence on the wettability and bonding performances of CNT reinforced epoxy composites. Due to better CNT dispersion state with CMC treatments, CMCs/CNTs reinforced epoxy composites had stronger interfacial adhesion, higher

toughness, bonding strength, and fracture strain compared to pristine CNTs reinforced epoxy composites.

CHAPTER 7. CONCLUSIONS

7.1. Main Conclusions

This dissertation investigated the bonding performance of epoxy-based composites with different surface roughnesses, bondline thicknesses, CNT weight fractions, CNT geometries, and a novel CNT mixing method using CMCs. The main conclusions of this study can be drawn as follows:

1) For neat epoxy resin, the bonding performance improved significantly with the increase of the surface roughness. The influence of surface roughness was more significant on smoother substrates and became less efficient on over-roughed substrates. While the reduction of bondline thickness greatly improved the toughness of epoxy-based composites, resulting in more plastic deformations and better bonding performance.
2) For CNT reinforced epoxy composites, surface roughness still had the same positive influence on the bonding performance of epoxy-based composites. With sufficient surface roughness and interfacial adhesion, the addition of CNTs significantly increased the bonding performance. Higher toughness and pulling-out of CNTs with improved fracture energy consuming efficiency were the reinforcing mechanisms. But when lacking sufficient interfacial adhesion due to low surface roughness, the bonding performance of the CNT reinforced epoxy composites still improved because the addition of CNTs could improve the interfacial adhesion, although the improvement was less significant.
3) CNT reinforced epoxy composites with higher CNT weight fraction (from 0% to 0.75%) had better bonding performance. The negative influence of bondline thickness of neat epoxy resin was still valid for CNT reinforced epoxy composites. Although thinner

CNT reinforced epoxy bondlines still yielded better bonding performance, the improvements become less significant as the increase of CNT weight fractions. The addition of CNTs could not eliminate the influence of bondline thickness, which was induced by the non-uniform dispersion and the aggregation of CNTs.

4) Epoxy composites reinforced by thicker CNTs had a more uniform CNT dispersion as a result of smaller particle size characterizations. Due to the better CNT dispersion, epoxy composites reinforced by thicker CNTs had better bonding performance not only in the higher bonding strength but also higher toughness. For the effect of CNT length, there was no evident difference between the dispersion characterizations of CNT suspensions with normal-length and short CNTs. However, the bonding performance of CNT reinforced epoxy composites with normal-length CNTs were much better than those with short CNTs.
5) A new physical surface treatment method using CMC as the surfactant was proposed to disperse CNTs. It is proved that CMC were well attached on the surface of CNTs leading to smaller CNT clusters and better dispersion characterizations, while the CMC treatment was more effective with higher CNT additions. Improved CNT dispersion characterizations also had a positive influence on the wettability and bonding performance of CNT reinforced epoxy composites.

7.2. Main Contributions

The main contributions of this dissertation lie in the following aspects:

1) The influence of surface roughness was investigated by several different roughness levels in a wide roughness range using the same surface treatment method instead of only comparing the substrates with or without a certain surface treatment.

2) The influence of bondline thickness on bonding performance of CNT reinforced epoxy composites was systematically investigated, and it was found for the first time that the negative effect of bondline thickness could be mitigated by CNT addition.
3) The dispersion characterization and bonding performance of CNT reinforced epoxy composites with different CNT geometries were investigated for the first time.
4) For the first time, CMCs were added into of CNT reinforced epoxy composites to improve the CNT dispersion, and the effectiveness of this newly-developed surface treatment method by CMCs was comprehensively proved.

7.3. Future Work

Future work applies to make comparisons among the three different CNT dispersion methods (mechanical mixing, chemical and physical surface treatments) and find the best dispersion method for optimizations of dispersion characterizations and bonding performance of CNT reinforced epoxy composites.

REFERENCES

[1] G.W. Ehrenstein, R.P. (Richard P.) Theriault, Polymeric materials : structure, properties, applications , Hanser, Munich, Germany, (2001).

[2] B. Tylkowski, K. Wieszczycka, R. Jastrzab, Polymer engineering , De Gruyter, Berlin, Germany, (2017).

[3] A. Afzal, A. Kausar, M. Siddiq, Role of polymeric composite in civil engineering applications: a review, Polym. Technol. Mater. 59 (2020) 1023–1040.

[4] A. Kumar, K. Sharma, A.R. Dixit, Carbon nanotube- and graphene-reinforced multiphase polymeric composites: review on their properties and applications, J. Mater. Sci. 55 (2020) 2682–2724.

[5] M.D. Banea, L.F.M. Da Silva, Adhesively bonded joints in composite materials: An overview, Proc. Inst. Mech. Eng. Part L J. Mater. Des. Appl. 223 (2009) 1–18.

[6] A. Ozel, B. Yazici, S. Akpinar, M.D. Aydin, Ş. Temiz, A study on the strength of adhesively bonded joints with different adherends, Compos. Part B Eng. 62 (2014) 167–174.

[7] S.B. Lyon, R. Bingham, D.J. Mills, Advances in corrosion protection by organic coatings: What we know and what we would like to know, Prog. Org. Coatings. 102 (2017) 2–7.

[8] M. Laurentiu, B. Lidia, D. Eliza, D. Valentin, Polymeric coatings used against marine corrosion of naval steel EN32, in: Key Eng. Mater., Trans Tech Publications Ltd, 699 (2016) 71–79.

[9] D. Baltzis, S. Orfanidis, A. Lekatou, A.S. Paipetis, Stainless steel coupled with carbon nanotube-modified epoxy and carbon fibre composites: Electrochemical and mechanical study, Plast. Rubber Compos. 45 (2016) 95–105.

[10] L. Zhang, H. Wu, Z. Zheng, H. He, M. Wei, X. Huang, Fabrication of graphene oxide/multi-walled carbon nanotube/urushiol formaldehyde polymer composite coatings and evaluation of their physico-mechanical properties and corrosion resistance, Prog. Org. Coatings. 127 (2019) 131–139.

[11] N. Parhizkar, B. Ramezanzadeh, T. Shahrabi, Corrosion protection and bonding performances of the epoxy coating applied on the steel substrate pre-treated by a sol-gel based silane coating filled with amino and isocyanate silane functionalized graphene oxide nanosheets, Appl. Surf. Sci. 439 (2018) 45–59.

[12] G.L. García, V. López-Ríos, A. Espinosa, J. Abenojar, F. Velasco, A. Toro, Cavitation resistance of epoxy-based multilayer coatings: Surface damage and crack growth kinetics during the incubation stage, Wear. 316 (2014) 124–132.

[13] G. Bahlakeh, B. Ramezanzadeh, A Detailed Molecular Dynamics Simulation and Experimental Investigation on the Interfacial Bonding Mechanism of an Epoxy Adhesive on Carbon Steel Sheets Decorated with a Novel Cerium-Lanthanum Nanofilm, ACS Appl. Mater. Interfaces. 9 (2017) 17536–17551.

[14] T. Semoto, Y. Tsuji, K. Yoshizawa, Molecular understanding of the adhesive force between a metal oxide surface and an epoxy resin, J. Phys. Chem. C. 115 (2011) 11701–11708.

[15] R.J. Moulds, T.R. Baldwin, Toughened adhesives for structural applications, Int. J. Adhes. Adhes. 3 (1983) 203-207.

[16] K.S. Kim, J.S. Yoo, Y.M. Yi, C.G. Kim, Failure mode and strength of uni-directional composite single lap bonded joints with different bonding methods, Compos. Struct. 72 (2006) 477–485.

[17] A.J. Kandeloos, M.M. Attar, The diffusion and adhesion relationship between free films and epoxy coated mild steel, Prog. Org. Coatings. (2019) 105405.

[18] X. Wu, K. He, Z. Gong, Z. Liu, J. Jiang, The shear strength of composite secondary bonded single-lap joints with different fabrication methods, J. Adhes. Sci. Technol. 34 (2020) 936–948.

[19] A.M. Pereira, J.M. Ferreira, F. V. Antunes, P.J. Bártolo, Analysis of manufacturing parameters on the shear strength of aluminium adhesive single-lap joints, J. Mater. Process. Technol. 210 (2010) 610–617.

[20] N. Saleema, D.K. Sarkar, R.W. Paynter, D. Gallant, M. Eskandarian, A simple surface treatment and characterization of AA 6061 aluminum alloy surface for adhesive bonding applications, Appl. Surf. Sci. 261 (2012) 742–748.

[21] Y. Lei, Y. Ma, B. Zhang, B. Lei, Y. Li, Enhancement the adhesion between epoxy coating and rusted structural steel by tannic acid treatment, Acta Metall. Sin. (English Lett. 27 (2014) 1105–1113.

[22] D. Fernando, ; J G Teng, M. Asce, ; T Yu, X.L. Zhao, F. Asce, Preparation and Characterization of Steel Surfaces for Adhesive Bonding, J. Compos. Constr. 17 (2013) 04013012

[23] Z. Zhai, L. Feng, Effect of oxygen plasma treatment on bonding strength of epoxy coating on steel substrate, Prog. Org. Coatings. 131 (2019) 36–41.

[24] R. Hunter, N. Ibacache, J. Möller, R. Betancourt, T. Mora, E. Diez, B. Pavez, Influence of roughness on the mechanical adhesion of single lap joints, J. Adhes. 88 (2012) 376–390.

[25] K. Uehara, M. Sakurai, Bonding strength of adhesives and surface roughness of joined parts, J. Mater. Process. Technol. 127 (2002) 179-181.

[26] S. Budhe, A. Ghumatkar, N. Birajdar, M.D. Banea, Effect of surface roughness using different adherend materials on the adhesive bond strength, Appl. Adhes. Sci. 3 (2015) 20.

[27] A. Ghumatkar, R. Sekhar, Experimental study on different adherend surface roughness on the adhesive bond strength-review under responsibility ofthe Committee Members of International Conference on Advancements in Aeromechanical Materials for Manufacturing (ICAAMM-2016), 2017.

[28] D. Zhang, Y. Huang, Influence of surface roughness and bondline thickness on the bonding performance of epoxy adhesive joints on mild steel substrates, Prog. Org. Coatings. 153 (2021) 106135.

[29] P. Davies, L. Sohier, J.Y. Cognard, A. Bourmaud, D. Choqueuse, E. Rinnert, R. Créac'hcadec, Influence of adhesive bond line thickness on joint strength, Int. J. Adhes. Adhes. 29 (2009) 724–736.

[30] M.D. Banea, L.F.M. Da Silva, R.D.S.G. Campilho, The effect of adhesive thickness on the mechanical behavior of a structural polyurethane adhesive, J. Adhes. 91 (2014) 331–346.

[31] R. Kahraman, M. Sunar, B. Yilbas, Influence of adhesive thickness and filler content on the mechanical performance of aluminum single-lap joints bonded with aluminum powder filled epoxy adhesive, J. Mater. Process. Technol. 205 (2008) 183–189.

[32] D. Castagnetti, A. Spaggiari, E. Dragoni, Effect of bondline thickness on the static strength of structural adhesives under nearly-homogeneous shear stresses, J. Adhes. 87 (2011) 780–803.

[33] L.F.M. da Silva, T.N.S.S. Rodrigues, M.A.V. Figueiredo, M.F.S.F. de Moura, J.A.G. Chousal, Effect of adhesive type and thickness on the bonding strength, J. Adhes. 82 (2006) 1091–1115.

[34] A. Akhavan-Safar, M.R. Ayatollahi, L.F.M. da Silva, Strength prediction of adhesively bonded single lap joints with different bondline thicknesses: A critical longitudinal strain approach, Int. J. Solids Struct. 109 (2017) 189–198.

[35] R.D. Adams, N. A. Peppiatt, Stress analysis of adhesive-bonded lap joints, J. Strain Anal. Eng. Des. 9 (1974) 185–196.

[36] L.D.R. Grant, R.D. Adams, L.F.M. da Silva, Experimental and numerical analysis of single-lap joints for the automotive industry, Int. J. Adhes. Adhes. 29 (2009) 405–413.

[37] D.B. Lee, T. Ikeda, N. Miyazaki, N.S. Choi, Effect of bond thickness on the fracture toughness of adhesive joints, J. Eng. Mater. Technol. Trans. ASME. 126 (2004) 14–18.

[38] A.D. Crocombe, Global yielding as a failure criterion for bonded joints, Int. J. Adhes. Adhes. 9 (1989) 145-153.

[39] M. Mariano, N. El Kissi, A. Dufresne, Cellulose nanocrystals and related nanocomposites: Review of some properties and challenges, J. Polym. Sci. Part B Polym. Phys. 52 (2014) 791–806.

[40] P. Jojibabu, M. Jagannatham, P. Haridoss, G.D. Janaki Ram, A.P. Deshpande, S.R. Bakshi, Effect of different carbon nano-fillers on rheological properties and bonding strength of epoxy adhesive joints, Compos. Part A Appl. Sci. Manuf. 82 (2016) 53–64.

[41] S.M. Park, M.Y. Shon, Effects of multi-walled carbon nano tubes on corrosion protection of zinc rich epoxy resin coating, J. Ind. Eng. Chem. 21 (2015) 1258–1264.

[42] J. Aakkula, O. Saarela, Silane based field level surface treatment methods for aluminium, titanium and steel bonding, Int. J. Adhes. Adhes. 48 (2014) 268–279.

[43] S. Iijima, Helical Microtubules of Graphitic Carbon, Nature 354 (1991) 56-58.

[44] J.-P. Salvetat, J.-M. Bonard, N.H. Thomson, A.J. Kulik, L. Forró, W. Benoit, L. Zuppiroli, Mechanical properties of carbon nanotubes, Appl. Phys. A. 69 (1999) 255–260.

[45] S. Yu, M.N. Tong, G. Critchlow, Use of carbon nanotubes reinforced epoxy as adhesives to join aluminum plates, Mater. Des. 31 (2010) S126-S129.

[46] G. Barra, L. Vertuccio, U. Vietri, C. Naddeo, H. Hadavinia, L. Guadagno, Toughening of epoxy adhesives by combined interaction of carbon nanotubes and Silsesquioxanes, Materials (Basel). 10 (2017) 1131.

[47] H. Khoramishad, M. Khakzad, Toughening epoxy adhesives with multi-walled carbon nanotubes, J. Adhes. 94 (2018) 15–29.

[48] M. Konstantakopoulou, G. Kotsikos, Effect of MWCNT filled epoxy adhesives on the quality of adhesively bonded joints, Plast. Rubber Compos. 45 (2016) 166–172.

[49] S.M.J. Razavi, M.R. Ayatollahi, A. Nemati Giv, H. Khoramishad, Single lap joints bonded with structural adhesives reinforced with a mixture of silica nanoparticles and multi walled carbon nanotubes, Int. J. Adhes. Adhes. 80 (2018) 76–86.

[50] D. Zhang, Y. Huang, Y. Wang, Bonding performances of epoxy coatings reinforced by carbon nanotubes (CNTs) on mild steel substrate with different surface roughness, Compos. Part A Appl. Sci. Manuf. 147 (2021) 106479.

[51] A. Kumar, K. Kumar, P.K. Ghosh, A. Rathi, K.L. Yadav, Raman, MWCNTs toward superior strength of epoxy adhesive joint on mild steel adherent, Compos. Part B Eng. 143 (2018) 207–216.

[52] M.R. Ayatollahi, A. Nemati Giv, S.M.J. Razavi, H. Khoramishad, Mechanical properties of adhesively single lap-bonded joints reinforced with multi-walled carbon nanotubes and silica nanoparticles, J. Adhes. 93 (2017) 896–913.

[53] B. Wang, Y. Bai, X. Hu, P. Lu, Enhanced epoxy adhesion between steel plates by surface treatment and CNT/short-fibre reinforcement, Compos. Sci. Technol. 127 (2016) 149–157.

[54] K. Li, B. Gu, K.-T. Hsiao, J. Alms, S.G. Advani, Use of epoxy/multiwalled carbon nanotubes as adhesives to join graphite fibre reinforced polymer composites, Nanotechnology 14 (2003) 791-793.

[55] S.J. Marshall, S.C. Bayne, R. Baier, A.P. Tomsia, G.W. Marshall, A review of adhesion science, Dent. Mater. 26 (2010) e11-e16.

[56] S.A. Sydlik, J.H. Lee, J.J. Walish, E.L. Thomas, T.M. Swager, Epoxy functionalized multi-walled carbon nanotubes for improved adhesives, Carbon N. Y. 59 (2013) 109–120.

[57] S.R. Yeomans, Galvanized steel reinforcement: Corros. Steel Concr. Struct., Elsevier Inc. (2016) 111–129.

[58] D. Zhang, Y. Huang, The bonding performances of carbon nanotube (CNT)-reinforced epoxy adhesively bonded joints on steel substrates, Prog. Org. Coatings. 159 (2021) 106407.

[59] A. Thess, R. Lee, P. Nikolaev, H. Dai, P. Petit, J. Robert, Crystalline ropes of metallic carbon nanotubes, Science 273 (1996) 483+.

[60] E. Gao, W. Lu, Z. Xu, Strength loss of carbon nanotube fibers explained in a three-level hierarchical model, Carbon N. Y. 138 (2018) 134–142.

[61] G. Pandey, E.T. Thostenson, Carbon nanotube-based multifunctional polymer nanocomposites, Polym. Rev. 52 (2012) 355–416.

[62] J.N. Coleman, U. Khan, Y.K. Gun'ko, Mechanical reinforcement of polymers using carbon nanotubes, Adv. Mater. 18 (2006) 689–706.

[63] E. Mainini, H. Murakawa, P. Piovano, U. Stefanelli, Carbon-nanotube geometries as optimal configurations, Multiscale Model. Simul. 15 (2017) 1448–1471.

[64] A. Anvari, The Influence of CNT Structural Parameters on the Properties of CNT and CNT-Reinforced Epoxy, Int. J. Aerosp. Eng. 2020 (2020) 4873426.

[65] W.S. Bao, S.A. Meguid, Z.H. Zhu, Y. Pan, G.J. Weng, Effect of carbon nanotube geometry upon tunneling assisted electrical network in nanocomposites, J. Appl. Phys. 113 (2013) 234313.

[66] R.J. Warzoha, A.S. Fleischer, Effect of carbon nanotube interfacial geometry on thermal transport in solid-liquid phase change materials, Appl. Energy. 154 (2015) 271–276.

[67] P.C. Ma, N.A. Siddiqui, G. Marom, J.K. Kim, Dispersion and functionalization of carbon nanotubes for polymer-based nanocomposites: A review, Compos. Part A Appl. Sci. Manuf. 41 (2010) 1345–1367.

[68] G. Gkikas, N.M. Barkoula, A.S. Paipetis, Effect of dispersion conditions on the thermo-mechanical and toughness properties of multi walled carbon nanotubes-reinforced epoxy, Compos. Part B Eng. 43 (2012) 2697–2705.

[69] H. Yang, Y. Yang, Y. Liu, D. He, J. Bai, Multi-scale study of CNT and CNT-COOH reinforced epoxy-based composites: dispersion state, interfacial interaction vs mechanical properties, Compos. Interfaces. 28 (2021) 381–393.

[70] A.H. Korayem, M.R. Barati, S.J. Chen, G.P. Simon, X.L. Zhao, W.H. Duan, Optimizing the degree of carbon nanotube dispersion in a solvent for producing reinforced epoxy matrices, Powder Technol. 284 (2015) 541–550.

[71] K.G. Dassios, P. Alafogianni, S.K. Antiohos, C. Leptokaridis, N.M. Barkoula, T.E. Matikas, Optimization of sonication parameters for homogeneous surfactant assisted dispersion of multiwalled carbon nanotubes in aqueous solutions, J. Phys. Chem. C. 119 (2015) 7506–7516.

[72] Y.P. Sun, K. Fu, Y. Lin, W. Huang, Functionalized carbon nanotubes: Properties and applications, Acc. Chem. Res. 35 (2002) 1096–1104.

[73] J. Wang, Z. Fang, A. Gu, L. Xu, F. Liu, Effect of amino-functionalization of multi-walled carbon nanotubes on the dispersion with epoxy resin matrix, J. Appl. Polym. Sci. 100 (2006) 97–104.

[74] P.C. Ma, J.K. Kim, B.Z. Tang, Effects of silane functionalization on the properties of carbon nanotube/epoxy nanocomposites, Compos. Sci. Technol. 67 (2007) 2965–2972.

[75] J. Li, Z. Fang, L. Tong, A. Gu, F. Liu, Improving dispersion of multiwalled carbon nanotubes in polyamide 6 composites through amino-functionalization, J. Appl. Polym. Sci. 106 (2007) 2898–2906.

[76] G.L. Burkholder, Y.W. Kwon, R.D. Pollak, Effect of carbon nanotube reinforcement on fracture strength of composite adhesive joints, J. Mater. Sci. 46 (2011) 3370–3377.

[77] M. Monthioux, B.W. Smith, B. Burteaux, A. Claye, J.E. Fischer, D.E. Luzzi, Sensitivity of single-wall carbon nanotubes to chemical processing: an electron microscopy investigation, Carbon N. Y. 39 (2001) 1251-1272.

[78] Z. Qi, Y. Tan, H. Wang, T. Xu, L. Wang, C. Xiao, Effects of noncovalently functionalized multiwalled carbon nanotube with hyperbranched polyesters on mechanical properties of epoxy-based composites, Polym. Test. 64 (2017) 38–47.

[79] Y. Chen, W. Wei, Y. Zhu, J. Luo, X. Liu, Noncovalent functionalization of carbon nanotubes via co-deposition of tannic acid and polyethyleneimine for reinforcement and conductivity improvement in epoxy-based composite, Compos. Sci. Technol. 170 (2019) 25–33.

[80] J. Cha, S. Jin, J.H. Shim, C.S. Park, H.J. Ryu, S.H. Hong, Functionalization of carbon nanotubes for fabrication of CNT/epoxy nanocomposites, Mater. Des. 95 (2016) 1–8.

[81] M.S. Rahman, M.S. Hasan, A.S. Nitai, S. Nam, A.K. Karmakar, M.S. Ahsan, M.J.A. Shiddiky, M.B. Ahmed, Recent Developments of Carboxymethyl Cellulose, Polymers (Basel). 13 (2021) 1345.

[82] J. Fu, D. Li, G. Li, F. Huang, Q. Wei, Carboxymethyl cellulose assisted immobilization of silver nanoparticles onto cellulose nanofibers for the detection of catechol, J. Electroanal. Chem. 738 (2015) 92–99.

[83] L. Long, F. Li, M. Shu, C. Zhang, Y. Weng, Fabrication and application of carboxymethyl cellulose-carbon nanotube aerogels, Materials (Basel). 12 (2019) 1867.

[84] K.C. Shin, J.J. Lee, The manufacturing process of co-cured single and double lap joints and evaluation of the load-bearing capacities of co-cured joints, in: J. Mater. Process. Technol. 138 (2003) 89–96.

[85] D. Sen, N.M. Chavan, D.S. Rao, G. Sundararajan, Influence of grit blasting on the roughness and the bond strength of detonation sprayed coating, J. Therm. Spray Technol. 19 (2010) 805–815.

[86] E.S. Gadelmawla, M.M. Koura, T.M.A. Maksoud, I.M. Elewa, H.H. Soliman, Roughness parameters, J. Mater. Process. Technol. 123 (2002) 133–145.

[87] F.J. Guild, A.J. Kinloch, A.C. Taylor, Particle cavitation in rubber toughened epoxies: The role of particle size, J. Mater. Sci. 45 (2010) 3882–3894.

[88] J.H. Park, J.H. Choi, J.H. Kweon, Evaluating the strengths of thick aluminum-to-aluminum joints with different adhesive lengths and thicknesses, Compos. Struct. 92 (2010) 2226–2235.

[89] M.J. Suriani, A. Ali, A. Khalina, S.M. Sapuan, S. Abdullah, Detection of defects of kenaf/epoxy by thermography analyses, IOP Conf. Ser. Mater. Sci. Eng. 36 (2012) 012013.

[90] F. Ali, N. Ishfaq, A. Said, Z. Nawaz, Z. Ali, N. Ali, A. Afzal, M. Bilal, Fabrication, characterization, morphological and thermal investigations of functionalized multi-walled carbon nanotubes reinforced epoxy nanocomposites, Prog. Org. Coatings. 150 (2021) 105962.

[91] S. Han, Q. Meng, S. Araby, T. Liu, M. Demiral, Mechanical and electrical properties of graphene and carbon nanotube reinforced epoxy adhesives: Experimental and numerical analysis, Compos. Part A Appl. Sci. Manuf. 120 (2019) 116–126.

[92] Y.L. Liang, Z.B. Wang, J. Zhang, J.B. Zhang, K. Lu, Enhanced bonding property of cold-sprayed Zn-Al coating on interstitial-free steel substrate with a nanostructured surface layer, Appl. Surf. Sci. 385 (2016) 341-348.

[93] X. Chen, I.J. Beyerlein, L.C. Brinson, Curved-fiber pull-out model for nanocomposites. Part 1: Bonded stage formulation, Mech. Mater. 41 (2009) 279–292.

[94] S. Parveen, S. Rana, R. Fangueiro, M.C. Paiva, Characterizing dispersion and long term stability of concentrated carbon nanotube aqueous suspensions for fabricating ductile cementitious composites, Powder Technol. 307 (2017) 1–9.

[95] A. Haque, A. Ramasetty, Theoretical study of stress transfer in carbon nanotube reinforced polymer matrix composites, Compos. Struct. 71 (2005) 68–77.

[96] M.M. Shokrieh, R. Rafiee, Investigation of nanotube length effect on the reinforcement efficiency in carbon nanotube based composites, Compos. Struct. 92 (2010) 2415–2420.

[97] V. V. Mokashi, D. Qian, Y. Liu, A study on the tensile response and fracture in carbon nanotube-based composites using molecular mechanics, Compos. Sci. Technol. 67 (2007) 530–540.

[98] L. Chia, Y. Huang, P. Lu, A.N. Bezbaruah, Surface Modification of Carbon Nanotubes Using Carboxymethyl Cellulose for Enhanced Stress Sensing in Smart Cementitious Composites, IEEE Sens. J. 21 (2021) 15218–15229.

[99] C.E. Pizzutto, J. Suave, J. Bertholdi, S.H. Pezzin, L.A.F. Coelho, S.C. Amico, Study of epoxy/CNT nanocomposites prepared via dispersion in the hardener, Mater. Res. 14 (2011) 256–263.

[100] P. Jojibabu, Y.X. Zhang, A.N. Rider, J. Wang, B. Gangadhara Prusty, Synergetic effects of carbon nanotubes and triblock copolymer on the bonding strength of epoxy adhesive joints, Compos. Part B Eng. 178 (2019) 107457.

[101] L. Bokobza, J. Zhang, Raman spectroscopic characterization of multiwall carbon nanotubes and of composites, Express Polym. Lett. 6 (2012) 601–608.

[102] M. Bourchak, K.A. Juhany, N. Salah, R. Ajaj, A. Algarni, F. Scarpa, Determining the Tensile Properties and Dispersion Characterization of CNTs in Epoxy Using Tem and Raman Spectroscopy, Mech. Compos. Mater. 56 (2020) 215–226.